Solubility and permeability as *in vitro* predictors for *in vivo* performance of fenofibrate IR solid dosage forms

Dissertation

zur Erlangung des Grades

„Doktor der Naturwissenschaften“

im Promotionsfach Pharmazie

am Fachbereich Chemie, Pharmazie und Geowissenschaften

der Johannes Gutenberg-Universität

in Mainz

Philipp Buch

geb. in Frankfurt am Main

Mainz, den 02.06.2010

D77 (Mainzer Dissertation)

Dekan:

1. Berichterstatter:

2. Berichterstatter:

Tag der mündlichen Prüfung: 25.06.2010

Die vorliegende Arbeit wurde in der Zeit von April 2005 bis März 2010 an der Johannes Gutenberg-Universität in Mainz durchgeführt.

Für meine Eltern

Danksagung

Table of contents

Abbreviations

AUC	Area under the curve
BCS	Biopharmaceutics classification system
BSA	Bovine serum albumin
Caco-2	Human colon carcinoma epithelial cell line
C_{max}	Maximum plasma concentration
CMC	Critical micelle concentration
Cryo-TEM	Cryogenic transmission electron microscopy
DLS	Dynamic light scattering
D-MEM	Dulbecco's modified eagle medium
D/P system	Dissolution/permeation system
EDTA	Ethylenediaminetetraacetic acid
FaSSIF	Fasted state simulated intestinal fluid
$FaSSIF_{mod}$	Modified fasted state simulated intestinal fluid
FBS	Fetal bovine serum
FDA	Food and Drug Administration
FeSSIF	Fed state simulated intestinal fluid
$FeSSIF_{mod6.5}$	Modified fed state simulated intestinal fluid
GI	Gastrointestinal
HBSS	Hank's balanced salt solution
HEPES	4-(2-hydroxyethyl)-1-piperazineethanesulfonic acid
HPLC	High performance liquid chromatography
IDD-P™	Insoluble Drug Delivery-MicroParticle
IR	Immediate release
IVIVC	*In vitro*/*in vivo* correlation
IVIVR	*In vitro*/*in vivo* relationship
k	Rate constant
MDCK	Madin-Darby canine kidney epithelial cell line
n/a	Not available
NaTC	Sodium taurocholate
NEAA	Nonessential amino acids
p.o.	per oral
R^2	Coefficient of correlation
rpm	Revolutions per minute
SANS	Small-angle neutron scattering
SD	Standard deviation

SDS	Sodium dodecyl sulfate
SEM	Standard error of the mean
SIF	Simulated intestinal fluid
TEER	Transepithelial electrical resistance
TM	Transport medium
t_{max}	Time of maximum plasma concentration
TR	Time-resolved
USP	United States Pharmacopeia
UV	Ultraviolet

1. Introduction into absorption models

Drug absorption from the gastrointestinal tract is a complex process arising from the diversity of interactions between the drug, its dosage form properties and physiological mechanisms. Accordingly, numerous variables affect the relationship between drug intake and clinical response. The major cause for variabilities in drug response can be attributed to differences in drug bioavailability, namely the rate and extent of drug absorption.

The rate and extent of absorption via the oral route are primarily controlled by two factors, the solubility and the permeability of a drug. According to these two factors, Amidon et al. [1] classified drugs into four different groups in what is referred to as the Biopharmaceutics Classification System (BCS). Taking into account these drug properties, dissolution and subsequent permeation across the gastrointestinal (GI) wall are processes in oral drug absorption whereby each of those may be rate limiting. Therefore, dissolution and permeation studies have been modified over the last decades to more closely simulate the characteristics of the GI tract *in vitro* in order to predict the rate and extent of drug absorption *in vivo*.

Hereafter, the most important physiological factors of the GI tract which affect the dissolution and absorption of drugs are shortly summarized, followed by an overview of *in vitro* methods mimicking the GI tract conditions. Furthermore, possibilities to correlate data obtained *in vitro* with *in vivo* clinical data are presented, leading finally to the aims of the thesis.

1.1 The gastrointestinal tract

The GI tract is composed of three major anatomical regions: the stomach, the small intestine and the colon. Due to its large surface (about 200 m^2 [2]) the small intestine is the most important site for drug absorption. It measures about 550 cm in length [3]. Numerous physiological parameters affect drug dissolution and permeation across intestinal epithelia such as gastric emptying, GI motility, microclimate pH, the stagnant water layer, bile salts, intestinal blood and lymph flow, as the most important.

1.1.1 The intestinal epithelium

About 90% of the cell population in the intestinal epithelium is composed of enterocytes providing the primary anatomical barrier against oral drug absorption. The lamina propria is found beneath the basal side of the enterocytes and is comprised of connective tissue matrix, smooth muscle cells, plasma cells, lymphocytes, macrophages and cells that make up blood and lymphatic cells [4,5]. A drug molecule enters the blood and/or lymphatic circulations or both after transversing the epithelium and the lamina propria.

Three physiological characteristics of the small intestine, namely the Kerckring fold, the villi and microvilli increase the area available for absorption. The permeability differs along the crypt-villus axis i.e., the high permeability drugs are rapidly and completely absorbed through the villus tips, whereas the low permeability drugs reside longer in the intestinal lumen and may diffuse down the length of the crypt-villus axis prior to absorption. Thus the drug is presented to a larger surface area in a region of leakier paracellular pathway [6].

Adjacent to the brush border of the epithelial villi is a stagnant water layer (posing a hydrophilic barrier) which the compounds have to permeate before they can be absorbed [7]. It exerts major resistance to mucosal uptake of lipophilic substances [8].

Drugs can cross the intestinal epithelium in two ways, either through the cell (transcellular route) or between the cells (paracellular route). The physicochemical characteristics as well as membrane features, e.g., transport proteins, determine the primary route of drug transport. In general hydrophilic drugs cross the biological membrane paracellularly and lipophilic drugs cross the membrane transcellularly [9].

1.1.2 Factors affecting gastrointestinal absorption

1.1.2.1 Intestinal transit rate

The absorption of orally administered drugs is affected by the permeability of GI mucosa, but also by the transit rate in the GI tract, due to the fact that the drug molecules need to be exposed to their absorption site for a definite period. It is well known that gastric emptying rate is a crucial factor influencing the plasma concentration profile of orally administered drugs [10] as very little absorption of most drugs occurs from the stomach relative to the small intestine [11]. Gastric emptying is affected by the type of the dosage form as well as the presence of food in the stomach. The half-emptying time for the stomach is prolonged by food intake (0.5 to 3 h) compared to the fasted state (8 to 15 min) [12]. Whereas the residence time in the small intestine (about three hours) is independent of the dosage form and fed state [13], with mean axial transport rates of 1.5 and 1.3 cm/min in the fasted and fed state, respectively [14].

1.1.2.2 Intestinal pH

It is well known that intestinal pH influences solubility, but also permeability of drugs. Furthermore, the pH in the GI tract is affected by the intake of food. In the absence of food the pH has been measured to be 1-2.5 in the stomach, increasing through 6.6 ± 0.5 in the proximal, to 7.5 ± 0.4 in the distal small intestine [15]. In the presence of food the pH in the stomach increases to about 6.4 [16]. Through the contents of the stomach entering the duodenum after food intake the pH is lowered to about 5, whereas the pH in the following parts of the intestine are not altered [17].

1.1.2.3 Intestinal fluid volume

Food influences a further physiological parameter of the GI tract, namely the fluid volume in which dissolution takes place. In the literature the detected values for GI volumes vary to a large extent. The following table presents an overview of published fluid volumes in the GI tract.

Table 1.1. Fluid volumes in the gastrointestinal tract.

	Stomach		Small intestine	
Author	Fasted	Fed	Fasted	Fed
Jantratid [18]	30-50	500	200	1000
Sunesen [14]	20-30	n.d.	120-350	n.d.
Custodio [19]	300-500	800-900	500	900-1000
Schiller [20]	45	686	105	54

The presented data are mean values [15]

Since a crucial hypothesis of this doctoral thesis is based on the data of liquid content in the GI tract obtained by Schiller et al. [20], these findings will be outlined briefly. Their observed fluid volumes in the stomach under fasted and fed states resemble the well known results from the literature, excluding the publication of Custodio et al. [19] in terms of the fasted state. Whereas in the small intestine Schiller et al. detected a comparatively small mean fluid volume in the fasted state, which in fact decreased significantly after the meal. Interestingly, the fluid was observed in separated pockets, surrounded by “dry” segments. In the small intestine of the fasting patients typically less than 100 ml fluid was found in up to six pockets located mainly in distal segments. That was a significant outcome since the volunteers drank 850 ml water in total during the previous 7 h before the data acquisition.

Additionally, the location of orally administered capsules was followed throughout the GI tract. About a quarter of the capsules located in the small intestine were not in contact with fluid pockets. Therefore Schiller et al [20]. concluded that compendial dissolution tests (for further details, please refer to [21]) may not exhibit appropriate systems to predict the *in vivo* release from oral dosage forms.

1.1.2.4 Bile and the effect of food

Bile plays a major role in the solubilization of lipid digestion products and poorly water-soluble drugs. Bile acids promote the absorption of dietary lipids and their digestion products by solubilizing them as mixed micelles. Furthermore, the mixed micelles may improve diffusion through the unstirred water layer representing a significant barrier to the absorption of increasingly lipophilic substances [8].

Ingestion of food stimulates the secretion of bile, which is comprised of (average, in mole percent of total lipid): 76% bile acids, 18% phospholipids and 6% cholesterol [22]. It has been shown that a change in the concentration of bile components in the GI tract has a vast impact on the absorption of orally administered poorly water-soluble drugs. Since their dissolution in the GI tract is typically the rate-determining step to the intestinal absorption, the presence of food may lead to an increase in their solubility, dissolution and bioavailability. This so called food effect is particularly seen with BCS class II (low solubility, high permeability) drugs [17,23,24].

1.2 *In vitro* models to study oral absorption

1.2.1 Dissolution - predicting the effect of food

Due to the increasing number of poorly water-soluble drugs in the pharmaceutical industry, the effect of food on bioavailability poses a major challenge to formulation scientists. The potential for food to change the pharmacokinetics of drug products was recognized by the United States Food and Drug Administration (FDA) which led to the establishment of standards for the design of clinical food effect studies [25]. Significant food effects hamper the development of new drug products, particularly when clinical studies are required to control and/or monitor food intake in relation to dosing. Therefore, the prediction from *in vitro* data of whether a drug or drug formulation will show a food effect in human would be time- and cost-saving.

To examine influences of food intake on dissolution of drugs and drug formulations biorelevant media, simulating the fasted (FaSSIF) and the fed state (FeSSIF) in the upper jejunum, have been introduced [26]. In recent years these simplified models of the GI composition have been modified in terms of bile salt and/or phospholipid content, pH or inclusion of lipolysis products to increase the physiological relevance of the media [18,27,28]. Although the *in vivo* performance of formulations containing poorly soluble drugs have been better predicted using biorelevant media instead of compendial media, it is particularly challenging to develop a universal simulated fed state models which can be used with all drugs. That is due to the change in composition of *in vivo* fed state fluids with different ingested meals resulting in different colloidal structures that could solubilize hydrophobic compounds. The nature of these colloidal structures depends on the relative concentrations of biliary lipids, bile salts and products of lipid digestion and is, therefore, constantly changing [29,30].

The colloidal structures in biorelevant media have barely been investigated and in several publications the media were examined in combination with drugs or drug formulations. Nielsen et al. [31] characterized a self-nanoemulsifying drug delivery system in FaSSIF and FeSSIF via dynamic light scattering (DLS) and small-angle X-ray scattering. Additionally, cryogenic transmission electron microscopy (cryo-TEM) measurements were utilized to examine colloidal structures in biorelevant media [32]. Sunesen et al. [33] determined the size distribution of micelles and vesicles in biorelevant media by means of DLS.

Although the compositions of biorelevant media are slightly modified in nearly every new publication, it can be generalized that in media comparable with FaSSIF and FeSSIF, the detected colloidal structures are vesicles and micelles, respectively. The micelle-to-vesicle transition which may occur whilst concentrated bile is secreted into and transported in the small intestine has not been examined to date in physiological relevant bile salt-phospholipid ratios.

The most widely recognized molecular model for the structure of bile salt-phospholipid mixtures is the mixed disk model suggested by Mazer et al. [34]. Mixed micelles are described as disk-like portion of a lecithin bilayer surrounded on its perimeter by bile salt molecules which reduce the unfavorable exposure of the phospholipid hydrocarbon tails to the external aqueous solution. The hydrophilic surfaces of the bile salts are in contact with the aqueous solvent and their hydrophobic surfaces interact with the phospholipid molecules. Furthermore, the lecithin bilayer is interspersed with dimers of bile salts.

Hjelm et al. [35] investigated the effects of dilution on the particle morphology in bile salt-phospholipid mixtures. The observed transition from micelles to vesicles might occur during the dilution of secreted bile in the small intestine, although a non-physiological bile salt-phospholipid ratio was used in this study. Upon secretion of bile into the upper intestine bile salts partition from the mixed micelles into the aqueous phase when reaching an environment which is depleted in bile lipids. Therefore, the structures formed at higher lipid concentration cannot be maintained and finally vesicles are formed.

The bile salt and phospholipid concentrations in the biorelevant media are mean values derived from investigations in human aspirates [17], which lead to rather static systems compared to the *in vivo* situation. *In vivo*, concentrated bile is secreted into the duodenum where its colloidal structures are changed during the transport through the small intestine due to dilution, uptake of bile ingredients or interaction with luminal components (e.g., food).

Nevertheless, these model systems have been generally accepted as *in vitro* methods to predict the food effect in dissolution of poorly water-soluble drugs [36]. The following table lists a summary of biorelevant media. FaSSIF$_{mod}$, FeSSIF$_{mod6.5}$ and HBSS SIFs differ from the additionally listed media as their composition was modified to make them usable in permeation studies with cell lines. They are based on Hank's balanced salt solution which contains a physiological salt concentration. The additionally listed media can only be used in dissolution experiments.

Table 1.2. Summary of biorelevant media.

Components [mM]	$FaSSIF_{mod}$ [27]	$FeSSIF_{mod6.5}$ [27]	HBSS SIFs [28]	FaSSIF [26]	FeSSIF [26]	FaSSIF-V2 [18]	FeSSIF-V2 [18]	Early FeSSIF [18]	Middle FeSSIF [18]	Late FeSSIF [18]
$CaCl_2$	1.26	1.26	1.26							
KCl	5.33	5.33	5.33	103.29	203.90					
$MgCl_2$	0.49	0.49	0.49							
$MgSO_4$	0.41	0.41	0.41							
KH_2PO_4	0.44	0.44	0.44	28.68						
$NaHCO_3$	4.17	4.17	4.17							
NaCl	138.0	138.0	138.0			68.62	125.5	145.2	122.8	51
Na_2HPO_4	0.34	0.34	0.34							
NaOH						34.8	81.65	52.5	65.3	72
Glucose	19.45	19.45	25.0							
HEPES	10.0	10.0								
MES			20.0							
Maleic acid						19.12	55.02	28.6	44	58.09
Acetic acid					144.05					
NaTC	3.0	15.0	5.0-15.0	3.0	15.0	3	10	10	7.5	4.5
Lecithin	0.75	3.75	1.25-3.75	0.75	3.75	0.2	2	3	2	0.5
Fatty acids			0 or 0.50				0.8	40	30	0.8
Monoglycerides			0 or 0.25				5	6.5	5	1
pH	6.5	6.5	6.0	6.5	5.0	6.5	5.8	6.5	5.8	5.4
Osmolality [mOsm/kg H_2O]	311.7 ± 0.6	325.7 ± 0.6	334-360	270 ± 10	635 ± 10	180 ± 10	390 ± 10	400 ± 10	390 ± 10	240 ± 10

1.2.2 Permeation

Various methods are used as model systems for intestinal epithelial permeability. The comprehensive review of Deferme et al. [37] may serve as an overview regarding permeation studies. As this doctoral thesis focuses on *in vitro* methods to predict the *in vivo* performance of orally administered drug products, two models as examples for artificial membrane and cell culture systems are presented in this section.

Although artificial membranes lack transporter proteins they can be used for permeability screening, since a remarkable number of drug molecules cross the intestinal membrane via diffusion. Corti et al. [38] introduced an *in vitro* permeation method based on cellulose acetate-nitrate membranes which were impregnated with a mixture of lipids. They reported an excellent correlation between the artificial membrane permeability of 21 mainly passively transported drugs and their fraction absorbed in humans. Interestingly, the relationship between *in vitro* and *in vivo* data was linear which rarely occurs with permeation methods. Therefore, the approach of Corti et al. has shown its potential as a high-throughput screening permeation method in the early stages of drug discovery.

Cell culture models are suitable both to study the mechanistic basis of drug transport and as permeability screening models for new drugs. The human carcinoma cell line, Caco-2, has been extensively used over the last decades as a model of the intestinal barrier because it displays many of the morphological characteristics of the *in vivo* intestinal epithelial [39], such as tight junctions, microvilli, metabolizing enzymes and an array of transporters [40,41]. Several studies have presented a good correlation between transport rates of passively absorbed drugs in Caco-2 cells and the fraction absorbed in humans [39,42]. Furthermore, drug-carrier mediated absorption and secretion across Caco-2 cell monolayers have been reported as relevant factors for a variety of drugs, including enalapril [43], digoxin [44] and talinolol [45].

Although the Caco-2 cell line resembles in their characteristics the intestinal barrier, a few variations from the human epithelium hamper the prediction of *in vivo* performance in drug transport from *in vitro* data. It has been shown that this cell line exhibits a variable and commonly lower expression of transporters than seen *in vivo* [42]. Therefore a scaling factor has to be introduced to adjust for the different expressions of the carrier system in human and in Caco-2. Moreover, due to the origin of this colon-derived cell line the permeability values of hydrophilic drugs more closely resemble those seen in the human colon [46].

1.2.3 Rationale for the connection of dissolution and permeation

In contrast to *in vitro* dissolution, which is primarily determined using dosage forms, *in vitro* permeation studies are commonly conducted with pure drug solutions. Neither dosage forms nor physiological solubilizing substances are utilized. Accordingly, permeability of an active substance is considered to be a property exclusively attributed to the compound.

This may be due to some practical reasons arising from the experimental conditions in the most commonly used method, Caco-2 cells in a standard Transwell® device. By testing a complete solid dosage form, the apical dissolution volume and the permeation area provided by the cell monolayer would be too small to simulate the *in vivo* conditions. Moreover, the viability of the cell monolayer would be affected by the mechanical load through the dosage form and the huge osmotic pressure differences [47] between the small apical and basolateral compartments.

However, by applying pure drug solutions to the permeation assay, one disregards the precedent dissolution step occurring *in vivo*. Therefore, possible solubility issues of active substances which could limit absorption from the GI tract are neglected. Moreover, the high drug concentrations in common permeation assays do not simulate clinical doses. Thus, the drug concentrations in the donor solution typically stay constant over time, not resembling the *in vivo* situation.

As has been stated in section 1.2.1 the *in vivo* performance of solid dosage forms can be predicted by dissolution studies. It is assumed that increasing fractions of drug dissolved *in vitro* will lead to a better performance *in vivo*. This assumption can be maintained when permeation is not the rate-limiting step in absorption and excipients of the dosage form do not interfere with the intestinal epithelium.

On the contrary, formulation excipients and food have been shown to affect not only dissolution but also permeation of orally administered drugs [48,49]. Over the last decades, a variety of drugs has been detected as substrates for active transporters which accelerate their uptake [43] or efflux [45]. Simultaneously, the interaction of several excipients and food components with intestinal epithelium has been reported. Applying intralumenal conditions and relevant excipient concentrations in *in vitro* permeation studies would unveil the *in vivo* situation, as stated by Brouwers et al. [50]. The review of Aungst [51] provides an overview concerning pharmaceutical additives and food components as potential permeation enhancers of orally administered drugs.

In conclusion, the major parameters of oral drug absorption, dissolution and permeation, should both be simulated under physiological conditions to better predict the *in vivo* performance of drugs and drug products. Thereby clinical doses and intestinal volumes should be regarded leading to the actual concentrations in the intestine. This may provide useful information for

formulation scientists regarding the physiologically relevant concentrations of active substances and excipients and their potential interaction with intestinal epithelium.

A possibility to more closely resemble the fate of an orally administered active substance is the combination of dissolution and permeation measurements since both factors are related *in vivo*. A model in which dissolution and permeation across a membrane (e.g., Caco-2 or artificial membrane) would occur sequentially and simultaneously would match the physiological situation. A combined measurement of dissolution and permeation under physiological conditions may provide a deeper insight into the determinants of drug absorption. A potential outcome of such measurements would be a substantially accurate prediction of the *in vivo* performance of a drug or drug formulation in humans prior to animal or clinical studies.

1.3 Combination of dissolution and permeation models

1.3.1 First attempts to combine dissolution and permeation

Starting in the 1960's, several approaches have been introduced to mimic the physiological process of oral absorption by combining dissolution and permeation in one device. Initially, simulation of the intestinal membrane has been recognized as the core issue. Two methods of simulation have emerged: distribution models and membrane models. Distribution models commonly consist of three fluid phases. Two aqueous phases represent the luminal and the blood compartment. Both parts are divided by a lipid phase, the "membrane", which the drug has to cross. Approaches of this kind were introduced by Rosano et al. [52] and Koch [53].

One example for a membrane model is the apparatus Resomat developed by Dibbern et al. [54]. This device is comprised of an aqueous phase and chloroform, separated by a lipid-treated artificial membrane. After permeation through the membrane into the chloroform the drug is considered to be absorbed. One of the major points of criticism of both basic concepts is the application of non-physiological organic solvents to simulate the *in vivo* membrane. By choice of a lipid phase or an artificial membrane active substances absorbed via passive diffusion could be tested, which is the general absorption mechanism. However, these ostensive devices revealed the choice of the suitable *in vitro* membrane to be the major issue in dissolution/permeation systems.

Over the last decade several approaches combining drug dissolution and permeation across a Caco-2 monolayer have been introduced. Continuous dissolution/Caco-2 systems can be divided in open and closed systems which is dependent on the dissolution part of the system. Dissolution takes place either in a flow through cell (open system) or a dissolution vessel (closed system). Accordingly, no drug is allowed to exit the experimental setup in the closed systems.

1.3.2 Closed dissolution/Caco-2 systems

1.3.2.1 Dissolution/Caco-2 system by Ginski et al.

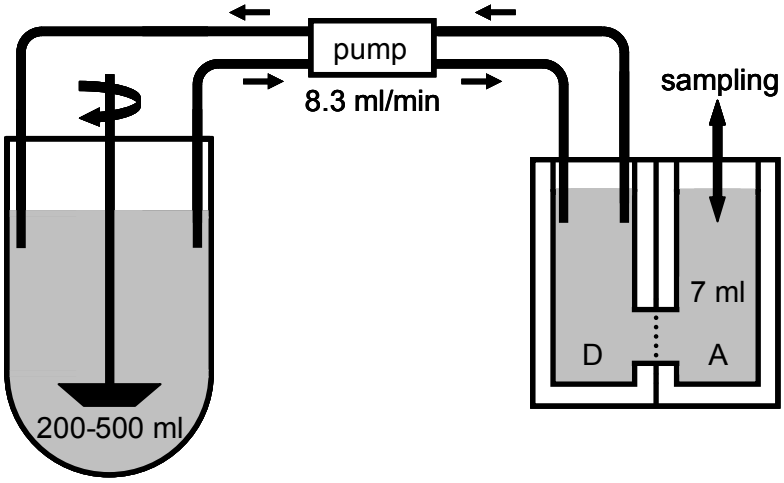

Figure 1.1. Dissolution/Caco-2 system by Ginski et al.; donor compartment (D), acceptor compartment (A)

The first system for simultaneous evaluation of dissolution and permeation was introduced by Ginski et al. [55] in 1999. Their approach is composed of a paddle apparatus (USP apparatus 2) and a side-by-side diffusion cell (Figure 1.1.). Donor and receiver compartment are connected through a Caco-2 monolayer grown on a polycarbonate Snapwell^{TM} filter. The transport of the dissolved drug from the dissolution medium to the diffusion cell is conducted via a peristaltic pump (flow rate: 8.3 ml/min). HBSS (pH 6.8) is used as dissolution and permeation media. This system may be seen as an advancement of a previous work where they first generated dissolution samples which were subjected to conventional Caco-2 flux studies in a second step.

Several objectives were pursued to investigate dissolution/absorption relationships: (1) testing whether the experimental data fit to the previously described mathematical model determining the relationship, (2) estimation of the effect of croscarmellose sodium on the relationships, (3) detection of possible effects of the formulation (solubilizing agents) on the relationships.

Validation of their *in vitro* tool with *in vivo* data using metoprolol, piroxicam, and ranitidine solid dosage formulations with varying release kinetics were confirmed. It qualitatively matched observed dissolution/absorption relationships from clinical studies, and usually matched clinical profiles quantitatively. Croscarmellose sodium revealed its permeation enhancing property, presumably caused by sequestering calcium. This was a false positive *in vitro* finding, because binding of all extracellular calcium may not happen *in vivo*. As assumed by the authors solubilizing agents only affected dissolution, not permeation. The results revealed the great

potential of this *in vitro* tool in the biopharmaceutical characterization of oral solid dosage form performance.

1.3.2.2 Dissolution/Caco-2 system by Kataoka et al.

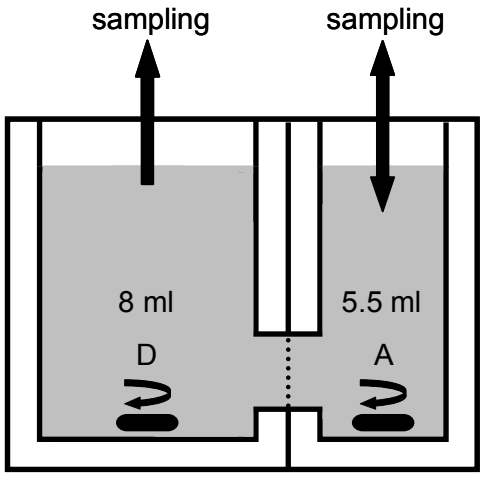

Figure 1.2. Dissolution/Caco-2 system by Kataoka et al.; donor compartment (D), acceptor compartment (A)

An additional continuous dissolution/Caco-2 system in a closed form was established by Kataoka et al. [56] in 2003. Validation of this dissolution/Caco-2 system was one goal of the current work. Throughout this doctoral thesis it is referred to as the dissolution/permeation (D/P) system. Kataoka et al. focused on the prediction of the oral absorption of poorly water-soluble drugs. For simplicity, compared to the approach by Ginski et al. this tool is only comprised of the side-by-side diffusion cell (Figure 1.2.).

Simulating clinical doses in a dissolution/Caco-2 system was the fundamental new aspect presented by this model. The miniaturized dissolution vessel is assumed to contain 1/100 of the *in vivo* dissolution volume (8 ml). Accordingly, the applied dose of the drug has to be reduced to the same scale. The dissolved drug has to permeate a Caco-2 monolayer which is mounted between the donor and the acceptor compartment (5.5 ml).

5 mM taurocholate (the concentration ranged between fasted and fed state) was added to the donor solution, containing griseofulvin. Therefore the permeated fraction for griseofulvin was increased which was mainly driven by higher dissolution rate and solubility. Applying 4.5% bovine serum albumin (BSA) to the receiver chamber promoted the *in vitro* permeation due to improved sink conditions for permeation.

The relationship between the human absorption of several drugs and their permeated fraction in the D/P system were observed at different time points. A good correlation was found using the permeation data after 2 h which is close to the average transit time in the small intestine (3 h) [13], the main organ for oral drug absorption.

In a following study [27] the simulation of the physiological conditions of the human GI tract under fasted and fed conditions was approached. Various kinds of simulated intestinal fluids were tested in the D/P system, including FaSSIF and FeSSIF (see Table 1.2.). The authors finally employed modified versions of the original FaSSIF and FeSSIF that did not affect the integrity of the Caco-2 monolayer. Therefore, human *in vivo* data from thirteen drugs could be successfully correlated with *in vitro* data obtained from the D/P system under fasted and fed conditions, respectively. Additionally, they could predict the reduction of the food effect on danazol formulated as self-emulsifying system.

1.3.3 Open dissolution/Caco-2 systems

1.3.3.1 Dissolution/Caco-2 system by Miyazaki et al.

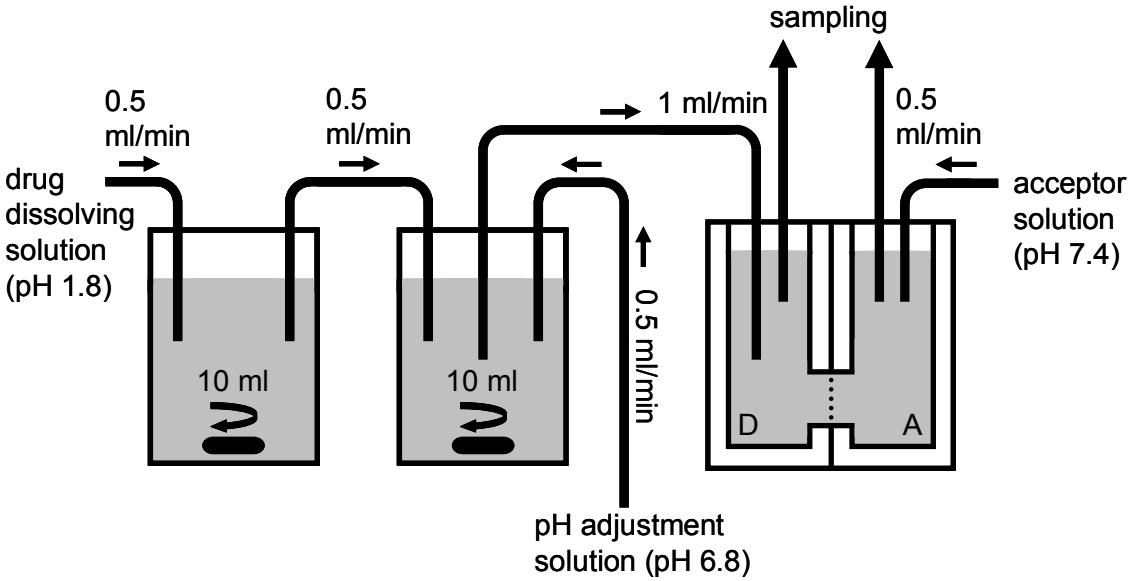

Figure 1.3. Dissolution/Caco-2 system by Miyazaki et al.; donor compartment (D), acceptor compartment (A)

In 2001, Miyazaki et al. [57] introduced the first dissolution/Caco-2 system in an open form. It is comprised of two vessels and a diffusion chamber, containing a Caco-2 monolayer (Figure 1.3.). Dissolution takes place in the first vessel, representing the stomach. The dissolved drug is constantly pumped into a pH adjustment vessel, representing the intestine. Finally, the drug solution is transferred into the permeation unit.

Over the last years the experimental tool has been slightly modified (e.g., extension of the vessel volumes from 3 to 10 ml) but the basic setup has been maintained. Compared to the closed dissolution/Caco-2 systems it is possible to simulate various effects of pH on dissolution (i.e., precipitation of the weak base albendazole in the pH adjustment vessel) [58]. However, it exhibits the downside that the pH values acting on the drug formulation in the dissolution vessel simulating the stomach can not be changed in one experiment. *In vivo* the undissolved drug is transferred to the small intestine with its increasing pH values, which is not reflected in this device. The introduction of different gastric acid models in a later publication [59] could only attenuate this drawback.

However, the results obtained from this approach were promising. A good relationship was shown between the fraction cumulatively permeated through the Caco-2 monolayer and the fraction absorbed in humans either from pure drugs or formulations [57,60]. Using either Caco-2 cells or rat intestine the authors were able to simulate the metabolism of the prodrug pivampicillin to ampicillin [60]. While passaging the *in vitro* permeation barriers pivampicillin was partly cleaved which correlated well with *in vivo* data.

1.3.3.2 Dissolution/Caco-2 system by Motz et al.

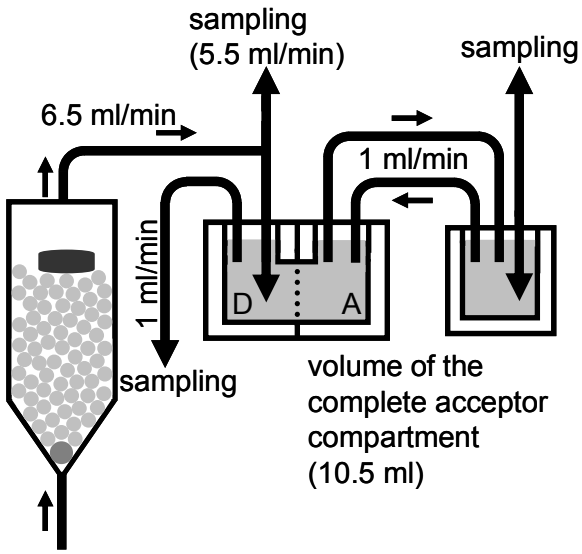

Figure 1.4. Dissolution/Caco-2 system by Motz et al.; donor compartment (D), acceptor compartment (A)

Probably the most complex continuous dissolution/Caco-2 system was published by Motz et al. [61]. Their apparatus is composed of a flow through dissolution cell (USP apparatus 4) and a permeation module containing a Caco-2 monolayer (Figure 1.4.). Sampling and quantification

was automated leading to a high sampling frequency. In contrast to the apical side, the basolateral compartment is a closed system in order to enable higher concentrations compared to those in an open system, facilitating more convenient analysis of the permeated drug. For successful applications they had to interpose a stream splitter between the dissolution unit and the permeation unit. Therefore, the flow rate in the permeation module was adjusted to a lower value compared to the flow rate in the dissolution device maintaining the integrity and viability of the Caco-2 monolayer. An experiment time of either 120 or 180 min resulted in a total dissolution volume of 780 and 1170 ml, respectively.

The authors tested several propranolol (BCS class I) solid dosage forms, varying in dosage strength or in release characteristics. An increase in dosage strength and moderate retardation of release was reflected in the permeation profiles. The drawback to this approach is that less than a sixth of the dissolved drug passes the stream splitter towards the permeation. This may hamper the appearance of detectable amounts of poorly soluble drugs on the basolateral side as only a small fraction of the dose will be dissolved and presented to the apical side of the monolayer. Furthermore, to date, no attempt was made to correlate *in vitro* data obtained from this approach with *in vivo* data.

1.3.4 Dissolution/permeation systems - alternatives to Caco-2

Besides the expounded dissolution/Caco-2 systems two additional noteworthy models, which belong to the class of continuous dissolution/permeation systems, are presented in the following section. Compared to the aforementioned models these two systems vary in the absorption unit.

1.3.4.1 Dissolution/hollow fiber system by Blanquet et al.

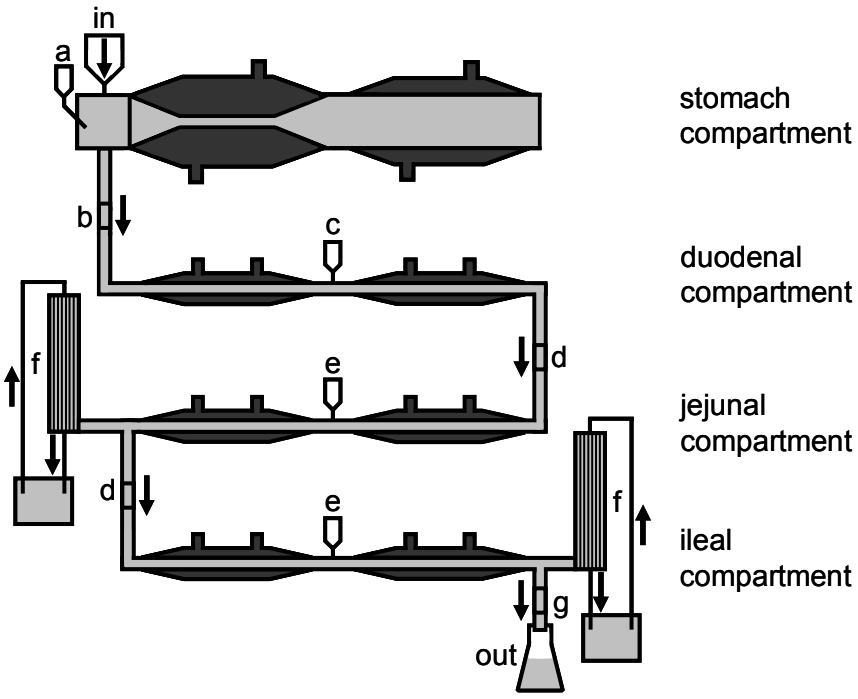

Figure 1.5. Dissolution/hollow fiber system by Blanquet et al.; stomach secretion (a), pyloric valve (b), duodenal secretion (c), peristaltic valve (d), jejunal/ileal secretion (e), hollow fiber membrane (f), ileocecal valve (g)

A sophisticated model combining *in vitro* dissolution and permeation was published by Minekus et al. [62] in 1995, called TIM-1. It is a dynamic, multicompartmental, computer-controlled system which closely mimics the physiological processes in the stomach and the small intestine. Briefly, four connected glass jackets with flexible interior walls represent the stomach and the three segments of the small intestine: the duodenum, jejunum and ileum (Figure 1.5.). This enables the simulation of the peristaltic movements in the GI tract. By utilizing a pump system the authors were able to secrete digestive fluids such as simulated salivary, gastric, biliary and pancreatic juices into the corresponding compartments.

Drug molecules are absorbed through dialysis membranes which are located at the middle (jejunum) and end part (ileum) of the “small intestine”. Permeated fractions of administered

substances could be determined by measuring the drug concentration in the dialysis fluids passing the dialysis membranes.

This approach was developed in the area of nutritional research and recently suggested its usefulness in pharmaceutical studies. Therefore, validation experiments were primarily conducted with minerals, vitamins and food mutagens to demonstrate the predictive value of the system [63-65]. Souliman et al. [66] were able to visualize the impact of food on the absorption of paracetamol from a solid oral dosage form. The tablet was administered to the gastric compartment either with 200 g of water or with 100 g of a mixed solid standardized meal with 200 g water, simulating the fasted and the fed state, respectively. A point-to-point relationship could be developed between the absorbed fractions *in vivo* and *in vitro*.

The fed state differed from the fasted state conditions only in the pH values in the stomach and the delayed gastric emptying time. To date, the bile solution was not adjusted to the *in vivo* fed state conditions. Accordingly, a published experiment with a poorly soluble drug is still sought after as the differences in bile juice content have a marked effect on its absorption. Since absorption is performed via dialysis membranes, the experiments are limited to drugs which are absorbed via passive diffusion. In order to circumvent this issue the authors want to expand their in vitro device with intestinal epithelia to include the effect of transporters on absorption.

1.3.4.2 Dissolution/everted intestine system by Kale et al.

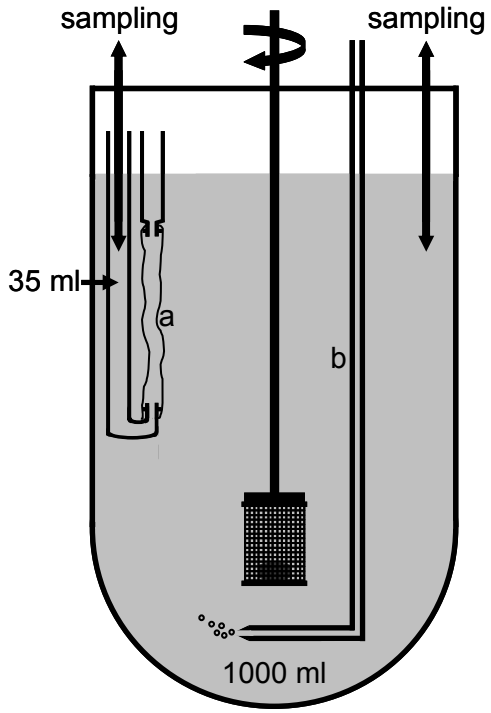

Figure 1.6 Dissolution/everted intestine system by Kale et al.; everted intestine (a), oxygen tube (b)

In 2007, Kale et al. [67] introduced a further approach which enabled simultaneous measurement of *in vitro* dissolution and permeation. Their system is comprised of a USP paddle apparatus and a permeation unit holding an everted intestine segment (Figure 1.6.). They used 1 l of distilled water as dissolution medium, whereas 35 ml of Krebs-Ringer solution was introduced to the absorption compartment. The everted intestine is mounted between two cannulae which are fixed at a constant distance. Chicken intestine was employed assuming that membrane permeability of compounds was not species-dependent.

Kale et al. tested different amounts of metformin in powder form and metformin formulated in two different slow-release oral dosage forms in their system. The studies led to the conclusion that the absorption of metformin may be permeation rate-limited which coincides with the assumption of Timmins et al. [68] that metformin may be subject to a saturable absorption process.

The combination of a compendial dissolution method with a modified everted sac technique represents an interesting approach. The primary drawback to the presented system is the permeation unit due to the lacking *in vitro* absorption studies conducted with chicken intestine. For successful application the chicken intestine has to be confirmed as suitable model for the human intestinal epithelium.

1.3.5 The D/P system by Kataoka et al. as method of choice

Among the aforementioned systems which combine *in vitro* dissolution and permeation assays the approach by Kataoka et al. (see section 1.3.2.2) seems to be the most promising model. As described in section 1.2.3 dissolution and permeation should be examined under conditions which reflect the actual physiological conditions. The authors attempt to fulfil this demand by applying clinical doses and biorelevant media to their D/P system. In contrast to the device by Blanquet et al. (see section 1.3.4.1) an IVIVC for various pure drugs under fasted and fed conditions was established. Moreover, Kataoka et al. were able to predict the *in vivo* performance of a danazol formulation. Due to the described characteristics, the D/P system was selected as the preferred device to examine oral drug formulations under physiologically relevant conditions. One goal of this thesis was to investigate if this approach is appropriate to develop an IVIVC with respect to different formulations containing the same compound.

1.4 *In vitro*/*in vivo* correlations

In the previous sections the determinants of oral absorption and the most promising methods of simulating the absorption mechanisms *in vitro* were elucidated. Such *in vitro* models provided a deeper insight into mechanistic absorption mechanisms and/or yield data which could be correlated with *in vivo* pharmacokinetic results. Since the pioneering studies by Nelson [69] and Levy et al. [70] in correlating dissolution rates of theophylline and acetylsalicylic acid, respectively, with their *in vivo* performance after oral administration, an increasing number of researchers have attempted to reveal *in vitro* properties of drugs and drug substances influencing their behavior *in vivo*.

An FDA guidance [71] in terms of *in vitro*/*in vivo* correlations (IVIVC) was published in an effort to minimize unnecessary clinical studies. Nowadays it is generally recognized that *in vitro* dissolution can substitute *in vivo* bioequivalence studies to a certain extent, as discussed in the previously mentioned guidance (e.g., scale up and post-approval changes). Bioequivalence is achieved *in vivo* when the test product exhibits the same rate and extent of bioavailability. In practice, two one-sided tests are conducted using log-transformed data from the bioequivalence study to show that the 90% confidence intervals for the ratio of the population geometric means (test/reference) for AUC and C_{max} fall within the limits (80-125%) [72].

A prerequisite to establish an IVIVC is the presence of several formulations showing differences in an *in vitro* property (e.g., dissolution rate) which is reflected in their *in vivo* performance. The FDA established four different levels of IVIVC, namely A, B, C and multiple C [71]. A level A correlation is the most preferable, because it represents the correlation of the entire *in vitro* dissolution time course of a drug with the entire *in vivo* response time course. Level B correlations are based on statistical moment analysis and relate the mean *in vitro* dissolution time of the drug to the mean residence time in the body or the mean *in vivo* dissolution time. A single point relationship between an *in vitro* dissolution parameter (e.g., fraction dissolved at a particular time or the time required for dissolution of a given fraction) and a pharmacokinetic parameter (e.g., AUC or C_{max}) is provided in a level C correlation. A multiple level C correlation represents a relationship between the fraction of drug dissolved at several time points, to one or several pharmacokinetic parameters of interest. In a regulatory point of view level B and C correlations are least informative, however may be useful to formulation scientists in selecting pilot formulations.

In the FDA guidance it is stated that any *in vitro* dissolution method may be used for the establishment of an IVIVC. This signifies that, to date, no universal *in vitro* dissolution model exists which is able to simulate the appropriate *in vivo* conditions. Therefore, the development of an IVIVC needs to be carried out on a case-by-case basis. This might be the reason why

applications of an IVIVC are limited to minor formulation changes not altering the release mechanism. An approximation of the *in vitro* dissolution conditions towards more physiological relevant conditions and/or the application of a more reliable *in vitro* method would augment the IVIVC concept.

1.4.1 When is an *in vitro*/*in vivo* correlation likely?

To forecast the *in vivo* performance of an orally administered drug, a method is required which is capable of modelling the limiting factor of absorption *in vitro*. In the case of dissolution testing extended release formulations [73-75] and formulations containing BCS class II drugs are addressed (see section 1.1.2.4). In contrast, an IVIVC based on *in vitro* dissolution data from formulations containing compounds of BCS classes III and IV would usually not be obtained, since permeation rather than dissolution may be rate limiting to absorption. In this case, a permeation method conducted with the formulated drug under physiologically relevant concentrations would provide more suitable data for an IVIVC than *in vitro* dissolution does. In the case of adverse interactions of formulation excipients on drug permeation, physiologically relevant data even for BCS class I and II may be yielded.

To summarize, a successful combination of *in vitro* dissolution and permeation data would examine both potentially rate-limiting parameters of absorption. This may expand the possibility of an IVIVC on compounds of all BCS classes.

A change from dissolution to permeation or a combination of dissolution and permeation in one approach as the predictive *in vitro* method for an IVIVC would be in accordance with the FDA guidance. Although the FDA defines the levels of correlation using the example of dissolution studies, it is permitted to implement a different *in vitro* property as long as it describes the relationship to an *in vivo* response.

1.5 Fenofibrate as model compound for drugs that are affected by the effect of food

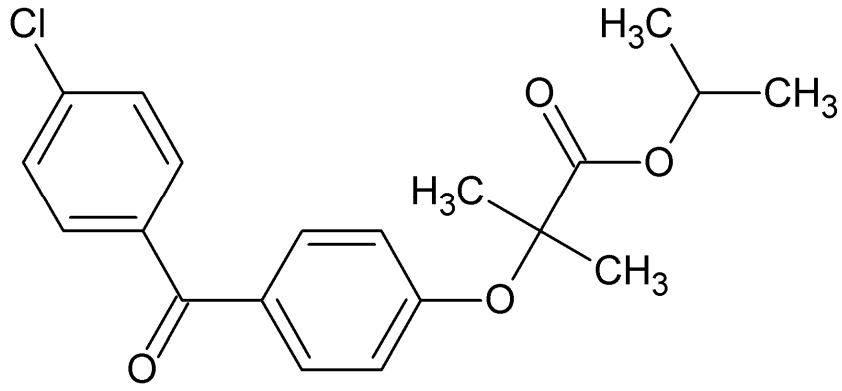

Figure 1.7. Fenofibrate

Fenofibrate, 2-[4-(4-Chlorobenzoyl)phenoxy]-2-methylpropanoic acid 1-methylethyl ester, is a poorly soluble ester of its active derivative fenofibric acid [76]. Fibric acid derivatives (fibrates) are a class of compounds which play an important role in the management of hypertriglyceridemia, combined hyperlipidemia, primary hypercholesterolemia, diabetic dyslipidemia and nephrotic syndrome [77-79]. The lipid-modifying effects of fenofibrate are mostly mediated by its ability to activate peroxisome proliferator-acivated receptors. Detailed information about this class of receptors and their interaction with fibrates is given in a review by Steinhilber et al. [80].

After oral administration, fenofibrate is rapidly converted through hydrolysis of its ester bond to fenofibric acid. Hydrolysis is catalyzed by both tissue and plasma esterases and appears to begin concomitantly with absorption. No unchanged fenofibrate can be detected in the blood after an oral dose [76]. Fenofibric acid is extensively protein bound (99%), primarily to albumin. Fenofibrate has a plasma half-life (22.1 h; range: 19.6-26.6 h) which ensures the therapeutic effectiveness of a once-daily 200 mg dosage [81]. Its metabolite fenofibric acid is eliminated largely in the urine as a conjugated derivative. Most (60-88%) of the dose is eliminated in the urine, with smaller fractions via the feces [76].

In this work an *in vivo* study in rats was conducted, since the rat has been recognized as an appropriate animal model to study the fraction of oral dose absorbed in humans [82]. As in humans, no unchanged fenofibrate is detected in the blood after an oral dose. In rats, approximately 70-80% of fenofibrate and its metabolites are recovered in the feces, with urinary excretion playing a secondary role [83]. Elimination in rats is rapid, with a mean terminal half-life around 10 h [84].

Fenofibrate is a neutral, lipophilic compound (log *P* = 5.24). It is practically insoluble in water, with an aqueous solubility at 37°C of < 0.2912 µg/ml. According to the BCS, fenofibrate is a class II drug having low solubility and high permeability [85]. It has the lowest and most variable bioavailability of the fibrates which is affected by the intake of food. This renders fenofibrate as a very suitable model in this thesis for examining the potential of the D/P system to differentiate between different formulations in terms of their ability to diminish the effect of food. Since fenofibrate is a neutral drug, no pH-controlled dissolution, as simulated to some extent in the approach of Miyazaki et al. (see section 1.3.3.1), is necessary.

The extent of absorption varies from 30-50% when fenofibrate is taken in the fasting state to 60-90% when it is given after a meal [86]. In general, due to their lipophilicity, the absorption of BCS class II drugs is substantially increased in the presence of food and, particularly, fat. Thus, the fed state may result in an increase in their solubility, dissolution and bioavailability [17].

However, in clinical practice the fenofibrate dosage schedule might be confused with the traditional schedule for statins and fenofibrate might be taken at bedtime on an empty stomach [87]. Additionally, patients may vary from day to day and from each other in their adherence to the limit of fat content of their meals and therefore may compromise the bioavailability of fenofibrate formulations.

Because the rate-limiting step in oral fenofibrate absorption is dissolution, improvements in this process have led to extended bioavailability. Increasing the rate and extent of dissolution of fenofibrate by micronization has been the major focus in the last decades. This has been shown to directly enhance bioavailability, which in turn enables dosage reduction and diminishes or abolishes the effect of food (more detailed information is presented in the following paragraphs).

1.5.1 Fenofibrate formulations

Fenofibrate has been marketed since the mid-1970's [88]. The initial dosage of the non-micronized formulation was 300 mg daily, taken in divided doses with food. The bioavailability of the original formulation of fenofibrate was improved through a micronization process. Thus the initial dosage regimen of the micronized formulation could be changed to 200 mg daily or three 67 mg capsules daily in divided doses, both with food [89].

Insoluble Drug Delivery-Microparticle (IDD-P^{TM}) fenofibrate tablets were developed to ensure fenofibrate bioavailability independent of food and its fat content. The technology used to develop this formulation involves reduction of particle size in the presence of phospholipids that associate at the freshly generated drug surface, preventing the microparticles from reaggregating. This approach preserves the expanded drug surface area that results from micronization. Upon oral administration the expanded drug surface area is exposed to the *in vivo*

dissolution, thereby increasing bioavailability [90]. Thus, 160 mg fenofibrate of the new tablet preparation is bioequivalent to 200 mg of the old capsule preparation. The purpose of equivalent extent of absorption under fed or fasting conditions could be fulfilled by the IDD-P™ fenofibrate 160-mg tablets.

By nanosizing fenofibrate its bioavailability could be raised compared to IDD-P™ fenofibrate 160 mg tablets which allowed a reduction of the dosage (145 mg tablet, 130 mg capsule). Neither fenofibrate 145 mg tablet nor fenofibrate 130 mg capsule interact with food, a property that may be associated with improved patient compliance. In the following table the four last mentioned fenofibrate formulations are listed.

Table 1.3. Summary of fenofibrate formulation.

Dosage [mg]	Fenofibrate particles	Dosage form	Brand name
200	Micronized	Capsule	Tricor®
160	Micronized (IDD-P™)	Tablet	Triglide®
145	Nanosized	Tablet	Tricor®
130	Nanosized	Capsule	Antara®

1.5.2 Several aspects of improving the bioavailability of poorly soluble drugs

To summarize, a reduction of the particle size of fenofibrate to the micrometer and nanometer range has led to a subsequent raise of oral bioavailability resulting in a reduction of the fenofibrate dosage. This positive effect of decreased particle sizes on bioavailability has been reported for several poorly water-soluble drugs [91,92] and has been attributed to an improved dissolution performance. Micro- and nanosizing have become generally accepted methods to improve the *in vivo* performance of poorly water-soluble drugs. In order to ensure the successful micronization, it has to be borne in mind that the interplay between active substance and formulation variables and not the pure drug alone, determines the optimal drug formulation.

For example, fine particles tend to agglomerate and aggregate due to their higher surface energy which commonly leads to lower dissolution rate and may result in lower bioavailability. Wettability and subsequent dissolution of the drug particles have been improved through the addition of surfactants, as reported by Perrut et al. [93] and Heng et al. [94]. Langguth et al. [95] showed in a rat study with different spironolactone formulations of different particle size, that the

choice of surfactant in the formulations had a greater impact on bioavailability enhancement than the degree of micronization.

An interesting finding in terms of adverse interactions of formulation components with the emulsifying systems of biorelevant media has been noticed by Abdalla et al. [96]. They examined a self-emulsifying drug delivery system which belongs to the field of lipid-based formulations providing a further strategy to optimize the oral delivery of poorly water-soluble drugs. The review of Porter et al. [97] gives an overview of this topic. Abdalla et al. investigated their formulation containing progesterone with respect to equilibrium solubility in FaSSIF and FeSSIF. The authors detected that *in vitro* digestion of the formulation induced a decrease in solubilization capacity which may be driven by adverse interactions between digestion products (e.g., hydroxystearate, middle chain fatty acids) and solubilizing structures. Abdalla et al., however, did not investigate the behavior of these solubilizing structures in the biorelevant media further.

By reviewing the literature one realizes that the colloidal structures in FaSSIF and FeSSIF and their modified versions have been barely investigated. Among those, DLS [33] and cryo-TEM [32] measurements are the most frequent. Only one publication was found characterizing biorelevant media by means of small-angle X-ray scattering [31].

1.5.3 Possible adjustments of dissolution and permeation methods

Although excipients (e.g., surfactants) are widely used in the pharmaceutical industry in terms of improving the bioavailability of poorly water soluble drugs, little is known about the effective excipient concentrations in the intestine and therefore their actual contribution to dissolution enhancement. Dissolution studies are generally conducted in 900 or 1000 ml dissolution medium, not representing the correct *in vivo* volumes (see section 1.1.2.3). It is focused rather on supplying sink conditions than on simulating the *in vivo* dissolution conditions which may at least partly include non-sink conditions for poorly water-soluble compounds. *In vitro* dissolution studies under physiologically relevant conditions (e.g., less dissolution volume) would emphasize the differences between the formulations and unveil their potential to improve the dissolution *in vivo*.

Appropriate physiological conditions should be met equally in permeation studies with drug formulations (see also section 1.2.3). Therefore, a deeper scientific insight into the potential of excipients to influence the *in vivo* permeation across the intestinal epithelium may be provided, resulting finally in a differentiation between drug formulations.

1.6 Aims of the thesis

According to the aspects discussed in the introduction the main aims of the thesis were to simulate more closely the major *in vivo* parameters of oral drug absorption, namely dissolution and permeation, and in this manner improve the ability to predict the *in vivo* performance from the properties of fenofibrate immediate release (IR) formulations. Moreover, several *in vitro* methods were conducted to get a deeper scientific insight into the contribution of the surfactants used in these formulations to the *in vivo* performance.

The goals of this thesis were:

- Validation of the D/P system as method of choice concerning a possible correlation between *in vitro* data and *in vivo* results from rats applying different fenofibrate formulations (including a self-developed lipid microparticle formulation) with biorelevant media simulating the fasted and fed state (chapter 2)

- Development of an IVIVC for different fenofibrate IR tablets in terms of C_{max} values observed from *in vivo* human studies by adjustment of *in vitro* solubility and permeation studies to physiologically relevant conditions (chapters 3 and 4)

- Investigation of the potential contribution of the surfactants used in these formulations to *in vivo* dissolution and permeation of fenofibrate by using the previously adjusted *in vitro* methods (chapters 3 and 4)

- Characterization of colloidal structures in biorelevant media with respect to their interaction with the surfactants used in these fenofibrate formulations (chapters 4 and 5)

- Investigation of the effect of dilution on structural particle changes during $FeSSIF_{mod6.5}$-to-$FaSSIF_{mod}$ transition (chapter 5)

2. IVIVC in oral absorption for fenofibrate immediate release tablets using a dissolution/permeation system

(Running chapter head: IVIVC for IR tablets using a dissolution/permeation system)

Philipp Buch[1], Peter Langguth[1], Makoto Kataoka[2], Shinji Yamashita[2]

[1]Department of Biopharmaceutics and Pharmaceutical Technology, Johannes Gutenberg-University, Staudingerweg 5, 55099 Mainz, Germany

[2]Faculty of Pharmaceutical Sciences, Setsunan University, Nagatoge-cho 45-1, Hirakata, Osaka 573-0101, Japan

J Pharm Sci. 2009; 98(6): 2001-2009

2.1 Abstract

The usefulness of the dissolution/permeation (D/P) system to predict the *in vivo* performance of solid dosage forms containing the poorly soluble drug, fenofibrate, was studied. Biorelevant dissolution media simulating the fasted and fed state conditions of the human gastrointestinal tract were used in order to simulate the effect of food on the absorption of fenofibrate. Moreover, the results obtained from the D/P system were correlated with pharmacokinetic parameters obtained following *in vivo* studies in rats. The *in vitro* parameter (fraction permeated in the D/P system) reflected well the *in vivo* performance in rats in terms of AUC and C_{max} of fenofibric acid. This study thus demonstrates the potential of the D/P system as valuable tool for absorption screening of dosage forms for poorly soluble drugs.

2.2 Introduction

The number of lipophilic active substances which exhibit poor water solubility is still increasing in pharmaceutical companies. Poor water solubility is a serious problem which frequently results in unpredictable *in vivo* performance in oral absorption, especially when the formulation is given in the fasted state.

It has always been a challenge for formulation scientists to overcome the issue of low bioavailability. In that respect, a screening system which can predict or at least rank order *in vivo* performance would be time- and cost-saving. Determination of *in vitro* behavior of solid oral dosage forms today is mainly based on *in vitro* dissolution testing whereas permeability screening is done by cell monolayer permeation assays (e.g., Caco-2). Although these methods have been used for years they still exhibit shortcomings because during permeability studies only pure compounds are tested. Neither dosage form excipients nor physiological solubilizing substances are applied which could alter the permeability of the drug. Furthermore, the high drug concentrations in the donor solution are far from mimicking clinical doses in that they tend to be constant over time in contrast to the *in vivo* situation. Also *in vitro* dissolution tests may not reflect the *in vivo* situation in GI tract for drug dissolution.

Therefore the necessary step was to create an *in vitro* system to determine a drug's permeability and solubility simultaneously under physiological conditions for prediction of drug absorption capacity *in vivo*. During the development of new chemical entities or new formulations of lipophilic drugs an *in vitro* screening method for predicting *in vivo* performance would be helpful. To that effect few systems have been developed over the last decade. A continuous dissolution/Caco-2 permeation system was first evolved by Ginski et al. [55]. Kobayashi et al. [57], and Sugawara et al. [58] focused on simulating the pH changes in the GI tract, whereas Kataoka et al. [56] invented the D/P system to which they applied an amount of drug corresponding to the clinical dose. Motz et al. [61,98] used a flow through setup to determine dissolution and permeation concomitantly. All these systems are based on a Caco-2 cell monolayer to determine the drug's permeability. Most *in vitro* systems are equipped with a pump to deliver the dissolved drug from the dissolution chamber to the permeation module. The application of a pump complicates the handling because different flow rates alter the drug's permeated fraction. Pressure variations caused by pulsating pumps may damage the pressure sensitive Caco-2 cell monolayer.

The equipment by Yamashita and co-workers consists of two half-chambers (one for dissolution, one as a receiver compartment) with a Caco-2 monolayer mounted in between. By using fasted and fed state simulating intestinal fluids ($FaSSIF_{mod}$ and $FeSSIF_{mod6.5}$) as apical solutions, the effect of food intake on the oral absorption of poorly water-soluble drugs has been studied

[19,48,99,100]. Furthermore, sticking of lipophilic drug to the tubing material is a frequently observed complication. This phenomenon is often seen with compounds of BCS class II, for which the presence of food may lead to an increase in their solubility, dissolution and bioavailability [17].

We tested several formulations with the D/P system and used $FaSSIF_{mod}$ and $FeSSIF_{mod6.5}$ as apical media. All formulations contained fenofibrate. Fenofibrate can be classified as BCS class II drug which exhibits a pronounced food effect on its bioavailability.

The main purpose of the present study was to validate the D/P system in terms of a possible correlation between *in vitro* results and *in vivo* data from rats. We expected the fasted state to be most discriminative for the compositions as fenofibrate shows a food effect and is only poorly absorbed in the fasted state [81]. Therefore, attempts were made to correlate the *in vitro* data obtained using $FaSSIF_{mod}$ as the apical medium with *in vivo* data from fasted rats. A further objective was to evaluate whether the D/P system operated under fed and fasted dissolution conditions would predict changes in the food effect depending on the formulation employed.

2.3 Materials and methods

Materials

The Caco-2 cell line was purchased from American Type Culture Collection (Rockville, MD) at passage 17. Dulbecco's modified Eagle medium (D-MEM) was purchased from Sigma-Aldrich (St. Louis, MO). Nonessential amino acids (NEAA), fetal bovine serum (FBS), $_{L}$-glutamate, trypsin (0.25%)-EDTA (1 mM) and antibiotic-antimycotic mixture (10,000 U/ml penicillin G, 10,000 mg/ml streptomycin sulfate and 25 mg/ml amphotericin B in 0.85% saline) were purchased from Gibco Laboratories (Lenexa, KS). Egg-phosphatidylcholine (lecithin) was purchased from NOF Corp. (Tokyo, Japan). Sodium taurocholate (NaTC) and BSA were purchased from WAKO Pure Chemical Industries, Ltd. (Osaka, Japan). All other chemicals were of analytical reagent grade.

Formulations employed

Formulation A: This formulation was based on the solid dispersion principle (MeltDose®-technique) and was used as delivered by the manufacturer [101]. It contains fenofibrate dispersed in a hydrophilic polymer and compressed to tablets following mixing with magnesium stearate, Avicel PH 200 and Polyplasdone XL.

Formulation B: This formulation is a fenofibrate nanoparticulate tablet formulation (TriCor®), containing fenofibrate, hypromellose 2910, docusate sodium, sucrose, sodium dodecyl sulfate (SDS), lactose monohydrate, silicified microcrystalline cellulose, crospovidone, magnesium stearate, polyvinyl alcohol, titanium dioxide, talc, soybean lecithin and xanthan gum. It was used as obtained.

Formulation C: This formulation contains micronized fenofibrate capsules (HEXAL® 160 mg Hartkapseln) containing also dimethicone-emulsion, gelatin, hypromellose, cornstarch, SDS, simethicone-emulsion, sucrose, talc, iron oxides and titanium dioxide.

Formulation D: Consists of lipid microparticles which were produced by a combination of atomizing and congealing [102-104]. A UP200S ultrasonic processor (Hielscher, Teltow, Germany) was used in a temperature controlled environment (4°C). The ultrasonic processor was placed upside down so that the sonotrode was on top. Softisan 138 and fenofibrate (15% w/w) were melted at 90°C under stirring [8,105-110]. Thereafter, the melt was pumped (feeding rate 2.7 ml/min) through a jacketed pipe at 80°C onto the oscillating top of the sonotrode. The top of the metal pipe was equipped with a metal ring which slightly touches the sonotrode's surface. When the liquid touched the sonotrode, the melt was atomized by ultrasound energy into small droplets, which subsequently solidify upon cooling. The metal ring which protrudes over the top of the sonotrode's surface forced the small droplets to fall to the ground and not to

be sprayed onto the pipe or any other part of the instrument. Eventually, the particles were sieved into a size fraction of 100–160 µm and stored at 4°C.

Formulation E: Consisted of micronized fenofibrate (5 µm average particle size) which was purchased from Labochim (Milan, Italy).

Formulation F: Consisted of bulk fenofibrate (28 µm average particle size) which was purchased from Labochim.

In vitro studies

Preparation of Caco-2 monolayer

Caco-2 cells were cultured in humidified air with 5% CO_2 at 37°C in culture flasks (Nippon Becton Dickinson Co., Ltd., Tokyo, Japan) using D-MEM supplemented with 10% FBS, 1% L-glutamate, 1% NEAA and 5% antibiotic-antimycotic solution. Cells were harvested with trypsin-EDTA and seeded at a density of 3 x 10^5 cells/filter onto polycarbonate filters (0.3 µm pores, 4.20 cm^2 growth area) inside a cell culture insert (Nippon Becton Dickinson Co., Ltd.). Culture medium (1.5 ml in the insert and 2.6 ml in the well) was changed every 48 h for the first 6 days and every 24 h thereafter. Cells were used for the experiments between days 18 and 21 postseeding.

D/P system

For these studies the previously described D/P system was used [56]. In short, the Caco-2 monolayer is fixed between two chambers, the donor and the receiver chamber. In the donor chamber the tested formulation dissolves, the dissolved drug permeates across the Caco-2 monolayer, and from the receiver chamber samples are taken for determining the concentration change over time. As master solution HBSS including 19.45 mM glucose and 10 mM HEPES was used (transport medium, TM).

$FaSSIF_{mod}$ and $FeSSIF_{mod6.5}$ were based on TM supplemented with NaTC 3 mM and lecithin 0.75 mM or five times higher concentrations of both substances, respectively [27,47]. The donor chambers contained 8 ml $FaSSIF_{mod}$ or $FeSSIF_{mod6.5}$, both adjusted to pH 6.5. 5.5 ml of TM containing 4.5% w/v BSA (pH 7.4) was used as receiver medium in each receiver chamber [111]. All the solutions and chambers were preheated to 37°C and maintained at that temperature. The solutions in both chambers were stirred at 200 rpm with magnetic stirrers (8 mm x 2 mm in size).

Permeability studies in the D/P system

Before the Caco-2 monolayer was fixed between the chambers of the D/P system, it was incubated for 20 min in the culture well with TM (pH 6.5) for the apical and TM containing 4.5% w/v BSA (pH 7.4) for the receiver side. After positioning the Caco-2 monolayer with support filter in the D/P system $FaSSIF_{mod}$ or $FeSSIF_{mod6.5}$ were filled in the apical chamber and receiver medium was filled in the receiver chamber. Drug products or pure drugs were added to the apical side as powder. The fenofibrate dose tested in vitro amounted to 1.45 mg, which corresponds to 1/100 of the clinically taken dose of 145 mg. Samples (200 µl) from the receiver solution were taken over 2 h and replaced by fresh medium. For HPLC analysis only the deproteinized supernatants (1.3 ml) of the samples containing BSA were used which were obtained by adding 1.4 ml of methanol followed by centrifugation (15,000 rpm, 20 min, 20°C). After all samples from the receiver compartment were gathered, apical solution was taken and filtered through cellulose acetate filter (pore size, 0.2 µm) for determining the final concentration of the dissolved drug. Fenofibrate and fenofibric acid concentrations were both determined in all samples as Caco-2 cells metabolized only a fraction of fenofibrate.

The transepithelial electrical resistance (TEER) values of the cell monolayers were monitored before and after the experiments by Millicell-ERS (MILLIPORE, Billerica, MA). The experiment's conditions had no effect on the integrity of the cell layers, as TEER-values did not decrease significantly and were higher than 300 Ω cm^2.

To estimate the *in vivo* absorption the *in vitro* permeated fraction of both fenofibrate and fenofibric acid (% of dose/2 h) in the D/P system was used in the following equation:

(2.1) $$\text{Predicted absorption}\,[\%] = \frac{\text{Abs}_{max}\ \text{x}\ \text{PA}^{\gamma}}{\text{PA}_{50}^{\gamma} + \text{PA}^{\gamma}}$$

Abs_{max} is the maximum absorption (defined as 100%), PA is the cumulative in vitro permeated fraction in the D/P system (% of dose/2 h), PA_{50} is the permeated fraction, which corresponds to 50% of the absorption *in vivo*, and γ is a Hill coefficient. PA_{50} and γ were obtained by a fitting procedure from the permeated fraction (PA) of drugs in the D/P system and their oral absorption in human by using MULTI program developed by Yamaoka et al. [112] The values for PA_{50} and γ were 0.334 ± 0.096 (SD) and 0.883 ± 0.178 in the fasted state, and 0.121 ± 0.021 and 1.334 ± 0.198 in the fed state, respectively.

Analysis of in *vitro* samples by HPLC

All samples were analyzed using a reversed-phase HPLC system (LC-10A, Shimadzu Co., Kyoto, Japan) with a binary pump, a vacuum degasser, an autosampler, a column oven and a variable wavelength ultraviolet detector (SPD-10A, Shimadzu Co.). The mobile phase was composed of 50 mM phosphate buffer (pH 2.5) (A) and acetonitrile (B) and the flow rate was 1.0 ml/min. All drugs were trapped and eluted from the analytical column (J'sphere ODS-H80 75 x 4.6 mm ID, YMC, Kyoto, Japan) held at 40°C using the following gradient conditions: 0–2.0 min, 50% A; 2.0–3.0 min, 50–30% A; 3.0–10.0 min, 30% A; and 10.0–13.0 min, 50% A. Fenofibrate and fenofibric acid were detected at a wavelength of 288 nm.

In vivo studies

Animals

All animal experiments were approved by the Ethical Review Committee of Setsunan University. Wistar male rats weighing 250 g were deprived of food with free access to water for 18 h before the experiments. Before the formulations were administered to the rats they were pulverized in a mortar if necessary and suspended in 0.5% methyl cellulose aqueous solution. Each rat was administered a volume of 1 ml containing fenofibrate in a concentration which corresponds to the clinical dose (145 mg/70 kg). Each formulation was administered to three rats.

At 0.5, 1, 2, 3, 4, 8, 24 h after administration, the rats were anesthetized using ether to collect blood samples (0.6 ml) from the jugular vein which was visualized through an incision on the shoulder. Blood samples were centrifuged and plasma was frozen at -70°C for subsequent measurement of fenofibric acid.

Analysis of plasma samples

All plasma samples were pretreated with 1.4 ml acetonitrile and centrifugation (15,000 rpm, 20 min and 20°C) and the deproteinized supernatant (1.3 ml) was used to determine the amount of fenofibric acid. All samples were analyzed with a reversed-phase HPLC system (LC-VP, Shimadzu Co.) consisting of a binary pump, a vacuum degasser, an autosampler, a column oven and a mass-spectrometer equipped with the electrospray ionization interface (LCMS-2010A, Shimadzu Co.). The mobile phase was composed of 0.1% formic acid in water (A) and acetonitrile (B) and the flow rate was 0.5 ml/min. Fenofibric acid was trapped and eluted from the analytical column (J'sphere ODS-H80 75 x 4.6 mm ID, YMC) held at 40°C using the following gradient conditions: 0–1.0 min, 95% A; 1.0–1.5 min, 95–5% A; 1.5–4.0 min, 5% A; and 4.0–6.0 min, 95% A. Selected ion monitoring was used for detection of protonated molecules of fenofibric acid (m/z 319.00). Data processing was carried out using LCMS Solution software (Shimadzu Co.).

Standard noncompartmental pharmacokinetic parameters were calculated using the pharmacokinetic program Topfit [113].

2.4 Results and discussion

***In vitro* results**

The fraction dissolved in the donor medium is given in Table 2.1. The rank order of the fractions of dose dissolved from the tested formulations was as follows: formulation B > formulation A > formulation C > formulation D > formulation E > formulation F for $FaSSIF_{mod}$ as well as for $FeSSIF_{mod6.5}$ [84,89]. In the case of dissolution in $FaSSIF_{mod}$, formulations A and B exhibited equal results. In $FeSSIF_{mod6.5}$ more fenofibrate was dissolved after 2 h from formulation B compared to A. This could be due to the inability of the filter materials to separate nanoscopic material from dissolved material.

Table 2.1. Fraction of fenofibrate dose dissolved after 2 h (mean ± SD, n ≥ 3) in the apical chamber of the D/P system.

Formulation	$FaSSIF_{mod}$ [%]	$FeSSIF_{mod6.5}$ [%]
A	7.49 ± 0.46	17.92 ± 0.76
B	7.67 ± 0.52	25.47 ± 0.87
C	5.33 ± 0.36	11.76 ± 0.94
D	1.54 ± 0.35	8.67 ± 3.85
E	0.74 ± 0.07	5.22 ± 1.23
F	0.71 ± 0.22	4.65 ± 0.72

For formulation B fenofibrate powder is downsized by wet-milling [114]. In the final tablet the particle size is in the nanometer range, such that some of the particles may pass through the cellulose acetate filter with a pore size of 0.2 µm following tablet disintegration. This could explain the equal or in the case of $FeSSIF_{mod6.5}$ better dissolution results for formulation B compared to A, and thus, most likely may contribute to an overestimation of the true fraction dissolved of formulation B in the apical chamber of the D/P system. These results also clearly demonstrate the advantage of the D/P system in which the oral absorption of drugs from various formulations can be evaluated not only from the dissolution but also from the permeation process without the necessity of having to separate colloidal particles. By taking the solubility of fenofibrate into consideration (14.3 ± 1.05 µg/ml in $FaSSIF_{mod}$ and 36.79 ± 0.39 mg/ml in $FeSSIF_{mod6.5}$, respectively, at 37°C) it becomes obvious that all experiments were run under non-sink conditions [115].

The permeation profiles of fenofibrate from all drug products and pure powders were determined in the D/P system using $FaSSIF_{mod}$ and $FeSSIF_{mod6.5}$ as apical media (Figure 2.1.a and b). The food effect of fenofibrate [116] which is seen in humans was particularly visible in the permeation profiles of the pure powders obtained by the D/P system.

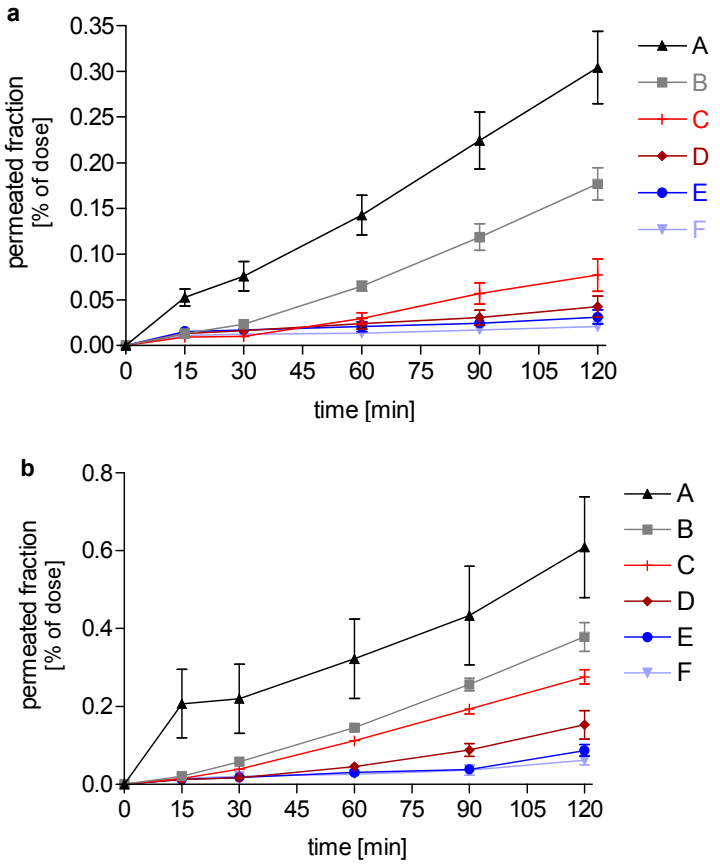

Figure 2.1. Effect of different formulations on permeation of fenofibrate in the D/P system with $FaSSIF_{mod}$ (a) and $FeSSIF_{mod6.5}$ (b) as apical medium. Each data point is the mean ± SEM of three to six independent experiments.

The calculated absorptions of fenofibrate from tested formulations are summarized in Table 2.2.

Table 2.2. Fraction of fenofibrate dose permeated after 2 h (mean, n ≥ 3) into the receiver chamber of the D/P system, the predicted absorptions and the ratio between the predicted absorptions, all based on the data obtained from the D/P system using $FaSSIF_{mod}$ and $FeSSIF_{mod6.5}$.

	Permeated fraction [% of dose/2h]		Predicted absorption [% of dose]		
Formulation	$FaSSIF_{mod}$	$FeSSIF_{mod6.5}$	$FaSSIF_{mod}$	$FeSSIF_{mod6.5}$	Ratio ($FeSSIF_{mod6.5}/FaSSIF_{mod}$)
A	0.304	0.625	47.94	88.95	1.86
B	0.177	0.379	36.32	82.09	2.26
C	0.077	0.276	21.5	75	3.49
D	0.043	0.153	14.64	57.71	3.94
E	0.031	0.087	10.97	39.29	3.58
F	0.02	0.062	7.82	29.22	3.74

Formulations E and F resulted in > 3 times higher absorption when tested in $FeSSIF_{mod6.5}$ compared to $FaSSIF_{mod}$. This is in accordance with pharmacokinetic data published previously (the extent of absorption varies from 30–50% to 60–90% when the drug is taken in the fasting state or when it is given after a meal, respectively) [81].

The smaller the ratio between the predicted absorptions using $FaSSIF_{mod}$ and $FeSSIF_{mod6.5}$, the more effective should the formulation reduce the food effect. The performances of formulations B and A showed that these formulations could diminish this ratio significantly, as seen in Table 2.2. As expected, all formulations revealed higher calculated absorption when $FeSSIF_{mod6.5}$ was used as apical solution in the D/P system. With formulation A the best results not only in minimizing the ratio but also in increasing the permeated fraction of fenofibrate and fenofibric acid in $FaSSIF_{mod}$ (Figure 2.1.a) and $FeSSIF_{mod6.5}$ (Figure 2.1.b) were achieved. Both formulations D and C performed as poor as the pure fenofibrate powders concerning the goal of reducing the food effect, but they raised the calculated absorption compared to the pure powders. The rank order of the drug formulations with respect to permeated fraction of fenofibrate and fenofibric acid followed almost completely the rank order in terms of fraction dissolved in the donor medium except for the A/B pair (explanation see above).

Pharmacokinetics in plasma

The plasma concentrations versus time profiles of fenofibric acid following oral administration are shown in Figure 2.2. The pharmacokinetic parameters following noncompartmental analysis are listed in Table 2.3. In agreement with the present in vitro results, formulation A presented the best intestinal absorption enhancement. The rank order of the formulations based on the $AUC_{0-24\ h}$ values was formulation A > formulation B > formulation C > formulation D > formulation F > formulation E. Except for the pure powders this reflects the results obtained with the D/P system. Formulation F had a higher $AUC_{0-24\ h}$ value than formulation E. The formulations were fed to the rats as a suspension. The higher surface energy of fine particles and subsequent stronger van der Waal attraction forces between nonpolar molecules could lead to aggregation and agglomeration during the process of homogenization. This phenomenon of insufficient wettability can explain a slower dissolution rate leading to lower bioavailability of formulation E [93,117-119]. Formulation A gave the highest peak concentration (C_{max}) for the fenofibric acid in rats. That is in accordance with the D/P system's permeation profile obtained from formulation A. In $FaSSIF_{mod}$ the sum of permeated fenofibrate and fenofibric acid was already after 15 min significantly higher ($p < 0.05$) for formulation A compared to the permeation values of the other formulations.

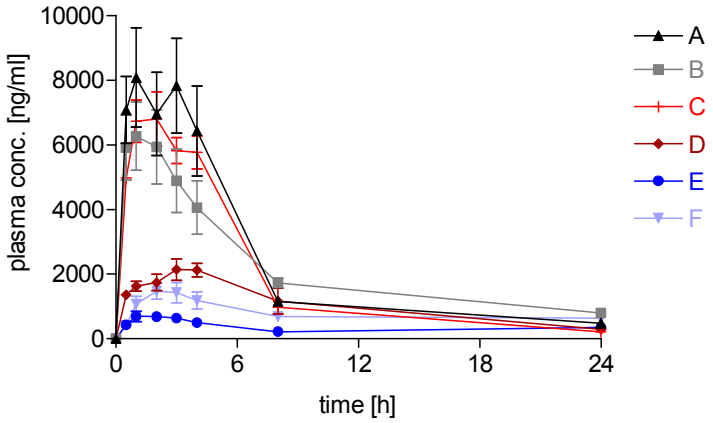

Figure 2.2. Average (± SEM) fenofibric acid plasma concentrations in rats (n = 3) after oral administration of different fenofibrate formulations.

Table 2.3. Mean pharmacokinetic parameters (± SD, n = 3) following oral administration of fenofibrate formulations at equal doses of 2.1 mg/kg.

Formulation	C_{max} [ng/ml]	t_{max} [h]	$AUC_{0\text{-}24\ h}$ [ng x h/ml]
A	9635.3 ± 2829.87	2.33 ± 1.15	64,135.45 ± 15,613.33
B	6265.64 ± 1823.49	1	52,224.76 ± 10,958.09
C	7179.1 ± 1004.52	2.33 ± 1.53	45,892.51 ± 4306.44
D	2226.47 ± 424.47	3.33 ± 0.58	24,997.64 ± 9493.6
E	737.86 ± 177.29	1.67 ± 1.15	8109.88 ± 2333.59
F	1496.7 ± 472.49	2.33 ± 0.58	18,673.64 ± 3162.45

In vitro/*in vivo* correlation

Formulation A showed the best results both based on calculated absorption and *in vivo* $AUC_{0-24\ h}$ values in rats, respectively. Comparing the results obtained in the D/P system using $FaSSIF_{mod}$ with the *in vivo* results in fasted rats (calculated absorptions vs. $AUC_{0-24\ h}$ values illustrated in Figure 2.3.) the ranking of the drug products were the same.

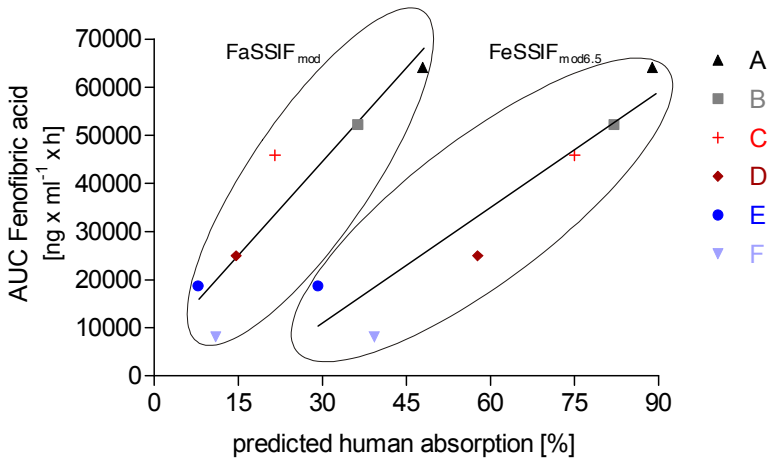

Figure 2.3. Plot of predicted absorptions of all fenofibrate formulations calculated from D/P data obtained with $FaSSIF_{mod}$ and $FeSSIF_{mod6.5}$ versus $AUC_{0\text{-}24\ h}$ values for all fenofibrate formulations.

However, the spread of the predicted extent of absorption from the D/P system (14.64–47.94% in $FaSSIF_{mod}$) for the fenofibrate drug products tested was much larger than the spread of the exposure data *in vivo* (38.98–100%, relative to formulation A). This could be due to the fact that the rat has no gall bladder and thus secrets bile constantly [2,82,120-123]. Zwart et al. [124] compared bile flow and total bile salt rate throughout the day in human and in rat (hepatic bile flow: in humans 2–22 ml/day/kg, in rats 48–92 ml/day/kg). Following their collected data the rat might not be the right model to predict absorption in the fasted state since the rat releases bile independent of food intake and in a higher amount which makes the fasted situation in rat and in human incomparable. This could be an explanation of the decreased differences between the drug products in the fasted rat compared to the differences in the *in vitro* data obtained with $FaSSIF_{mod}$ in the present study. In Figure 2.3., correlation between the calculated absorptions using $FeSSIF_{mod6.5}$ and $AUC_{0-24\ h}$ values in vivo in fasted rats was also incorporated. These results might indicate that, from the point of view of dissolution of poorly soluble drugs, GI tract conditions in fasted rats are close to that in human under fed state rather than under fasted state. This would be the next issue for our research to investigate the species differences in the food effect on oral drug absorption.

2.5 Conclusion

In conclusion, it appears that the D/P system in combination with biorelevant media can be used to predict relevant biopharmaceutic properties of different fenofibrate formulations in rats. Assays in the D/P system with modified FaSSIF and FeSSIF should be useful in formulation development, especially for lipophilic drugs which are known to show a positive food effect.

Further work will be necessary in order to challenge the D/P system for its predictability of formulation performance in humans.

2.6 Acknowledgments

P.B. received a scholarship from the German Academic Exchange Service (DAAD) during his stay in Hirakata. The authors thank Dr. Per Holm (LifeCycle Pharma) and Dr. Dieter Scherer (ApisPharma) for constructive comments and for the supply of the RD 24 formulation.

3. IVIVR in oral absorption for fenofibrate immediate release tablets using dissolution and dissolution permeation methods

(Running chapter head: IVIVR for IR tablets using dissolution and dissolution permeation methods)

Philipp Buch[1], Per Holm[2], Jesper Qvist Thomassen[2], Dieter Scherer[3], Makoto Kataoka[4], Shinji. Yamashita[4], Peter Langguth[1]

[1]Department of Biopharmaceutics and Pharmaceutical Technology, Johannes Gutenberg-University, Staudingerweg 5, 55099 Mainz, Germany

[2]LifeCycle Pharma A/S, Kogle Allé 4, 2970 Hørsholm, Denmark

[3]ApisPharma, Bahnhofstraße 6, 4242 Laufen, Switzerland

[4]Faculty of Pharmaceutical Sciences, Setsunan University, Nagatoge-cho 45-1, Hirakata, Osaka 573-0101, Japan

Pharmazie. (in press)

3.1 Abstract

In a previous study it has been demonstrated that the D/P system can discriminate between different IR fenofibrate formulations. The fractions permeated were correlated with fenofibrate's *in vivo* exposure in rats following p.o. administration.

In the present study more detailed investigations are presented using data from six fenofibrate tablets tested *in vivo* in humans. In these pharmacokinetic studies no significant differences between formulations in AUC but in C_{max} were found. Differences between the C_{max} values were not explained by the dissolution characteristics of the tablets but were rationalized on the basis of micellar entrapment and diminished mobility of the active ingredient by surfactants in the formulations. This was demonstrated by a permeation system using dialysis membranes. Thus a permeation step in addition to dissolution measurement may significantly improve the establishment of an IVIV relationship.

3.2 Introduction

Hydrophobicity and poor water solubility of new chemical entities represent an increasing problem in pharmaceutical development. As *in vivo* studies are time- and cost-intensive, a number of approaches simulating the *in vivo* situation for dosage forms for poorly soluble drugs have been introduced. For example, biorelevant media including FaSSIF and FeSSIF, representing the fasted and the fed state in the upper jejunum, respectively, were proposed by Galia et al. [26]. Dissolution studies conducted with these media better predicted the *in vivo* performance of formulations containing poorly soluble drugs compared to the use of compendial media [125].

Dissolution is not the only determining parameter for absorption of a compound. Following its dissolution the dissolved drug has to permeate biological membranes to become absorbed. To simulate this second step *in vitro* permeation methods were established.

The prevailed *in vitro* permeability assay in pharmaceutical research is based on cellular models, such as Caco-2 [39,40] and MDCK [126]. These permeation screening tools are used in early stages of drug discovery, but have limited applicability for testing of pharmaceutical formulations and evaluation of the effects of various excipients on permeability.

A combined dissolution/permeation step was first introduced by Ginski et al. [55] who evolved a continuous dissolution/Caco-2 permeation system which allowed the simultaneous determination of a drug's permeability and solubility.

Kataoka et al. [56] introduced the D/P system to determine solubility and permeation under physiological conditions for prediction of drug absorption capacity *in vivo*. They used biorelevant media as dissolution medium to evaluate the effect of food intake on the oral absorption of poorly water-soluble drugs [27]. The original FaSSIF and FeSSIF could not be used as dissolution media because their components would destroy the integrity of the cell culture monolayer. Therefore, they applied NaTC and lecithin as physiological solubilizing substances, using the same concentrations as in FaSSIF and FeSSIF. Furthermore HBSS was used as cell culture medium base for their biorelevant media, $FaSSIF_{mod}$ and $FeSSIF_{mod6.5}$. With this D/P system the fraction of fenofibrate permeated was correlated with its *in vivo* exposure in rats [127].

In the present study six IR fenofibrate tablet formulations were tested *in vivo* in humans. Fenofibrate belongs to the class of poorly soluble but highly permeable drugs [85]. Bioequivalence with a reference product (formulation B) in fasted-state conditions should be demonstrated in these randomized crossover studies. We tried to correlate these *in vivo* data with data from several *in vitro* methods, in order to predict their *in vivo* performance. As *in vivo* studies were conducted in the fasted state, attempts were made to correlate these data with

results obtained from the D/P system using $FaSSIF_{mod}$ as the apical medium. Besides the D/P system, dissolution studies of the fenofibrate tablets were evaluated and a permeation system was introduced to predict the *in vivo* performance in humans.

3.3 Materials and methods

Materials

The Caco-2 cell line was purchased from American Type Culture Collection at passage 17. D-MEM was purchased from Sigma-Aldrich. NEAA, FBS, L-glutamate, trypsin (0.25%)-EDTA (1 mM) and antibiotic-antimycotic mixture (10,000 U/ml penicillin G, 10,000 µg/ml streptomycin sulfate and 25 µg/ml amphotericin B in 0.85% saline) were purchased from Gibco Laboratories. Fenofibrate was purchased from Labochim (Milan, Italy). TriCor® (formulation B) was obtained from the manufacturer (Abbott Laboratories, Chicago, IL). RD 24, RD 25, RD 23, RD 22 and RD 18 were kindly provided by LifeCycle Pharma (Hørsholm, Denmark). Lecithin was purchased from NOF Corp. NaTC was kindly donated by Prodotti Chimici e Alimentari S.p.A. (Basaluzzo, Italy) via their German agent Alfred E. Tiefenbacher GmbH & Co. KG (Hamburg, Germany). BSA was purchased from WAKO Pure Chemical Industries, Ltd. All other chemicals were of analytical reagent grade.

Formulations employed

The RD formulations were based on the solid dispersion principle (MeltDose®-technique) and were used as delivered by the manufacturer [101]. RD 22 (formulation I) contains fenofibrate dispersed in a hydrophilic polymer and compressed to tablets following mixing with magnesium stearate. RD 24 (formulation A), RD 25 (formulation G), RD 23 (formulation H) and RD 18 (formulation J) additionally contain Avicel PH 200 and Polyplasdone XL as binder and disintegrant, respectively.

Formulation A contains a surfactant from the class of poloxamers (S1). Formulations H, I and J contain besides SDS a poloxamer (S2) which is different to the one employed in formulation A. S2 and a surfactant from the class of polyethoxylated castor oils (S3) are used as emulsifying agents in formulation G.

Formulation B: This formulation comprises fenofibrate particles in the nanometer range (< 200 nm) downsized by wet-milling [128,129]. The tablet formulation additionally contains hypromellose 2910, docusate sodium, sucrose, SDS, lactose monohydrate, silicified microcrystalline cellulose, crospovidone, magnesium stearate, polyvinyl alcohol, titanium dioxide, talc, soybean lecithin and xanthan gum. It was used as received.

In vitro studies

Preparation of Caco-2 monolayer

Caco-2 cells were cultured in humidified air with 5% CO_2 at 37°C in culture flasks (Nippon Becton Dickinson Co., Ltd.) using D-MEM supplemented with 10% FBS, 1% $_L$-glutamate, 1% NEAA and 5% antibiotic-antimycotic solution. Cells were harvested with trypsin-EDTA and seeded at a density of 3 x 10^5 cells/filter onto polycarbonate filters (0.3 µm pores, 4.20 cm^2 growth area) inside a cell culture insert (Nippon Becton Dickinson Co., Ltd.). Culture medium (1.5 ml in the insert and 2.6 ml in the well) was changed every 48 h for the first 6 days and every 24 h thereafter. Cells were used for the experiments between days 18 and 21 postseeding.

D/P system

For these studies the previously described D/P system was used [56]. In short, the Caco-2 monolayer is fixed between two chambers, the donor and the receiver chamber. In the donor chamber the tested formulation dissolves, the dissolved drug permeates across the Caco-2 monolayer, and from the receiver chamber samples are taken for determining the concentration change over time. As master solution HBSS including 19.45 mM glucose and 10 mM HEPES was used (transport medium, TM).

$FaSSIF_{mod}$ was based on TM supplemented with NaTC 3 mM and lecithin 0.75 mM [27,47]. The donor chambers contained 8 ml $FaSSIF_{mod}$, adjusted to pH 6.5. 5.5 ml of TM containing 4.5% w/v BSA (pH 7.4) was used as receiver medium in each receiver chamber [111]. All the solutions and chambers were preheated to 37°C and maintained at that temperature. The solutions in both chambers were stirred at 200 rpm with magnetic stirrers (8 mm x 2 mm in size).

Permeability studies in the D/P system

Before the Caco-2 monolayer was fixed between the chambers of the D/P system, it was incubated for 20 min in the culture well with TM (pH 6.5) for the apical and TM containing 4.5% w/v BSA (pH 7.4) for the receiver side. After positioning the Caco-2 monolayer with support filter in the D/P system $FaSSIF_{mod}$ was filled in the apical chamber and receiver medium was filled in the receiver chamber. Formulations A, B, G, H and J were ground in a mortar and added to the apical side as powder. The fenofibrate dose tested *in vitro* amounted to 1.45 mg, which corresponds to 1/100 of the clinically taken dose of 145 mg. Samples (200 µl) from the receiver solution were taken over 2 h and replaced by fresh medium. For HPLC analysis only the deproteinized supernatants (1.3 ml) of the samples containing BSA were used which were obtained by adding 1.4 ml of methanol followed by centrifugation (15,000 rpm, 20 min, 20°C).

After all samples from the receiver compartment were gathered, apical solution was taken and filtered through cellulose acetate filter (pore size, 0.2 µm) for determining the final concentration of the dissolved drug. Fenofibrate and fenofibric acid concentrations were both determined in all samples as Caco-2 cells metabolized only a fraction of fenofibrate.

The TEER values of the cell monolayers were monitored before and after the experiments by Millicell-ERS (MILLIPORE, Billerica, MA). The experiment's conditions had no effect on the integrity of the cell layers, as TEER-values did not decrease significantly and were higher than 300 Ω cm^2 [57].

To estimate the *in vivo* absorption the *in vitro* permeated fraction of both fenofibrate and fenofibric acid (% of dose/2 h) in the D/P system was used in the following equation:

(3.1) $$\text{Predicted absorption}\,[\%] = \frac{\text{Abs}_{\max} \times \text{PA}^{\gamma}}{\text{PA}_{50}^{\gamma} + \text{PA}^{\gamma}}$$

Abs_{max} is the maximum absorption (defined as 100%), PA is the cumulative *in vitro* permeated fraction in the D/P system (% of dose/2 h), PA_{50} is the permeated fraction, which corresponds to 50% of the absorption *in vivo*, and γ is a Hill coefficient. PA_{50} and γ were obtained by a fitting procedure from the permeated fraction (PA) of drugs in the D/P system and their oral absorption in human [27] by using MULTI program developed by Yamaoka et al. [112]. The values for PA_{50} and γ were 0.334 ± 0.096 (SD) and 0.883 ± 0.178.

Analysis of D/P system samples by HPLC

Samples were analyzed using a reversed-phase HPLC system (LC-10A, Shimadzu Co., Kyoto, Japan) with a binary pump, a vacuum degasser, an autosampler, a column oven and a variable wavelength ultraviolet detector (SPD-10A, Shimadzu Co.). The mobile phase was composed of 50 mM phosphate buffer (pH 2.5) (A) and acetonitrile (B) and the flow rate was 1.0 ml/min. All drugs were trapped and eluted from the analytical column (J'sphere ODS-H80 75 x 4.6 mm ID, YMC, Kyoto, Japan) held at 40°C using the following gradient conditions: 0-2.0 min, 50% A; 2.0-3.0 min, 50%-30% A; 3.0-10.0 min, 30% A; and 10.0-13.0 min, 50% A. Fenofibrate and fenofibric acid were detected at a wavelength of 288 nm.

Dissolution studies

Dissolution studies were performed on a fully calibrated dissolution apparatus using the paddle method at 50 rpm (apparatus: Sotax AT7, Sotax AG, Basel, Switzerland). The degassed dissolution medium consisting of 1.5% SDS in 1000 ml water was maintained at 37 ± 0.5°C. All dissolution studies were performed in triplicate.

Permeation studies

The permeation method using dialysis membranes was carried out using a DIANORM equilibrium dialysis equipment (Bachofer Laboratoriumsgeräte, Reutlingen, Germany). From all surfactants deployed in the tablet formulations (Table 3.1.) four were chosen for these permeation studies. Fenofibrate was added in excess to $FaSSIF_{mod}$ containing different amounts of the four surfactants. The resulting suspensions were shaken over night in an orbital shaker (37°C, 200 rpm). After a centrifugation step (5,000 rpm, 10min, 37°C) the dissolved amount of fenofibrate in the supernatant was analyzed and 4 ml of each solution were placed in the donor chamber of the dialysis cell. The dissolved fenofibrate permeates through the dialysis membrane (neutral cellulose, molecular weight cut-off 10,000 Dalton) to the receiver side, which contained the same volume and the same concentration of the deployed surfactant as the donor solution. After 4 hours the permeated fraction of fenofibrate was analyzed in the receiver chamber.

Table 3.1. Surfactant composition of the tablet formulations. S1 and S2 are surfactants from the class of poloxamers. S3 is a surfactant from the class of polyethoxylated castor oils.

Formulation	Surfactant (1)	Surfactant (2)	Surfactant (2) amount [mg/tablet]
A	S1	-	-
B	Docusate-Na	SDS	10.15
G	S2	S3	n/a
H	S2	SDS	19.32
I	S2	SDS	41.9
J	S2	SDS	40.22

Analysis of permeation samples by HPLC

Quantitative analysis of fenofibrate was carried out using an HPLC pump, a vacuum degasser, automatic sampler, and UV detector from Series 1050, Hewlett Packard (Palo Alto, CA). Data processing was carried out with the software package HPLC Chemstation Rev. A. 03.01 (Hewlett Packard). Samples were separated using a 125 x 4.6 mm LiChrospher 100 RP-18 (end-capped) column (5µm) (MZ Analysentechnik, Mainz, Germany). The mobile phase consisted of 0.1% diethylamine in a water/acetonitrile-mixture (20%/80%) which was adjusted with phosphoric acid to a pH of 4. Fenofibrate was detected at a wavelength of 289 nm.

In vivo studies

Two human studies were conducted with six solid dosage forms, four containing SDS. Bioequivalence with formulation B in fasted conditions should be demonstrated in these randomized crossover studies. The bioavailability studies were performed at Biovail Research Center, Toronto, ON, Canada and were approved by the Ontario Institutional Review Board.

Clinical study 1

Formulation B, formulation I and formulation J

12 healthy non-smoking human volunteers (6 male and 6 female), aged 20 to 73 years (mean 43.4 years), were selected. Each subject received one tablet in a randomized crossover manner. There was a washout period of 10 days between dosing. Tablets were administered at 7:00 AM following an overnight fast (min. 10 hours). No water was permitted from 1.0 hour predose to 1.0 hour postdose, with exception of 240 ml dosing water. Food was withheld for at least 4 hours postdose. At 4.5, 9.5 and 13.5 hours postdose, standardized meals with beverages were provided to the subjects. All meals and beverages were free of alcohol, grapefruit products, xanthine and caffeine and were identical for the three study periods. 21 blood samples (4 ml) were drawn at 0.00 (predose), 0.5, 1.0, 1.5, 2.0, 2.5, 3.0, 3.5, 4.0, 4.5, 5.0, 5.5, 6.0, 8.0, 10.0, 14.0, 24.0, 36.0, 48.0, 72.0, 96.0 hours postdose.

Clinical study 2

Formulation B, formulation A, formulation G and formulation H

20 healthy non-smoking human volunteers (12 male and 8 female), aged 26 to 77 years (mean 47.5 years), were selected. Each subject received one tablet in a randomized crossover manner. The experimental protocol used in this study was the same as described in study 1.

Analysis of plasma samples

Fenofibric acid and its internal standard, naproxen, were extracted from human plasma (0.2 ml), using dipotassium EDTA as an anticoagulant, by solid phase extraction into an organic medium, evaporated under nitrogen and reconstituted in 200.0 µl of mobile phase. An aliquot of this extract was injected into a HPLC system and detected using a UV detector. The analytes were separated by reverse phase chromatography. Evaluation of the assay, using defined acceptance criteria, was carried out by the construction of an eight point calibration curve (excluding zero concentration) covering the range 49.996 ng/ml to 12,798.8 ng/ml for fenofibric acid in human plasma. The slope and intercept of the calibration curves were determined through weighted linear regression analysis ($1/conc^2$). Two calibration curves and duplicate quality control samples (at three concentration levels) were analyzed along with each batch of the study samples. Peak height ratios were used to determine the concentration of the standards, quality control samples, and the unknown study samples from the calibration curves.

3.4 Investigations and results

The plasma concentration versus time profiles of fenofibric acid after single oral doses of 145 mg fenofibrate are shown in Figure 3.1. The pharmacokinetic parameters following noncompartmental analysis are depicted in Table 3.2. The results based on $AUC_{0\text{-inf}}$ values in humans showed no significant differences between the six fenofibrate formulations, since all formulations were within the 80-125% confidence interval (log transformed). Concerning the C_{max} values the rank order of the formulations was as follows: A > B > G > H > I > J. Formulations B, H, I and J contained 10.15, 19.32, 41.9 and 40.22 mg sodium dodecyl sulfate (SDS) per tablet, respectively. Formulations A and G contained different surfactants.

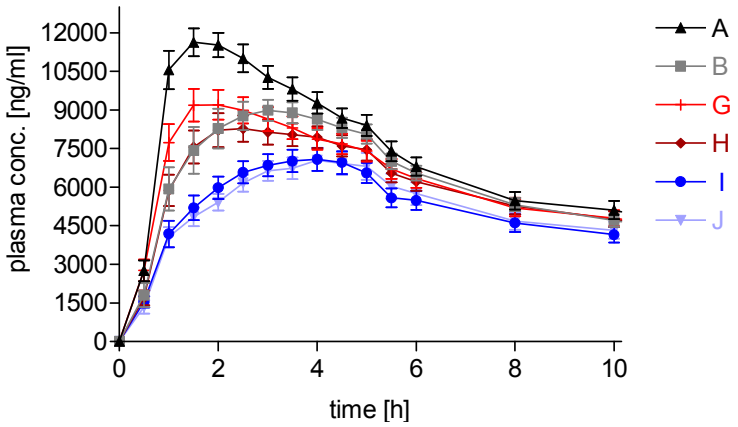

Figure 3.1. Average (± SD) fenofibric acid plasma concentrations in humans (n ≥ 12) after oral administration of different fenofibrate formulations. The data for formulations I and J were standardized to the values for formulation B obtained in clinical study 2. For a better differentiation between the formulations only the first 10 hours of the plasma profiles are shown.

The fraction of fenofibrate dissolved in the donor medium of the D/P system is given in Table 1. By taking the solubility of fenofibrate into consideration (14.3 ± 1.05 µg/ml in $FaSSIF_{mod}$) it becomes obvious that all experiments were run under non-sink conditions. This explains the low fractions of drug which were dissolved over the 2 hour time period. The fenofibrate dissolved from the tested formulations differed only marginally and was not useful to classify the formulations.

Table 3.2. Mean pharmacokinetic parameters (relative to formulation B, n ≥ 12) following oral administration of formulations containing 145 mg fenofibrate. Fraction of fenofibrate dose dissolved after 2 h (mean, n ≥ 3) in the apical chamber of the D/P system. Fraction of fenofibrate dose permeated after 2 h (mean, n ≥ 3) into the receiver chamber of the D/P system and the predicted absorptions, all in *vitro* data based on the results obtained from the D/P system using FaSSIF$_{mod}$.

Formulation	*In vivo* data		*In vitro* data (D/P system)		
	C_{max} [%]	$AUC_{0\text{-inf}}$ [%]	Dissolved fraction [%]	Permeated fraction [%]	Predicted absorption [%]
A	123.4	107.53	7.49	0.304	132.07
B	100	100	7.67	0.177	100
G	95.7	103.93	5.71	0.346	139.94
H	86.33	102.08	6.35	0.32	135.18
I	73.93	99.91	n/a	n/a	n/a
J	72.43	100.11	6.37	0.299	131.05

The results of permeation of fenofibrate from the tablet formulations A, B, G, H and J from the D/P system using FaSSIF$_{mod}$ as apical medium are depicted in Figure 3.2. and, the *in vivo* absorption relative to formulation B was calculated (Table 3.2.). Formulations A, G, H and J performed much better than B and their predicted absorptions were therefore approximately 25% higher than the calculated absorption from formulation B.

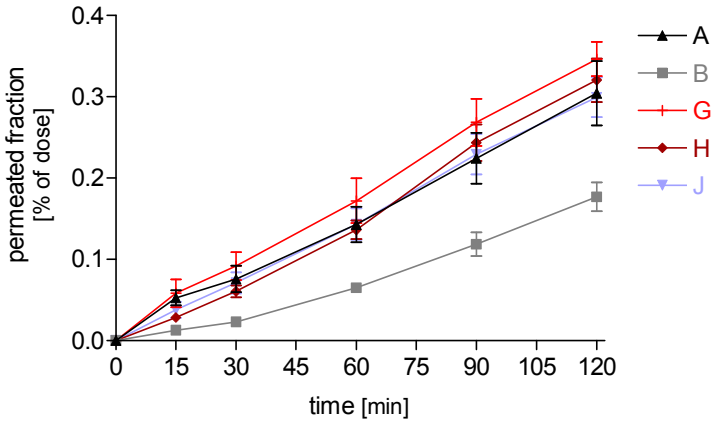

Figure 3.2. Effect of different formulations on permeation of fenofibrate in the D/P system with FaSSIF$_{mod}$ as apical medium. Each data point is the mean ± SEM of three to six independent experiments.

The permeation profiles of fenofibrate from formulations A, G, H and J showed almost the same characteristics which resulted in similar predicted absorptions. Formulation B's permeation profile of fenofibrate showed a flatter gradient which had a mandatory impact on its calculated absorption.

Dissolution testing in a USP paddle apparatus was carried out under sink conditions (Figure 3.3.). In 1000 ml water, containing 1.5% SDS, more than 65% of the fenofibrate content of the formulations were dissolved within 30 minutes. Formulation I showed the slowest dissolution in the first 30 minutes of all tested formulations, probably since it did not contain any disintegrants. Formulation B as well showed a slow initial dissolution rate, but after 20 minutes almost 90% of its fenofibrate dose were dissolved. Regarding the initial 15 minutes, formulations H and A showed the highest dissolution rate of fenofibrate.

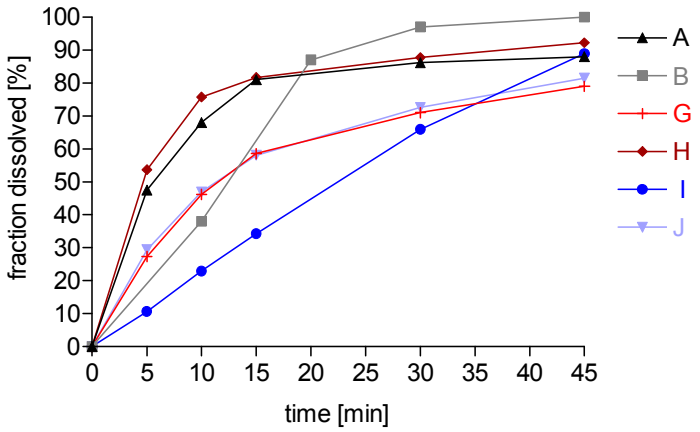

Figure 3.3. Mean dissolution profiles (n = 3) of different formulations containing 145 mg fenofibrate per tablet using the USP paddle apparatus (1000 ml water, 1.5% SDS, 50 rpm, 37°C)

As an additional *in vitro* tool, a modified permeation method was introduced to perform a closer analysis of the permeation step of fenofibrate in the presence of estimated intestinal surfactant concentrations. Whereas in the previously described D/P system 1% of the clinical applied dose was dissolved in 8 ml of apical medium corresponding to an intestinal volume of 500-1000 ml [17], a recent study by Schiller et al. [20] suggested much smaller intestinal volumes available for drug dissolution. The reported minimum and median volumes under fasted conditions in the stomach (13/47 ml) and the small intestine (45/83 ml) provoked a review of the tablet mass to dissolution volume proportion to be used in the D/P system under fasted conditions. Thus higher surfactant concentrations needed to be employed. In this case use of the original D/P system was not feasible because some surfactants (e.g., SDS) are toxic to the epithelial monolayer at

the concentrations needed in the modified D/P assay. That is why a permeation system using dialysis membranes was introduced in this manuscript.

The permeation of fenofibrate in $FaSSIF_{mod}$ containing different amounts of the surfactants which are used in the tablet formulations, i.e., SDS, two surfactants from the class of poloxamers (S1 and S2) and one surfactant from the class of polyethoxylated castor oils (S3), is depicted in Figure 3.4. It becomes obvious that the permeated fractions of fenofibrate decreased with rising concentrations of S1, S3 and SDS. Low concentrations of SDS seemed to have the least negative impact on fenofibrate permeation. But with rising surfactant concentrations the permeated proportion of fenofibrate obtained with SDS approximated the values gathered with S1 and S3. Only S2 seemed not to affect the permeability of fenofibrate, as the fraction permeated remained at the same high level even with rising surfactant concentration.

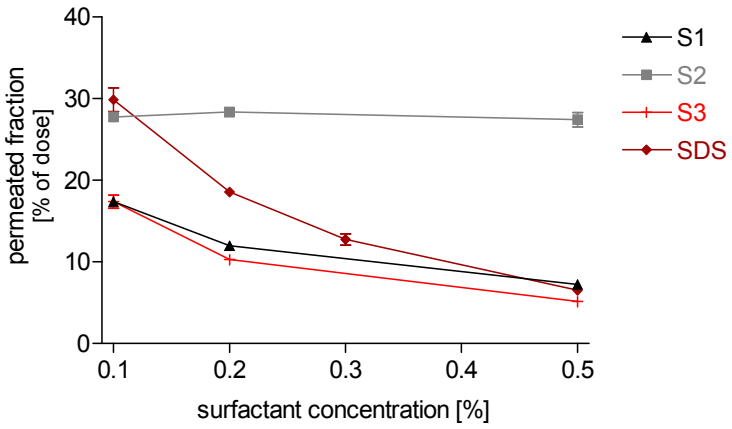

Figure 3.4. Fraction of fenofibrate permeated after 4 h (mean ± SD, n = 3) across the dialysis membrane (neutral cellulose, molecular weight cut-off 10,000 Dalton) to the receiver side. The four tested surfactants were dissolved in $FaSSIF_{mod}$.

Based on the results obtained with this modified permeation method, the permeated fractions of fenofibrate from the formulations were calculated at their respective surfactant composition. A dissolution volume of 50 ml *in vivo* was assumed. From all tested surfactants S2 was excluded from calculations as its rising concentrations did not affect the permeated fraction of fenofibrate. The calculated permeated fractions of fenofibrate correlated well with C_{max} values for formulations containing SDS, indicating a negative influence of SDS on the permeation of the dissolved fenofibrate (Figure 3.5.).

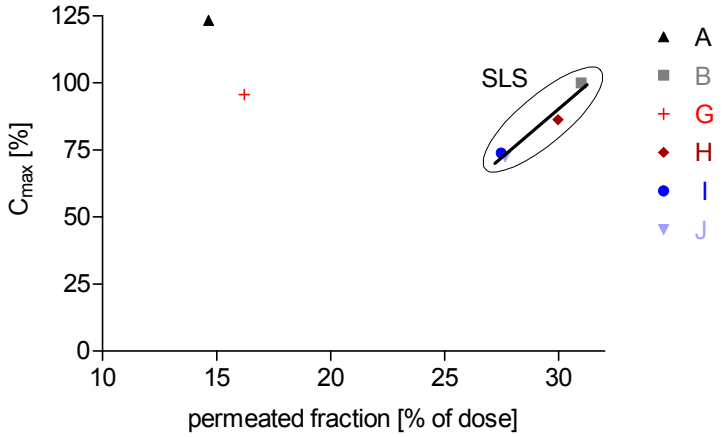

Figure 3.5. Plot of predicted permeated fractions of fenofibrate from the formulations calculated from permeation data obtained with the permeation method using dialysis membranes (50 ml *in vivo* dissolution volume were assumed) versus C_{max} values for the fenofibrate fomulations. Linear regression analysis was done on the formulations containing SDS.

3.5 Discussion

This study describes the elucidation of an *in vitro*/*in vivo* relationship for fenofibrate IR tablets using several *in vitro* methods. The outcome of the human studies was an obvious variation in C_{max} for the fenofibrate formulations, whereas the results based on $AUC_{0\text{-}inf}$ values showed no significant difference. Although the D/P system was developed to predict the *in vivo* systemic exposure in humans rather than absorption rates, it was tried to correlate the permeation profiles with the C_{max} values in humans. This was not successful. Using the D/P system, the predicted fenofibrate absorptions from formulations A, G, H and J showed almost the same performance which is consistent with the human *in vivo* studies. Only the calculated absorption from formulation B missed the result of the *in vivo* studies by being around 25% smaller compared to the predicted absorptions from the other formulations.

Similarly to the fraction permeated after 2 hours, permeation results at other time points did not result in significantly improved IVIV-relationships. Also traditional dissolution testing under sink conditions did not result in any useful IVIV-relationship between the dissolution profiles and C_{max} values in humans, demonstrating the inadequacy of the dissolution method to predict *in vivo* performance. For example, the good dissolution performance of formulation D was not reflected in humans. Likewise, the second highest fenofibric acid C_{max} value in humans was measured after the administration of formulation B, but its dissolution result after 10 minutes was only the second to last.

No improvement of prediction was seen when the solubilizing surfactant SDS in the dissolution medium was replaced by a bile salt based medium as e.g., $FaSSIF_{mod}$. Again, no improvement of differentiation and interpretability of the dissolution data from the formulations was obtained (data not shown) with generally fractions dissolved of less than 1% of the fenofibrate dose from the tablets over a period of 45 min in 50 ml $FaSSIF_{mod}$. Up to 10% of the fenofibrate was dissolved from the tablets after 45 min in 900 ml $FaSSIF_{mod}$, but no rank order of the formulations based on their dissolution profiles was established.

By introduction of a permeation method using cellulose-based membranes, higher surfactant concentrations as compared to the original D/P system were tested. It was discovered that the permeated fractions of dissolved fenofibrate decreased with rising concentrations of S1, S3 and SDS.

This lower permeability may be due to surfactant forming mixed micelles with the NaTC and lecithin contained in $FaSSIF_{mod}$, which prevent micellar entrapped fenofibrate from permeation across the dialysis membrane. The rising number of micelles due to increasing surfactant concentrations can explain the concurrently decreasing fractions of fenofibrate dissolved in the donor chamber which permeated across the membrane. Only with S2 the fractions of drug which

were detected in the receiver chamber remained at the same level, irrespective of the surfactant concentration. This confirms the hypothesis of micellar entrapment of fenofibrate regarding SDS, S1 and S3 because all tested S2 concentrations were below their critical micelle concentration (CMC = 6.3 mM at 37°C) [130]. The CMCs for SDS, S1 and S3 are 1.6 mM, 0.0004 mM and 0.012 mM, respectively [131-133].

The uptake of dissolved fenofibrate into micelles which reduced the free concentrations of drug in the intestinal lumen might serve as an explanation for the performance of these solid dosage forms in the human studies. The three RD formulations containing SDS in conjunction with S2 showed a poor performance in terms of C_{max} compared to the two formulations containing different surfactants instead of SDS and formulation B having the overall lowest surfactant concentrations. The micelles containing SDS seem to restrain dissolved fenofibrate from permeation across membranes by incorporation, as has been shown previously for tetracycline in combination with dioctyl sodium sulfosuccinate [134].

This theory is further supported by comparing the predicted permeated fractions of fenofibrate from the formulations with the C_{max} values for the fenofibrate formulations, assuming a 50 ml *in vivo* dissolution volume. The dissolution of tablet formulations containing low amounts of SDS will result in small numbers of SDS micelles or no micelles at all which could incorporate and therefore restrain dissolved fenofibrate from permeation across membranes.

3.6 Conclusion

Even for highly permeable substances dissolution testing may not always be a sufficiently predictive *in vitro* method for *in vivo* performance. An additional permeation step may need to be incorporated into the *in vitro* prediction models. The D/P system which combines dissolution and permeation seems to be a useful tool to predict the *in vivo* performance in humans in terms of exposure. To enable the prediction of the performance of absorption rate, more concentrated surfactant solutions in a permeation model using artificial membranes needs to be introduced.

Incorporation of dissolved fenofibrate in micelles containing SDS and subsequently reduced permeability of the fenofibrate/micellar complex was made responsible for the reduction in C_{max} of the three fenofibrate formulations which goes along with a reduced absorption velocity (permeability) of fenofibrate.

In tablet formulations containing a poorly soluble drug like fenofibrate, SDS is a frequently used excipient to improve the drug's solubility which is a prerequisite for absorption. But formulation scientists should keep in mind that the dissolved drug has to permeate biological membranes to become systematically available. As shown in this study an increase in surfactant concentration in a tablet formulation cannot guarantee improved absorption.

3.7 Acknowledgments

P.B. received a scholarship from the German Academic Exchange Service (DAAD) during his stay in Hirakata.

4. IVIVC for fenofibrate immediate release tablets using solubility and permeability as *in vitro* predictors for pharmacokinetics

(Running chapter head: IVIVC for IR tablets using solubility and permeability methods)

Philipp Buch[1], Per Holm[2], Jesper Qvist Thomassen[2], Dieter Scherer[3], Robert Branscheid[4], Ute Kolb[4], Peter Langguth[1]

[1]Institute for Pharmacy and Biochemistry, Biopharmacy and Pharmaceutical Technology, Johannes Gutenberg University, Staudinger Weg 5, 55128 Mainz, Germany

[2]LifeCycle Pharma A/S, Kogle Allé 4, 2970 Hørsholm, Denmark

[3]ApisPharma, Bahnhofstraße 6, 4242 Laufen, Switzerland

[4]Institute of Physical Chemistry, Johannes Gutenberg-University, Jakob-Welder-Weg 11, 55128 Mainz, Germany

J Pharm Sci. (in press)

4.1 Abstract

The goal of this study was to investigate the IVIVC for fenofibrate IR tablet formulations based on MeltDose®-technique. The *in vitro* determined drug solubility and permeability data were related to the C_{max} values observed from two *in vivo* human studies. Fenofibrate tablets were administered to healthy volunteers in two randomized crossover studies, blood samples were collected over 96 hours and assayed. Solubility and permeation studies of fenofibrate were conducted in medium simulating the fasted state conditions in the upper jejunum, containing the surfactant compositions of the six formulations at different concentrations. HBSS was additionally applied in the solubility studies. The behavior of all surfactant compositions in both solutions was characterized by determination of surface tension, DLS measurements and cryo-TEM studies.

The obtained solubility and permeation data were combined and compared with the C_{max} values for the fenofibrate formulations, assuming a 50 ml *in vivo* dissolution volume. A good IVIVC was

observed for five fenofibrate formulations which were based on the same manufacturing technique (R^2 = 0.94). The *in vitro* studies revealed that the formulation compositions containing SDS interfered with the vesicular drug solubilizing system of the biorelevant medium and antagonized its solubilization capacity.

The opposing interaction of surfactants with the emulsifying physiological constituents in intestinal juice should be taken into consideration in order to prevent unsatisfactory *in vivo* performance of orally administered formulations with low soluble active pharmaceutical ingredients.

4.2 Introduction

Up to 75% of new chemical entities are poorly soluble. Poor water solubility frequently results in unpredictable *in vivo* performance, especially when the formulation is given in the fasted state. Regarding the oral route, absorption of a drug depends upon its dissolution in the GI tract and its permeability across the GI wall. Therefore, several *in vitro* methods were established to determine a drug's dissolution rate and/or permeability under biorelevant conditions. Consequently time- and cost-intensive *in vivo* studies may be avoided to some extent.

Biorelevant dissolution media were introduced to better predict the *in vivo* performance of formulations containing poorly soluble drugs. FaSSIF and FeSSIF, simulating the fasted and fed state conditions in the upper jejunum, were proposed by Galia et al. [26] and are still the point of reference for modified versions [135].

For permeability screening in pharmaceutical research cellular models are extensively used and generally accepted. The human carcinoma cell line (Caco-2) is preferentially applied because it displays many of the morphological and functional properties of the *in vivo* intestinal epithelial [39,40]. This permeation method is used in the early stages of drug discovery when only pure compounds are tested. The applicability for testing pharmaceutical formulations is limited due to the cell monolayer's destruction by several excipients [136,137].

A combination of the aforementioned *in vitro* methods was the following step. Simultaneous determination of dissolution and permeation through Caco-2 can be conducted in two classes of apparatus, open [57,61] and closed [55] systems. The classification depends on the dissolution part of the system, using a flow through cell and a dissolution vessel, respectively.

Kataoka et al. [27] used biorelevant media as dissolution medium in their closed dissolution/permeation system to evaluate the effect of food intake on the oral absorption of poorly water-soluble drugs. The compositions of the original FaSSIF and FeSSIF had to be modified because their use as dissolution medium would destroy the integrity of the Caco-2 monolayer [27,138]. Several excipients, especially surfactants, show as well toxic effects on

Caco-2 cells. In this case the application of a permeation system using artificial membranes is inevitable.

In the present study several *in vitro* methods were applied to explain the differences between the C_{max} values gathered from two human studies. In these studies six fenofibrate IR formulations were tested in a randomized crossover manner. Bioequivalence with a reference product (formulation B) in fasted conditions should be demonstrated. Regarding the *in vitro* methods it was focused on the differences in solubility of fenofibrate in $FaSSIF_{mod}$ subject to the surfactant compositions of the six formulations. Finally, solubility data was combined with permeation data in terms of a possible IVIVC.

4.3 Materials and methods

Materials

Fenofibrate was purchased from Labochim. TriCor® (formulation B) was obtained from the manufacturer (Abbott Laboratories). RD 24, RD 25, RD 23, RD 22 and RD 18 were kindly provided by LifeCycle Pharma. Lecithin was purchased from Lipoid GmbH (Ludwigshafen, Germany). NaTC was kindly donated by Prodotti Chimici e Alimentari S.p.A. via their German agent Alfred E. Tiefenbacher GmbH & Co. KG. All other chemicals were of analytical reagent grade.

Formulations employed

The RD formulations were based on the solid dispersion principle (MeltDose®-technique) and were used as delivered by the manufacturer [101]. RD 22 (formulation I) contains fenofibrate dispersed in a hydrophilic polymer and compressed to tablets following mixing with magnesium stearate. RD 24 (formulation A), RD 25 (formulation G), RD 23 (formulation H) and RD 18 (formulation J) additionally contain Avicel PH 200 and Polyplasdone XL as binder and disintegrant, respectively. Formulation A contains a surfactant from the class of poloxamers (S1). Formulations H, I and J contain besides SDS a poloxamer (S2) which is different to the one employed in formulation A. S2 and a surfactant from the class of polyethoxylated castor oils (S3) are used as emulsifying agents in formulation G.

Formulation B: This formulation is a fenofibrate nanoparticulate tablet formulation, containing fenofibrate, hypromellose 2910, docusate sodium, sucrose, SDS, lactose monohydrate, silicified microcrystalline cellulose, crospovidone, magnesium stearate, polyvinyl alcohol, titanium dioxide, talc, soybean lecithin and xanthan gum. It was used as received.

In vitro studies

Solubility studies

As stock solutions for the solubility studies HBSS including 19.45 mM glucose and 10 mM HEPES (transport medium, TM), as well as TM including 3 mM NaTC and 0.75 mM lecithin were used (FaSSIFmod). TM and FaSSIFmod were adjusted to pH 6.5. An excess of fenofibrate (15 mg) was added to 15 ml of FaSSIFmod containing the surfactant compositions of the six tablet formulations (Table 4.1.) at different concentrations. The suspensions were agitated at 37°C in an orbital shaker at 200 rpm over night until equilibrium. Equilibrium was reached when concentration became uniform. For HPLC analysis the samples were centrifuged (5,000 rpm, 10 min, 37°C). Each experiment was run in triplicate.

Table 4.1. Surfactant composition of the tablet formulations. S1 and S2 are surfactants from the class of poloxamers. S3 is a surfactant from the class of polyethoxylated castor oils.

Formulation	Surfactant (1)	Surfactant (2)	Surfactant (2) amount [mg/tablet]
A	S1	-	-
B	Docusate-Na	SDS	10.15
G	S2	S3	n/a
H	S2	SDS	19.32
I	S2	SDS	41.9
J	S2	SDS	40.22

Dissolution studies

Dissolution studies were performed using the paddle method (apparatus: Erweka DT 7R, Erweka GmbH, Heusenstamm, Germany). The release profiles were examined in 900 ml $FaSSIF_{mod}$ using a paddle speed of 50 rpm. Each measurement was performed in triplicate.

Permeation studies

The permeation method using dialysis membranes was carried out using a DIANORM equilibrium dialysis equipment (Bachofer Laboratoriumsgeräte, Reutlingen, Germany). From all surfactants deployed in the tablet formulations (Table 4.1.) four were chosen for these permeation studies, namely S1, S2, S3 and SLS. Fenofibrate was added in excess to $FaSSIF_{mod}$ containing different amounts of the four surfactants. The resulting suspensions were shaken over night in an orbital shaker (37°C, 200 rpm). After a centrifugation step (5,000 rpm, 10 min, 37°C) the dissolved amount of fenofibrate in the supernatant was analyzed and 4 ml of each solution were placed in the donor chamber of the dialysis cell. The dissolved fenofibrate permeates through the dialysis membrane (neutral cellulose, molecular weight cut-off 10,000 Dalton) to the receiver side, which contained the same volume and the same concentration of the deployed surfactant as the donor solution. After 4 hours the permeated fraction of fenofibrate was analyzed in the receiver chamber.

Tensiometry

A Digital-Tensiometer K 10 (Krüss, Hamburg, Germany) was used to measure the surface tension of TM, $FaSSIF_{mod}$ and $FaSSIF_{mod}$ containing the surfactant compositions of the six tablet formulations (Table 4.1.) at different concentrations. A 20 ml volume of each solution was filled into a 50 ml glass beaker and placed onto the tensiometer platform. A platinum wire ring was submerged into the solution and then slowly pulled through the liquid-air interface, to measure the surface tension (N/m). Between each measurement, the ring was rinsed with distilled water before it was heated in the oxidizing portion of a gas flame above the reducing zone of a gas burner. Each measurement was performed in triplicate.

Analysis of *in vitro* samples by HPLC

Quantitative analysis of fenofibrate was carried out using an HPLC pump, a vacuum degasser, automatic sampler, and UV detector from Series 1050, Hewlett Packard. Data processing was by HPLC Chemstation Rev. A. 03.01 (Hewlett Packard). Samples were separated using a 125 x 4.6 mm MZ Analysentechnik LiChrospher 100 RP-18 (end-capped) column (5µm). The mobile phase consisted of 0.1% diethylamine in a water/acetonitrile-mixture (20%/80%) which was adjusted with phosphoric acid to a pH of 4.

Dynamic light scattering (DLS) measurements

The particle size distribution of the colloidal structures in $FaSSIF_{mod}$, and $FaSSIF_{mod}$ containing the surfactant compositions of the six tablet formulations (Table 4.1.) at different concentrations were analyzed by DLS at room temperature. A backscattering arrangement was used, the scattering angle being 170°C. Laser light (lambda = 632.8 nm) was used as the incident beam and the scattered light was detected by a single photon detection unit, connected to a correlator (ALV-7004, Langen, Germany). Measurements of 5 min duration of the autocorrelation function were performed. The time correlation functions were analyzed with ALV-Korrelator Software.

Cryogenic transmission electron microscopy

Samples for cryo-TEM were prepared on Quantifoil grids (Quantifoil Micro Tools, Jena, Germany) which had been treated with Argon plasma for hydrophilisation. The vitrification was done in a controlled environment of 36°C and 80% relative humidity with a Vitrobot device (FEI, Eindhoven, The Netherlands). Imaging of the vitrified specimens was performed at -175°C sample temperature with a Tecnai 12 BioTWIN transmission electron microscope (FEI) operating at 120 kV and a SIS MegaView III CCD camera (Olympus Soft Imaging Solutions, Münster, Germany).

In vivo studies

Two human studies were conducted with six solid dosage forms, four containing SDS. Bioequivalence with formulation B in fasted conditions should be demonstrated in these randomized crossover studies. The bioavailability studies were performed at Biovail Research Center (Toronto, ON, Canada) and were approved by the Ontario Institutional Review Board.

Clinical study 1

Formulation B, formulation I and formulation J

12 healthy non-smoking human volunteers (6 male and 6 female), aged 20 to 73 years (mean 43.4 years), were selected. Each subject received one tablet in a randomized crossover manner. There was a washout period of 10 days between dosing. Tablets were administered at 7:00 AM following an overnight fast (min. 10 hours). No water was permitted from 1.0 hour predose to 1.0 hour postdose, with exception of 240 ml dosing water. Food was withheld for at least 4 hours postdose. At 4.5, 9.5 and 13.5 hours postdose, standardized meals with beverages were provided to the subjects. All meals and beverages were free of alcohol, grapefruit products, xanthine and caffeine and were identical for the three study periods. 21 blood samples (4 ml) were drawn at 0.00 (predose), 0.5, 1.0, 1.5, 2.0, 2.5, 3.0, 3.5, 4.0, 4.5, 5.0, 5.5, 6.0, 8.0, 10.0, 14.0, 24.0, 36.0, 48.0, 72.0, 96.0 hours postdose.

Clinical study 2

Formulation B, formulation A, formulation G and formulation H

20 healthy non-smoking human volunteers (12 male and 8 female), aged 26 to 77 years (mean 47.5 years), were selected. Each subject received one tablet in a randomized crossover manner. The experimental protocol used in this study was the same as described in study 1.

Analysis of plasma samples

Fenofibric acid and its internal standard, naproxen, were extracted from human plasma (0.2 ml), using dipotassium EDTA as an anticoagulant, by solid phase extraction into an organic medium, evaporated under nitrogen and reconstituted in 200.0 µl of mobile phase. An aliquot of this extract was injected into a HPLC system and detected using a UV detector. The analytes were separated by reverse phase chromatography. Evaluation of the assay, using defined acceptance criteria, was carried out by the construction of an eight point calibration curve (excluding zero concentration) covering the range 49.996 ng/ml to 12,798.8 ng/ml for fenofibric acid in human plasma. The slope and intercept of the calibration curves were determined through weighted linear regression analysis ($1/conc^2$). Two calibration curves and duplicate quality control samples (at three concentration levels) were analyzed along with each batch of the study samples. Peak height ratios were used to determine the concentration of the standards, quality control samples, and the unknown study samples from the calibration curves.

4.4 Results

The plasma concentration versus time profiles of fenofibric acid following oral administration are shown in Figure 4.1. The pharmacokinetic parameters following noncompartmental analysis are summarized in Table 4.2. No significant difference in $AUC_{0\text{-}inf}$ values was noted between the six fenofibrate formulations, since all formulations were within the 80-125% confidence interval (log transformed). Regarding the C_{max} values a differentiation was obvious. The rank order of the drug formulations with respect to the C_{max} values was as follows: A > B > G > H > I > J.

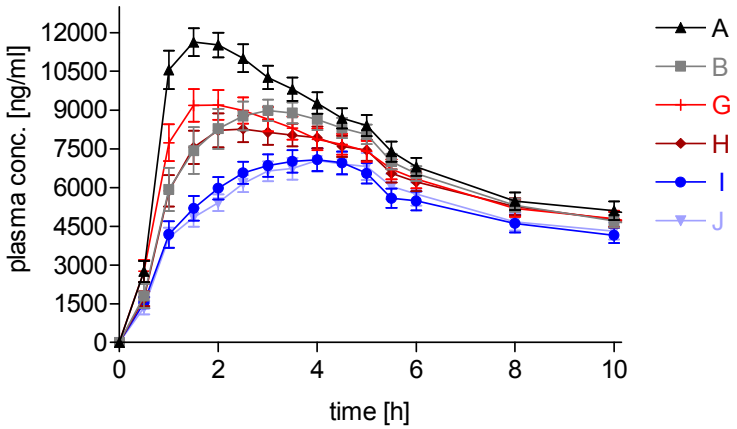

Figure 4.1. Average (± SD) fenofibric acid plasma concentrations in humans (n ≥ 12) after oral administration of different fenofibrate formulations. The data for formulations I and J were standardized to the values for formulation B obtained in clinical study 2. For a better differentiation between the formulations only the first 10 hours of the plasma profiles are shown.

Table 4.2. Mean pharmacokinetic parameters (n ≥ 12) following oral administration of fenofibrate formulations at equal doses of 145 mg [% relative to formulation B].

	In vivo data	
Formulation	C_{max} [%]	$AUC_{0\text{-}inf}$ [%]
A	123.4	107.53
B	100	100
G	95.7	103.93
H	86.33	102.08
I	73.93	99.91
J	72.43	100.11

The results of the solubility experiments are depicted in Figure 4.2.a ($FaSSIF_{mod}$) and Figure 4.2.b (TM). No significant alteration of the solubility of fenofibrate in $FaSSIF_{mod}$ was observed at the lowest concentration of all surfactant compositions in $FaSSIF_{mod}$. The solubility of fenofibrate increased with rising surfactant concentration, regarding the surfactant compositions of formulations G and A. Their highest tested surfactant concentration in $FaSSIF_{mod}$ could double and almost triple fenofibrate's solubility in $FaSSIF_{mod}$, respectively. With the surfactants of formulations B, H, I and J dissolved in $FaSSIF_{mod}$ fenofibrate's solubility declined compared to its performance in $FaSSIF_{mod}$ alone. From these four formulations containing SDS only B and J were able to raise the solubility of fenofibrate at their highest surfactant concentration. Formulations A and G contained other surfactants than SDS.

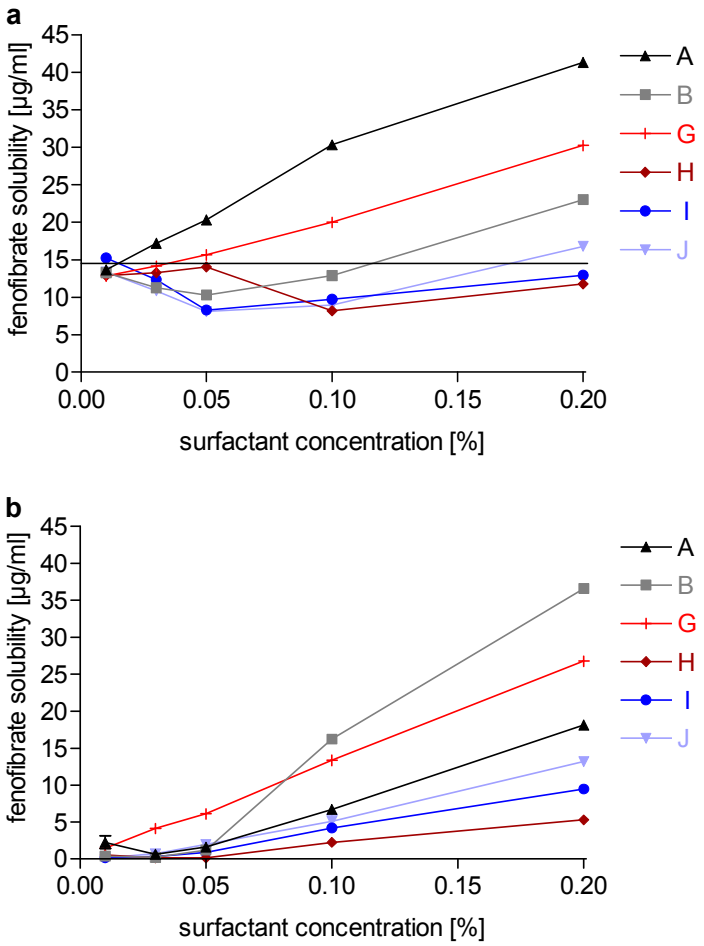

Figure 4.2. Solubility of fenofibrate as a function of surfactant composition for the six tablet formulations in $FaSSIF_{mod}$ (a) and TM (b). The given percentages reference the only surfactant or the main surfactant in the formulation. Each data point is the mean ± SD of three independent experiments. The solubility of fenofibrate in $FaSSIF_{mod}$ is marked with a black line.

All surfactant compositions increased the solubility of fenofibrate in TM (0.29 ± 0.12 µg/ml) with rising surfactant concentration. As seen in $FaSSIF_{mod}$, formulations H, I and J showed the least effect in raising fenofibrate's solubility in TM. The rank order of fenofibrate dissolved in TM containing the surfactant compositions at the highest tested concentration was as follows for the first three formulations: B > G > A.

The dissolution profiles of the formulations A, G, H, I and J are shown in Figure 4.3. Formulations A, H and J seem to reach the dissolution plateau after five minutes with only a slight change in fenofibrate fractions dissolved till the termination of the assay. At the end of the dissolution study around six to eight percent of their fenofibrate content is in solution. The dissolution profile of formulation I resembles the aforementioned ones with the exception that the plateau is reached after 10 minutes. Only formulation G shows an obvious increase in dissolved fraction over a longer period, reaching the maximum fraction dissolved after 30 minutes (about 10%).

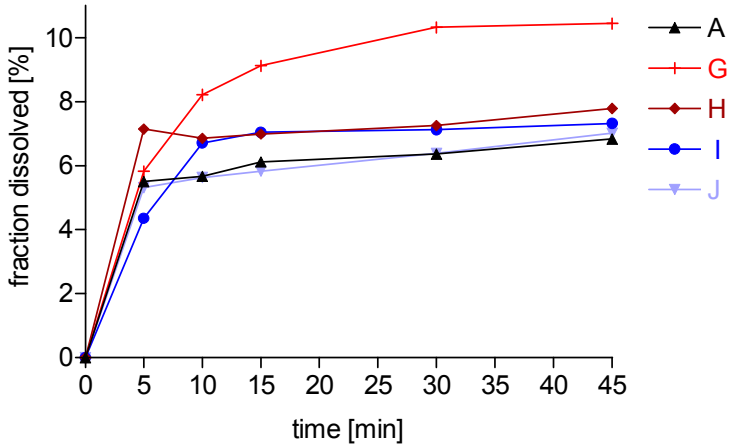

Figure 4.3. Mean dissolution profiles (n = 3) of different formulations containing 145 mg fenofibrate per tablet using the USP paddle apparatus (900 ml $FaSSIF_{mod}$, 50 rpm, 37°C)

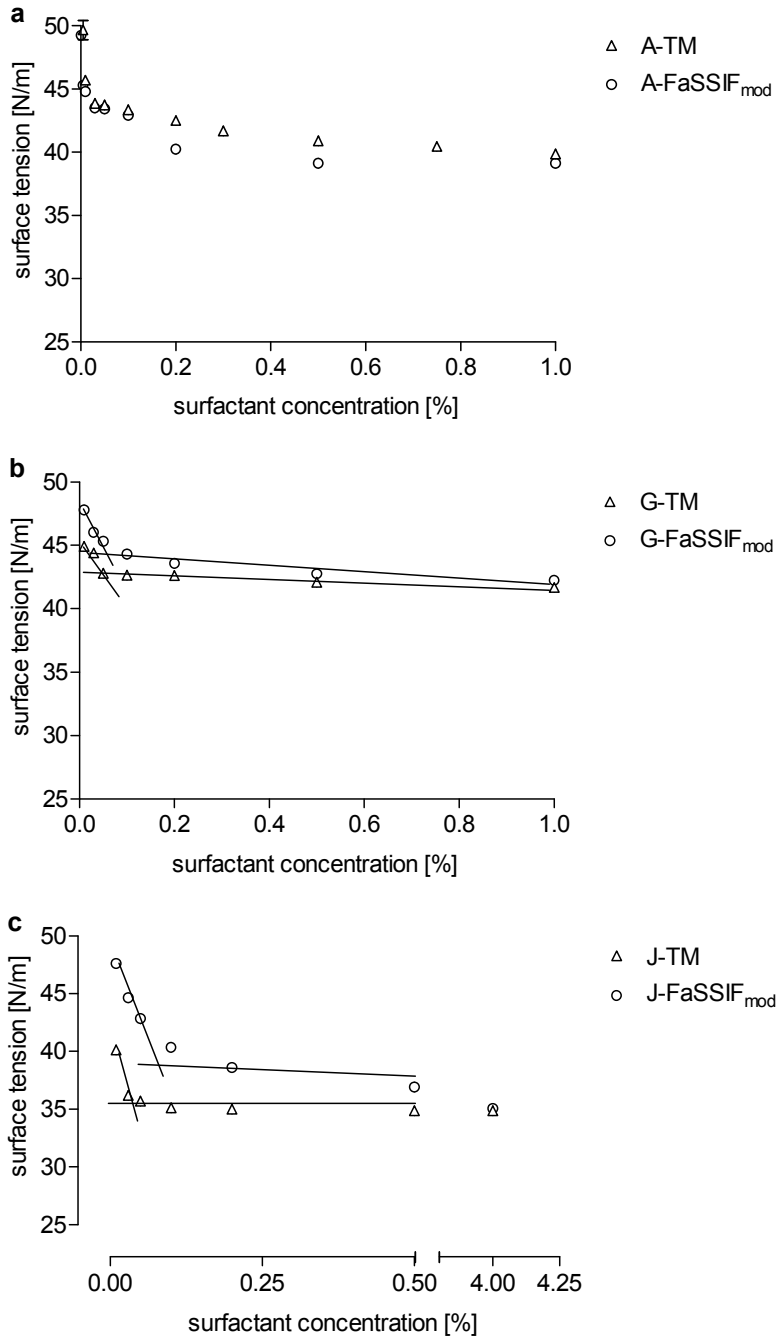

Figure 4.4. Surface tension as a function of surfactant composition for formulations A (a), G (b) and J (c) in TM and FaSSIF$_{mod}$. The given percentages reference the only surfactant or the main surfactant in the formulation. Each data point is the mean ± SD of three independent experiments.

Figure 4.4. shows the surface tension as a function of surfactant composition for formulations A, G and J in TM (70.6 N/m) and FaSSIF$_{mod}$ (52.2 N/m). The data show that the surface tension in TM and FaSSIF$_{mod}$ is lowered with rising concentration to an equilibrium value of approximately 40, 42 and 35 N/m for formulations A, G and J, respectively. Especially at concentrations around the break-point, which indicate the formation of aggregates, [139,140] formulation A's surfactant S1 exhibits similar surface activities in both solutions with the surface tensions being slightly

smaller in $FaSSIF_{mod}$ (Figure 4.4.a). Similar results were obtained with the surfactant composition of formulation G with the surface tensions being slightly higher in $FaSSIF_{mod}$ (Figure 4.4.b). On the other hand, the surfactant composition of formulation J results at low concentrations in obviously different surface tensions in TM and $FaSSIF_{mod}$, the surface tension showing higher values in $FaSSIF_{mod}$ (Figure 4.4.c). The break-point concentration in $FaSSIF_{mod}$ (0.08%) is more than twice as high as in TM, and the leveling off of the surface tension in $FaSSIF_{mod}$ takes place at much higher surfactant concentrations compared to formulations A and G.

Concerning the curve shapes gathered from the tensiometric measurements the formulations can be divided into two groups. One group comprises formulations A and G which show similar results. The second group consists, beyond formulation J, of formulations B, H and I, all four containing SDS. All characteristics of formulation J can be found in the results gathered with formulations B, H and I (data in the appendix, see Figure A.4.). At low surfactant concentrations the surface tensions in TM and $FaSSIF_{mod}$ are obviously different, regarding each surfactant composition separately. At high surfactant concentrations (approx. 4%) the surface tension curves obtained from both solutions converged. In this group of formulations the surface tensions in $FaSSIF_{mod}$ are consistently higher at low surfactant concentrations. Therefore, the break-point concentrations in $FaSSIF_{mod}$ are consequently higher when compared to the results determined in TM.

The results from the DLS measurements are depicted in Figure 4.5. The particle size distributions from $FaSSIF_{mod}$ and from mixtures of $FaSSIF_{mod}$ with surfactants employed in the formulations were investigated. Analysis of $FaSSIF_{mod}$ resulted in a median diameter of 80 nm (Figure 4.5.a). A similar particle size distribution was observed when 0.1 g S1 was dissolved in $FaSSIF_{mod}$ to a final volume of 100 ml (Figure 4.5.b). Formulation G's surfactant composition at a concentration of 0.1% in $FaSSIF_{mod}$ resulted in two particle populations (median 15.9 and 94.6 nm) (Figure 4.5.d). In a 0.1% solution of formulations B's, H's, I's and J's surfactant composition in $FaSSIF_{mod}$ the particle size decreased significantly to a median value of 8.6, 8.6, 5.2 and 15 nm, respectively (Figure 4.5.c, e-g). Whereas at a concentration of 0.01% all tested solutions showed a similar particle size distribution compared to $FaSSIF_{mod}$.

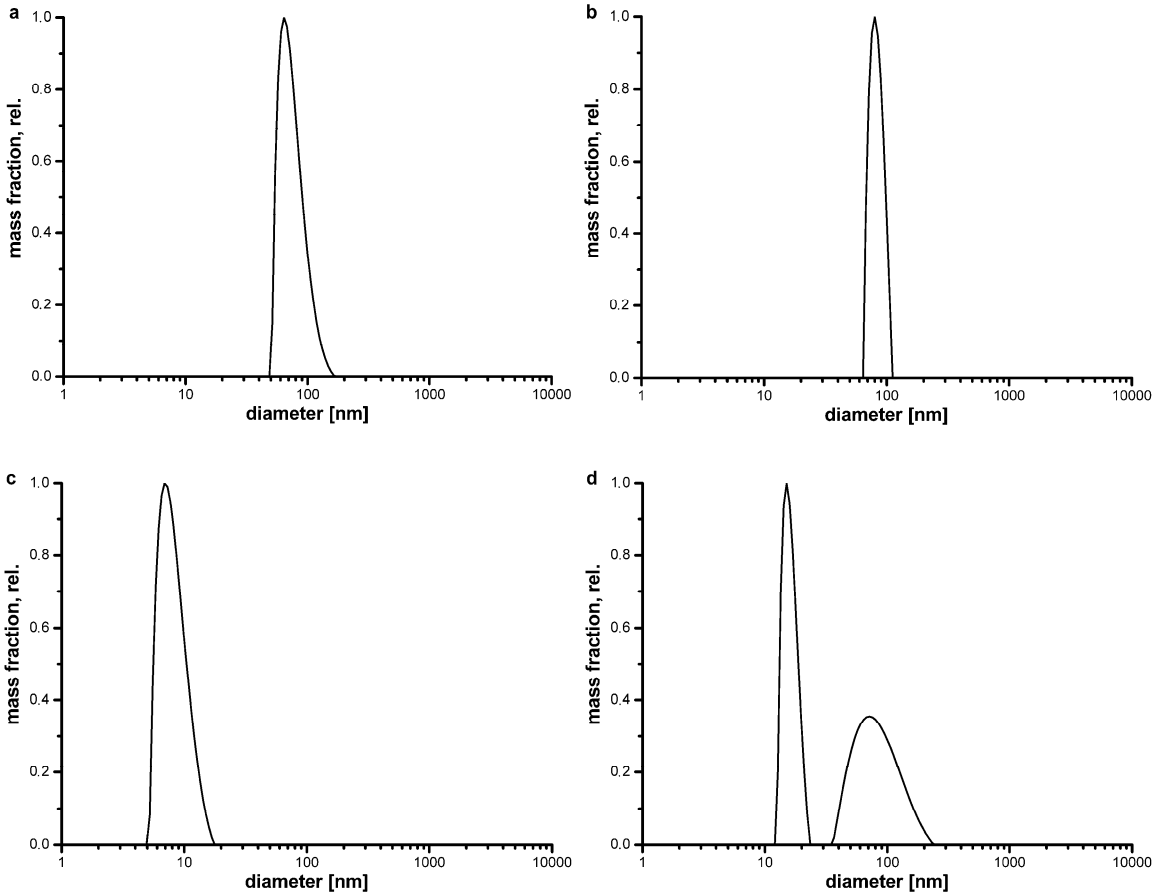

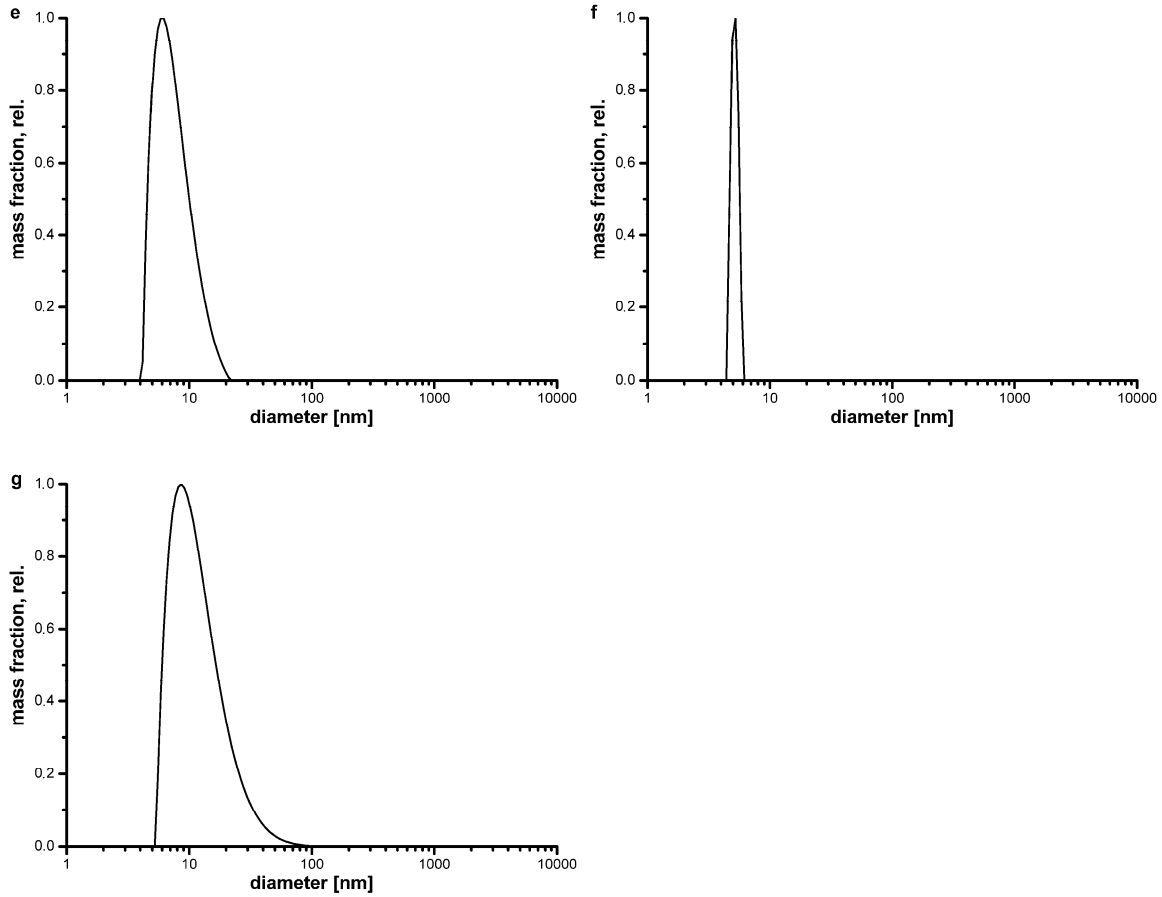

Figure 4.5. Hydrodynamic size data as obtained from a mass weighted size distribution analysis of $FaSSIF_{mod}$ (a) and 0.1% solutions of formulations A's (b), B's (C), G's (d), H's (e), I's (f) and J's (g) surfactant composition in $FaSSIF_{mod}$. The given percentage references the main surfactant in the formulation.

Three of the solutions whose particle size distributions are shown in the former Figure were imaged by cryo-TEM. In $FaSSIF_{mod}$ unilamellar vesicles are observed (Figure 4.6.a). Their size is consistent with the findings from the DLS measurements. The same applies for the results obtained from a 0.1% solution of formulation A's surfactant S1 in $FaSSIF_{mod}$ (Figure 4.6.b). Whereas no vesicles were detected in a solution of formulation F's surfactant composition in $FaSSIF_{mod}$ at a concentration of 0.1% (Figure 4.6.c).

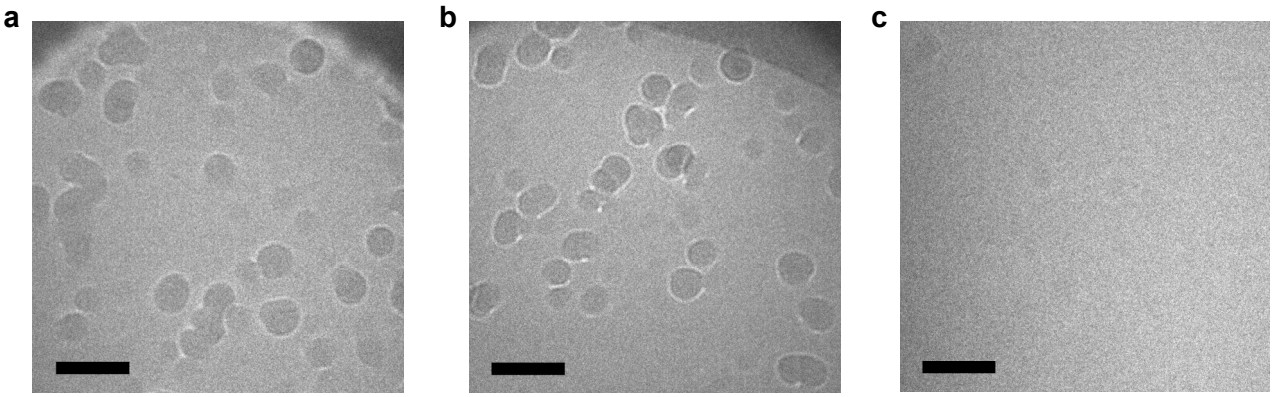

Figure 4.6. Cryo-TEM micrographs of $FaSSIF_{mod}$ (a), a 0.1% solution of formulation A's surfactant S1 in $FaSSIF_{mod}$ (b) and a 0.1% solution of formulation J's surfactant composition in $FaSSIF_{mod}$ (c). Given percentages reference the main surfactant in the formulation. The pictures were taken at a slight defocus to obtain high-quality images. The scale bars represent 100 nm.

Based on the results obtained with the solubility studies, solubilities of fenofibrate from the formulations were calculated at their respective surfactant composition (Table 4.3.). A dissolution volume of 50 ml *in vivo* was assumed as it was done for the calculation of the permeated fractions of fenofibrate from the formulations at their respective surfactant composition (Table 4.3.).

Table 4.3. Calculated solubilities and permeated fractions of fenofibrate from the formulations in $FaSSIF_{mod}$ at their respective surfactant composition, assuming a 50 ml *in vivo* dissolution volume.

Formulation	Solubility [µg/ml]	Permeated fraction
A	36.8	0.146
B	10.7	0.31
G	24.2	0.162
H	11.7	0.3
I	11.3	0.275
J	12.4	0.277

The products of these permeation data and the calculated solubilities of fenofibrate were related to the C_{max} values gathered from two human studies (Figure 4.7.). Formulation B was excluded from linear regression analysis because it is based on a totally different manufacturing technique compared to formulations A, G, H, I and J. There was a close correlation between the calculated permeability-solubility product of formulations A, G, H, I and J and their *in vivo* rate of absorption as expressed by C_{max} (coefficient of determination = 0.94).

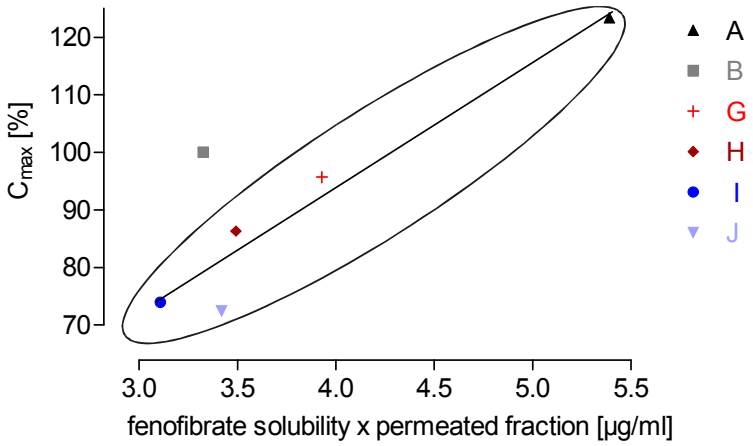

Figure 4.7. Plot of C_{max} values for six fenofibrate formulations versus the products of calculated dissolved fenofibrate and the calculated permeated fractions of fenofibrate from these formulations (see Table 4.3.). A dissolution volume of 50 ml was assumed. Linear regression analysis was done on the formulations A, G, H, I and J.

4.5 Discussion

In this study the effect of the surfactant composition designed to enhance the dissolution and solubility of fenofibrate from IR formulations was studied. Solubilities and permeated fractions of fenofibrate from six formulations were determined at their respective surfactant composition, assuming a 50 ml *in vivo* dissolution volume. The product of these solubility and permeation data was compared with the C_{max} values for the fenofibrate formulations. A close correlation was shown between the *in vitro* characteristics of formulations A, G, H, I and J and their *in vivo* performance. Formulation B was excluded from the analysis because its performance in humans is probably the result of the drug's small particle size (< 200 nm) [91]. The fenofibrate particle size in all other formulations was approximately 1 µm. However, the effect of fenofibrate's particle size on the performance in human was not investigated in this study, as all experiments were carried out with micronized fenofibrate (5 µm average particle size).

Furthermore, it was examined with several *in vitro* methods why four of the tested surfactant compositions decreased fenofibrate's solubility in $FaSSIF_{mod}$. Synergistic effects between $FaSSIF_{mod}$ and surfactant composition in improving the solubility of fenofibrate were only exhibited with formulations G and particularly A, containing S2, S3 and S1 as surfactants. Based on these results, the tablet formulations could be divided into two groups. One group consisted of the formulations B, H, I and J containing SDS which decreased the intrinsic solubilization capacity of the biorelevant medium $FaSSIF_{mod}$. Solubility studies, conducted with S2 and SDS alone, revealed that S2 had no effect on fenofibrate's solubility in $FaSSIF_{mod}$, whereas SDS reduced fenofibrate's solubility in $FaSSIF_{mod}$ at low surfactant concentrations (data not shown). The other group comprised formulations A and G. However, their surfactant compositions demonstrated synergistic effects with the biorelevant medium, suggesting their preferred use in drug formulations with low soluble compounds.

A change in solubility of fenofibrate was shown by applying the different surfactant compositions to $FaSSIF_{mod}$. It would have been illuminating to show a similar effect on drug dissolution from the fenofibrate formulations. For several practical reasons the performance of a differentiating dissolution study was unsuccessful. In 50 ml $FaSSIF_{mod}$, corresponding to the solubility study, less than 0.5% of the fenofibrate dose were dissolved from the tablets over a period of 45 min (data not shown). This was expected based on the result of the solubility study. In 900 ml $FaSSIF_{mod}$ up to 10% of fenofibrate was dissolved from the tablets after 45 min, but no rank of the formulations based on their dissolution profiles could be established. Similarly, no correlation was found between the dissolution profiles of the fenofibrate tablets gathered in 1.5% SDS solution as dissolution medium and their C_{max} values in humans (data not shown).

Due to the solubility of fenofibrate in $FaSSIF_{mod}$ (14.3 ± 1.05 µg/ml in $FaSSIF_{mod}$, at 37°C) a fraction of the tablet was tested in a compendial dissolution vessel under sink conditions. Grinding was the method chosen to prepare an appropriate fragment of the tablet. In the following, several dissolution studies under non-sink and sink conditions were performed using this ground material. The results lead to the conclusion that dissolution studies had no potential to account for a differentiation between the tablets reflecting their *in vivo* performance (data not shown). Since no predictive dissolution was established, further treatment of the data in terms of obtaining a level A IVIVC were not conducted.

In contrast to the surfactant compositions of formulations A and G the surfactant compositions of the tablets containing SDS yielded different surface tensions in TM and $FaSSIF_{mod}$ with higher values in $FaSSIF_{mod}$, when low concentrations were investigated. Furthermore, the fact that high surfactant concentrations were needed to lower the surface tensions in $FaSSIF_{mod}$ to similar values as in TM indicate an interaction between SDS and the emulsifying constituents of biorelevant media. This interaction prevents saturation of the liquid surface with surfactant at low concentrations. We thus show that higher surfactant concentrations had to be applied to saturate the liquid surface. The theory of interaction between the emulsifying contents was confirmed by higher break-point concentrations in $FaSSIF_{mod}$ providing higher critical micellar concentrations for the formulations containing SDS.

This theory and the classification of the fenofibrate formulations into two groups were affirmed by DLS data. The curve of particle size distribution resulted in a median of 80 nm for $FaSSIF_{mod}$ which was unchanged in the presence of surfactants from formulations A and G. By contrast, this characteristic $FaSSIF_{mod}$-peak was caused to vanish by the equally concentrated surfactant compositions containing SDS, indicating a loss of drug solubilizing surfactant vesicles in the presence of additional SDS.

Cryo-TEM images were taken from $FaSSIF_{mod}$ and from the surfactant compositions of formulations A and J in $FaSSIF_{mod}$, each presenting an example for one group of formulations. Vesicles were observed in $FaSSIF_{mod}$ and a solution of S1 in $FaSSIF_{mod}$. The surfactant composition of formulation J seemed to destroy these colloidal structures as no vesicles were recovered by imaging a solution of formulation J's surfactants in $FaSSIF_{mod}$.

The vesicle system in the biorelevant medium seems to become disordered by SDS which results in low fenofibrate solubility, reflected in low C_{max} values in humans for the fenofibrate formulations containing SDS. The vesicular phase seems to play an important role in drug solubilization, as has been shown previously especially for high log *P* drugs [141].

4.6 Conclusion

Drug solubility in biorelevant media may be modified by surfactants contained in solid formulations as exemplified for fenofibrate in MeltDose®-formulations. Interactions between naturally occurring phospholipid solubilizers and SDS may decrease rather than increase solubility. Thus SDS must be avoided in formulations with the intention to raise fenofibrate's solubility and thus dissolution rate *in vivo*. This was affirmed by several *in vitro* experiments which showed that surfactant compositions containing SDS interfered with the vesicle system of the biorelevant medium, $FaSSIF_{mod}$, and therefore its solubilization capacity. Solubility and permeability of the solubilized drug may be used to predict the *in vivo* performance of the dosage forms (R^2 = 0.94).

Further work will be necessary in order to investigate the influence of surfactants on other drug's solubility and permeability when dissolved in biorelevant media which might prevent unsatisfactory *in vivo* performance of orally administered formulations by choosing the appropriate surfactant composition.

5. Liposome formation from bile salt-lipid micelles in the digestion and drug delivery model FaSSIF$_{mod}$ estimated by combined time-resolved neutron and dynamic light scattering

(Running chapter head: Liposome formation in FaSSIF$_{mod}$)

Thomas Nawroth[1], Philipp Buch[1], Karl Buch[1], Peter Langguth[1], Ralf Schweins[2]

[1]Institute for Pharmacy and Biochemistry, Biopharmacy and Pharmaceutical Technology, Johannes Gutenberg-University, Staudinger Weg 5, 55128 Mainz, Germany

[2]Institut Laue-Langevin, Large Structure Group LSS, Avenue des Martyrs, 38042 Grenoble, France

5.1 Abstract

The flow of bile secretion into the human digestive system was simulated by dilution of a bile salt-lipid micellar solution. The structural development upon the dilution of the fed state bile model FeSSIF$_{mod6.5}$ to the fasted state bile model FaSSIF$_{mod}$ was investigated by neutron small-angle scattering and dynamic light scattering in crossed beam experiments in order to observe small and large structures in a size range of 1 nm to 50 µm in parallel. Because of the physiologically low lipid and surfactant concentrations of 2.625 mM lecithin and 10.5 mM taurocholate the sensitivity of the neutron structural investigations was improved by partial solvent deuteration with 71% D_2O, with control experiments in H_2O. Static experiments of initial and end state systems after 6 days development revealed the presence of mixed bile salt-lipid micelles of 5.1 nm size in the initial state model FeSSIF$_{mod6.5}$, and large liposomes in FaSSIF$_{mod}$, which represent the late status after dilution of bile secretion in the intestine in the fasted state. The liposomes depicted a size of 34.39 nm with a membrane thickness of 4.75 nm, which indicates medium to large size unilamellar vesicles. Crossed beam experiments with time-resolved neutron and light scattering experiments after fast mixing with a stopped-flow device, revealed a stepwise structural dynamics upon dilution by a factor of 3.5. The liposome formation was almost complete five minutes after bile dilution. The liposomes 30 min after dilution

resembled the liposomes found after 6 days and depicted a size of 44.56 nm. In the time regime between 3 and 100 s a kinetic intermediate was observed. In a further experiment the liposome formation was abolished when the dilution was conducted with a surfactant solution containing sodium dodecyl sulfate.

5.2 Introduction

Pharmacokinetic studies have become more and more time- and cost-intensive. Therefore, one major focus of the pharmaceutical industry is to minimize the number of clinical studies or better to avoid them. Simulating physiological conditions *in vitro* has gained a critical role in the preformulation step of new drug candidates. As solubility and permeability of a drug are the fundamental determinants of its oral bioavailability, a number of substitute models for both of these parameters have been introduced.

Hydrophobic drugs interact during the delivery and uptake with the bile and lipid systems in the gastrointestinal tract, which have been investigated at non-physiological concentrations in structure and dynamics [142,143]. Biorelevant media including FaSSIF and FeSSIF, representing the fasted and the fed state in the upper jejunum, were proposed by Galia et al. [26]. Dissolution studies conducted with these media better predicted the *in vivo* performance of formulations containing poorly soluble drugs compared to the use of compendial media [144]. Through FaSSIF and FeSSIF dissolution testing has gained a new aspect in the last decade. Besides studying the batch to batch quality of dosage forms, dissolution studies become more and more interesting as predictive model because relevant physiological parameters are taken into account.

In recent years the compositions of FaSSIF and FeSSIF have been modified to update the simulation in the upper small intestine or to make them usable in permeation studies conducted with cell lines. Kataoka et al. [27] utilized the cell culture medium buffer HBSS as base for their biorelevant dissolution media, FaSSIF$_{mod}$ and FeSSIF$_{mod6.5}$, and took over the physiological solubilizing substances, NaTC and lecithin, in the same concentrations as in FaSSIF and FeSSIF. The dissolution media in their original compositions would destroy the integrity of the Caco-2 monolayer which Kataoka et al. use in their dissolution/permeation system. With this system two critical parameters of a drug's oral availability, dissolution and permeability, can be determined at the same time.

In a previous study FaSSIF$_{mod}$ was applied as stock solution in solubility and permeation studies [145]. A good *in vitro*/*in vivo* correlation was observed when the in vitro data from both studies were combined and compared with the C_{max} values for five fenofibrate IR formulations.

Investigating the interactions between the surfactant compositions of all formulations and the emulsifying constituents of biorelevant media it was observed that SDS interfered with the vesicle system of $FaSSIF_{mod}$ and therefore its solubilization capacity.

In the present study small-angle neutron scattering (SANS) and dynamic light scattering (DLS) was applied to get a deeper understanding of the colloidal structures in $FaSSIF_{mod}$. It was focused on characterizing the vesicular system in $FaSSIF_{mod}$ which was detected in FaSSIF before [146] and its interaction with a surfactant formulation containing SDS and a surfactant from the class of poloxamers (S2). The structural dynamics was studied by a fast mixing dilution technique with a stopped-flow device in combination with synchronous time-resolved neutron and dynamic light scattering (TR-SANS and TR-DLS) in a novel double beam technique. This gives information about the structural conversion between the simulated fed to the fasted state as well as during the transport of bile and food in the upper gastrointestinal system.

5.3 Materials and methods

Materials

Lecithin was purchased from Lipoid GmbH. NaTC was kindly donated by Prodotti Chimici e Alimentari S.p.A. via their German agent Alfred E. Tiefenbacher GmbH & Co. KG. All chemicals were at least of analytical grade and purchased from Sigma-Aldrich (Steinheim, Germany) and Merck-VWR (Darmstadt, Germany). The samples and solutions were sterile filtered after preparation. The physiologic salt buffers HBSS and PBS were purchased as sterile solutions from Invitrogen (Carlsbad, CA).

Preparation of $FaSSIF_{mod}$, $FeSSIF_{mod6.5}$ and surfactant solution

As master solution HBSS including 19.45 mM glucose and 10 mM HEPES was used (transport medium, TM). $FeSSIF_{mod6.5}$ was based on TM supplemented with NaTC 15 mM and lecithin 3.75 mM. $FaSSIF_{mod}$ was prepared by diluting $FeSSIF_{mod6.5}$ five times with TM.

The surfactant solution for control experiments contained 1 g/l S2 and 0.747 g/l SDS in TM, based on H_2O or 99.75% D_2O.

Stopped-flow mixing

The stopped-flow experiment should simulate the preparation of $FaSSIF_{mod}$ by diluting $FeSSIF_{mod6.5}$ five times with TM. $FeSSIF_{mod6.5}$ had to be prediluted before the time-resolved experiments because the syringe volumes of the stopped-flow mixing device allowed only a 3.5 times dilution of $FeSSIF_{mod6.5}$.

The DLS was observed at 170° backscattering angle with a ProSpecD 500 projecting DLS optics device from Nanovel (Langenlonsheim, Germany) connected to a single photon detector SIPC-II and a ALV-7001 correlator from ALV. The ProSpecD 500 projecting DLS device contained a polarised Helium-Neon Laser of 5 mW power and mode T_{m00} at 638 nm wavelength and revealed a detection volume of 25 x 25 x 400 µm in 70 mm distance from the device front. The data collection and basic evaluation was done with the ALV3 software for Windows-XP. For the time-resolved experiments the data were collected in 30 s frames using the autoscript modus. The samples were investigated in 2 ml autosampler vials from Chromacol Ltd. (Herts, UK), or directly in 10 x 1 mm quartz cuvettes for neutron scattering, purchased from Hellma (Müllheim, Germany).

For the time-resolved experiments the samples were mixed with a modified pressurized air stopped-flow device SFxM20 from HighTech Scientific (Oxford, UK) connected to a SFC220 triple stopped-flow remote controller from Nanovel. A mixing ratio of 1 + 2.5 (bile salt-lipid solution $FeSSIF_{mod6.5}$: TM or surfactant solution) was selected by the drive-syringes A and B, 1

ml and 2.5 ml, from Kloehn (Las Vegas, NV). The third channel C of the mixing device (1 ml) was used as visco-elastic brake, and drived the stop-syringe D (1ml) bearing the ready-switch by transfer of a viscous 50% glycerol solution through a thin teflon tube (0.3 mm) of 20 cm length. The components from syringes A and B, i.e., bile salt-lipid micelle solution and buffer, were delivered by teflon tubings of 0.8 mm inner diameter to an external 4-channel Tefzel® mixer, which was equipped with a purge valve and a short tubing to the sample cuvette. The sample cuvette was equipped with a bent 0.96 mm steel needle at the side for filling and removal of the used sample after each experiment. For each shot the cuvette was flushed and drained. The filling time was adjusted to 1s by the visco-elastic brake (syringe C) and the driving air pressure (4 bar). The signal from the stop syringe (sample ready) was amplified and converted to a TTL-pulse with the SFC220 controller, and used as trigger signal for starting the data collection of the D11 instrument.

The neutron small-angle scattering experiments were done 2009 with the improved flux version of the D11 instrument [147] at the high flux reactor of the Institut Laue Langevin (Grenoble, France). The instrument has now a flux of 10^8 N/s x cm^2 at the sample at 6.0 Å wavelength. The scattering profiles were observed at 1.2 and 8 m detector-sample distance and collimation using a position sensitive 128 x 128 pixel ^{3}He-detector. The sample cuvette for the time-resolved experiments and additional cuvettes for static samples and references were located in parallel in the standard sample changer device of the D11-instrument, which can take up to 30 samples.

For the double beam SANS-DLS experiments, the projecting DLS device was mounted on a positioning drive from Isel, Eichenzell, 130° tilted above the sample, which was located together with the mixer, purge valve and purge syringe and some reference samples in the standard sample changer device of the D11-instrument. The 170° backscattering detection plane of the projecting DLS was located rectangular to the neutron beam-DLS laser plane.

The experimental setup is shown in Figure 5.1. A parallel monochromatic neutron beam is delivered to a flat Quartz sample cuvette in the D11 instrument. The projecting DLS device containing a Helium-Neon Laser and the detection unit in backscattering geometry was adjusted to the same sample area from above. The laser focus was adjusted ~300 µm behind the entrance window, which avoids light scattering from windows attached particles.

For the time-resolved experiments the DLS data collection with a constant frame width of 30 s was started manually ~3 min before closing the interlock system and triggering the stopped-flow device. The data collection of the SANS after the shot ready signal was done with an initial time resolution of 1 s and logarithmically increase of the frame width by 5.3%/frame.

The neutron data basic evaluation, machine specific corrections and radial averaging, was done with the SANS program pack from Ron Gosh, and GRASP from Charles Dewhurst, both online

available at www.ill.eu. Further evaluation of SANS and DLS data was done using our programs Kinex-Dacon3 from Nanovel, and the datasheet evaluation and plot program SigmaPlot.

a

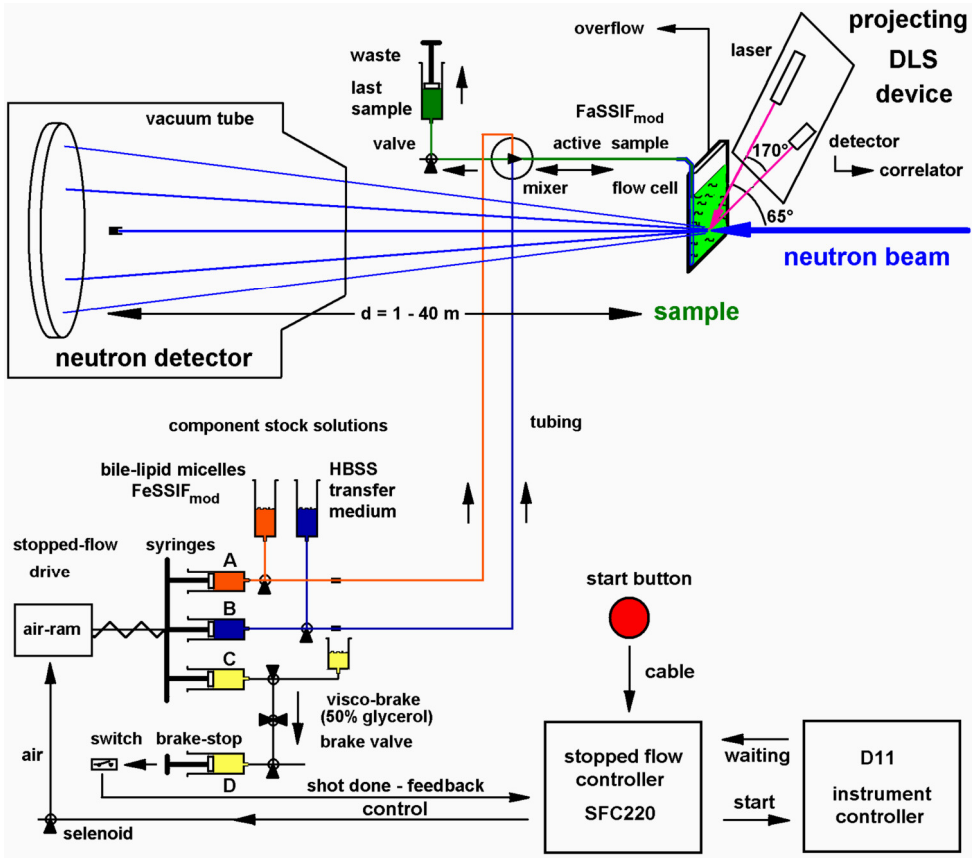

b

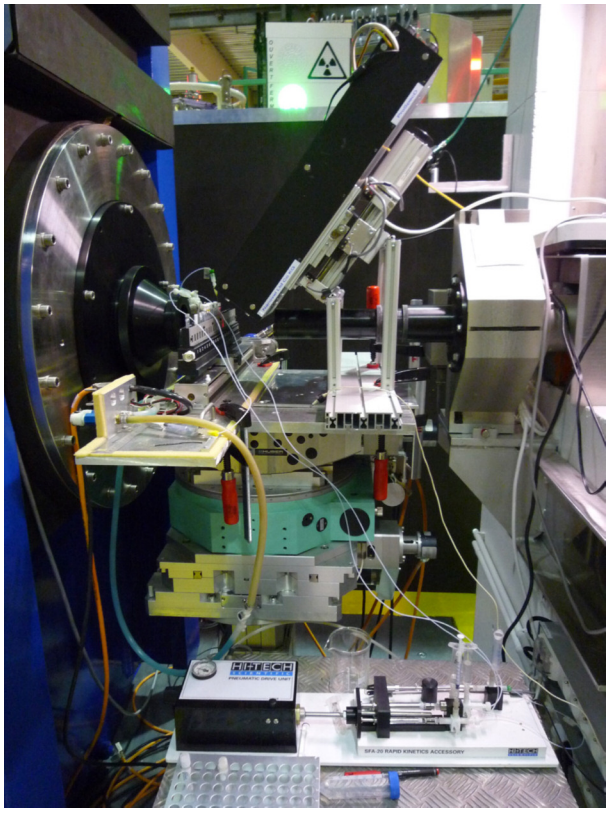

Figure 5.1. Setup for structure dynamics investigation of liposome formation by time-resolved neutron and dynamic light scattering: scheme (a), situation at the instrument ILL-D11 (b).

The scattering profiles were expressed wavelength independent in terms of the momentum transfer q (scattering vector) which was calculated from the neutron wavelength λ and the half scattering angle θ, according to Equation (5.1). The radius of gyration R_g of the liposomes as well as the bilayer thickness d were obtained by Guinier and Kratky-Porod plots [148-150] of the neutron scattering profiles according to Equation (5.2) and Equation (5.3). The radius of gyration R_g is defined as the geometric averaged distance of the scatters from the centre of the object. In case of a solid sphere it is by a factor of $\sqrt{5}/_3$ smaller as the outer particle radius r. It is obtained from the leftmost part of the scattering profile according to Equation (5.2).

(5.1) $q = \frac{4\pi}{\lambda}\sin\theta$ **scattering vector, momentum transfer**

(5.2) $\ln(I(q) = \ln(I_0) - \frac{R_g^{\,2}}{3}q^2$ **logarithmic Guinier equation**

(5.3) $\ln(I_d(q)) = \ln(I_{do})$ - $R_d q^2$ **logarithmic Kratky-Porod equation**

(5.4) $I_d(q) = I(q) \cdot q^2$ **thickness scattering profile I_d(q)**

(5.5) $d = R_d \cdot \sqrt{12}$ **membrane thickness d**

(5.6) $s = 2 \cdot r_m + d \cong 2 \cdot R_g + d$ **liposome size s from SANS**

The thickness radius R_d is obtained from the logarithimic evaluation of the thickness profile $I_d(q)$, which is calculated from the middle part of the scattering profile $I(q)$ by multiplication by the thickness factor q^2 according to Equation (5.4). It is linear, if one dimension of the particle is much smaller than the others, e.g., in case of a plate or a thin walled hollow sphere. With Equation (5.5) the thickness of the membrane d is obtained by multiplication of R_d by root of 12.

In case of spherical unilamellar liposomes the radius of gyration R_g is equivalent to the membrane radius r_m [151]. The Guinier plot allows determination of the radius of gyration R_g of the liposomes by taking the slope m = - $R_g^{\,2}/_3$ of the linear part of the leftmost curve part [152]. The Kratky-Porod plot permits determination of the thickness radius R_d and is related to the membrane thickness d = $R_d \cdot \sqrt{12}$ of the liposomes by taking the slope m = R_d^2 of the linear part of the curve [151]. The size s of the liposomes can be estimated by small-angle scattering by Equation (5.6).

In the DLS experiments the temporal fluctuations of the scattered light were observed at a fixed angle of 170°. This back scattering setup avoids artefacts from multiple scattering [153]. The scattering signal was detected from the scattering object only, i.e., without a reference beam in autobeating mode. The autocorrelation according to Equation (5.7) reveals the intensity

fluctuations in time by varying interparticular interference upon particle motion. In case of moderate particle numbers in the detection volume, ~1000...10^6, the correlation time corresponds to the particle Diffusion coefficient *D*. For solutions of moderate concentration, where the particles do not form a crowded network or gel, the average particle radius *r* is obtained with the Stokes-Einstein relation (Equation (5.8)) from the diffusion coefficient *D*, the solvent viscosity η and the temperature *T*. With the ALV software the evaluation was done by automatic iteration using the "regularized fit" function up to the non-weighted distance distributions *S*(*r*), which represent the composition of the scattered light from contributions of particles of different size (populations). In these raw data the large particles are strongly overweighted as compared to mass-weighted particle size distributions.

(5.7) $G2(\tau) = C(\tau) = \lim_{M\to\infty} \frac{1}{2M} \int_{t=-M}^{M} I(t) * I(t+\tau) dt$ **autocorrelation function in the measure time *M***

(5.8) $D = \frac{k_b T}{6\pi\eta r}$ **Stokes-Einstein diffusion law**

(5.9) $r_{dls} = \sqrt{\frac{a^2 + b^2 + c^2}{3}}$ **average size r_{dls} for solid particles with the main axes *a*, *b*, *c***

(5.10) $C_{m3} = \frac{S(r)}{r^3}$ **particle mass distribution $C_{m3}(r)$ for solid particles, micelles**

(5.11) $C_{m2} = \frac{S(r)}{r^2}$ **particle mass distribution $C_{m2}(r)$ for liposomes**

(5.12) $I_{int} = I_1 \exp[-kt] + I_2 (1 - \exp[-kt])$ **exponential development of SANS of final product (I_2) from a precursor (I_1) without an intermediate**

The further evaluation to mass-weighted particle size distributions $C_m(r)$ was done due to common scattering laws depicted in Equation (5.10) and Equation (5.11): The particle mass as well as the scattering wave amplitude of a single particle is proportional to the number of atoms within. This is for a solid particle proportional to the third power of the radius, but for a hollow sphere as a liposome to the product of second power of the radius and the membrane span, which is constant. The observed intensity is the square of the scattering amplitude value. Thus the mass-weighted solid particle size distribution $C_{m3}(r)$ was estimated by division of the non-weighted size distributions $S(r)$ by r^3 according to Equation (5.10) in case of solid particles, e.g., micelles. But the mass-weighted size distribution $C_{m2}(r)$ for hollow particle were calculated by division of $S(r)$ by r^2 according to Equation (5.11) in case of liposomes, where the membrane

span *d* does not increase with the particle size. In both cases the size of the most frequent particles and the average size represented by the median were estimated.

The radius obtained by DLS experiments r_{dls} is the geometric average of the particle main axes *a*, *b*, *c* according to Equation (5.9), including the hydration shell. Thus it is often larger than the radius obtained by other methods, e.g., in case of bulky headgroups in stealth liposomes [154]. Due to the observation of the fluctuations only, backscattering DLS without angle variation has a typical size error of 10-20%.

5.4 Results

For the observation of the structural development in the bile salt-lipid system in the small intestine we have adapted the FeSSIF$_{mod6.5}$ model, which is suitable to the physical conditions of a fast mixing system with a stopped-flow device and neutron small-angle scattering in double beam experiments. The setup as used at the Institut Laue-Langevin is shown in Figure 5.1. The active sample FaSSIF$_{mod}$ was produced in an external mixer by fast mixing of prediluted bile salt-lipid solution and TM during 1 s and observed during up to 1 h. Static samples were investigated as above, but without mixing in a further cuvette located in the sample changer device (left middle in Figure 5.1.b.

For long structural development time static samples were prepared 6 days before the structural investigation. A homologous sample pair was prepared in H_2O, and 71% D_2O systems in order to improve the particle contrast [155]. The small-angle neutron scattering profiles of the end product FaSSIF$_{mod}$ in 71% D_2O and H_2O are shown in Figure 5.2.a and b. With the resolution of the experiment, the scattering profiles are equivalent, while the profile of the sample in H_2O is rather noisy.

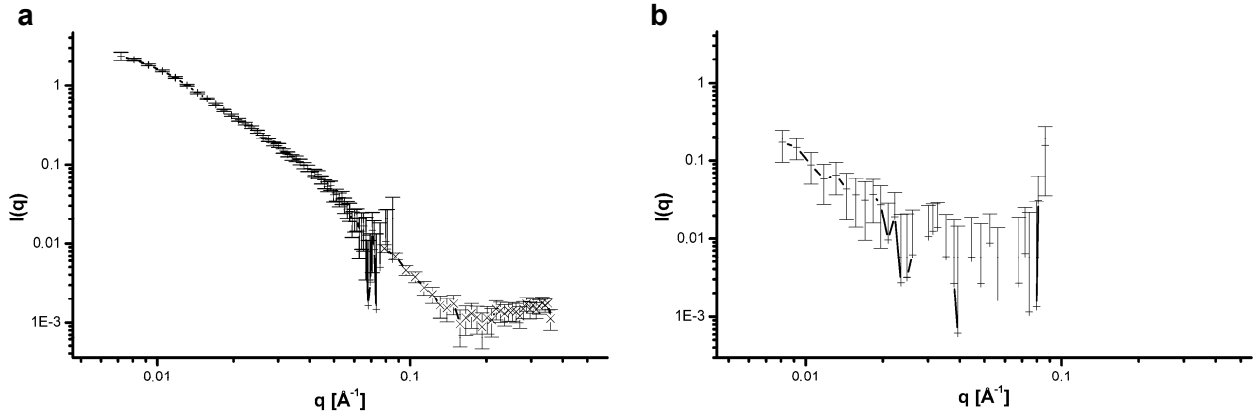

Figure 5.2. Small-angle neutron scattering profiles of the bile salt-lipid mixture FaSSIF$_{mod}$ in 71% D_2O (a) and H_2O (b) 6 d after the dilution of FeSSIF$_{mod6.5}$ (end point). The profile was estimated at sample-detector distances of 1.2 m (a) and 8 m (a and b).

The evaluation of the neutron scattering of the static $FaSSIF_{mod}$ sample in 71% D_2O by the Guinier representation is shown in Figure 5.3.a. From the plot a radius of gyration of R_g = 14.82 ± 0.21 nm was calculated. Figure 5.3.b depicts the evaluation of the same scattering profile by a Kratky-Porod plot, which yields the thickness of the particle in case of flat particles. The plot indicates a lipid layer thickness of d = 4.75 ± 0.21 nm. The combination of both results according to Equation (5.6) yields a liposome size s = 34.39 ± 0.63 nm.

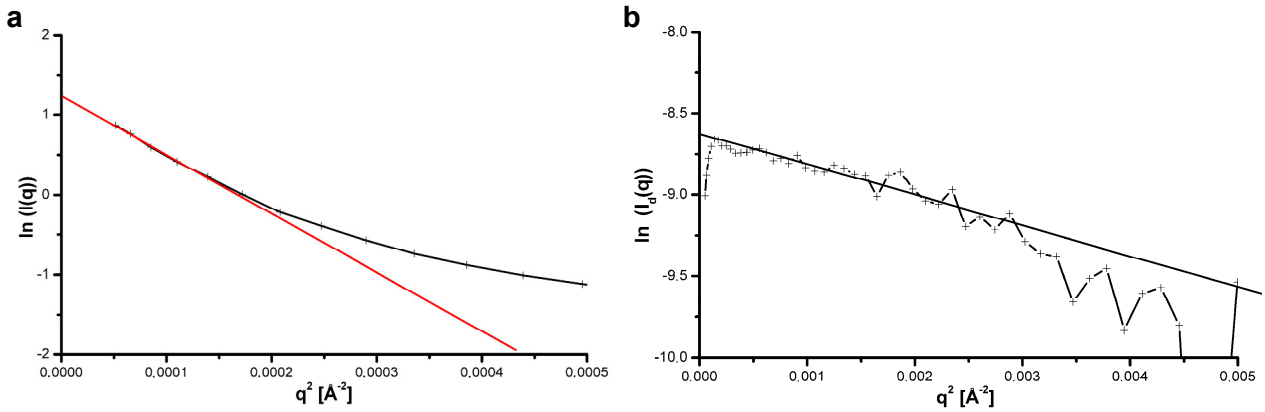

Figure 5.3. SANS evaluation of liposomes in the bile salt-lipid mixture $FaSSIF_{mod}$ in 71% D_2O 6 d after the dilution of $FeSSIF_{mod6.5}$ (end point):
a) the Guinier plot yields a radius of gyration of R_g = 14.82 ± 0.21 nm
b) the Kratky-Porod representation indicates a lipid layer thickness of d = 4.75 ± 0.21 nm. The combination yields a liposome size s = 34.39 ± 0.63 nm.

The 6 day old end product $FaSSIF_{mod}$ sample (diluted) and the initial bile salt-lipid solution $FeSSIF_{mod6.5}$ (concentrated) were investigated by DLS. Figure 5.4. shows the obtained size distributions for the H_2O-samples in a representation depicting the mass fraction of micelles (a) and liposomes (b) according to Equation (5.10) and Equation (5.11), respectively. The D_2O samples were similar (not shown).

With the initial solution $FeSSIF_{mod6.5}$ the particle size distribution in Figure 5.4.a was obtained. The calculated average size of s_{av} = 5.1 nm and most frequent size of s_{max} = 4.1 nm indicates micelles.

The $FaSSIF_{mod}$ end product in Figure 5.4.b revealed an average particle size of s_{av} = 80.3 nm, and a most frequent size of s_{max} = 54.7 nm. This indicates the formation of liposomes in $FaSSIF_{mod}$ from micelles by dilution of the initial solution $FeSSIF_{mod6.5}$.

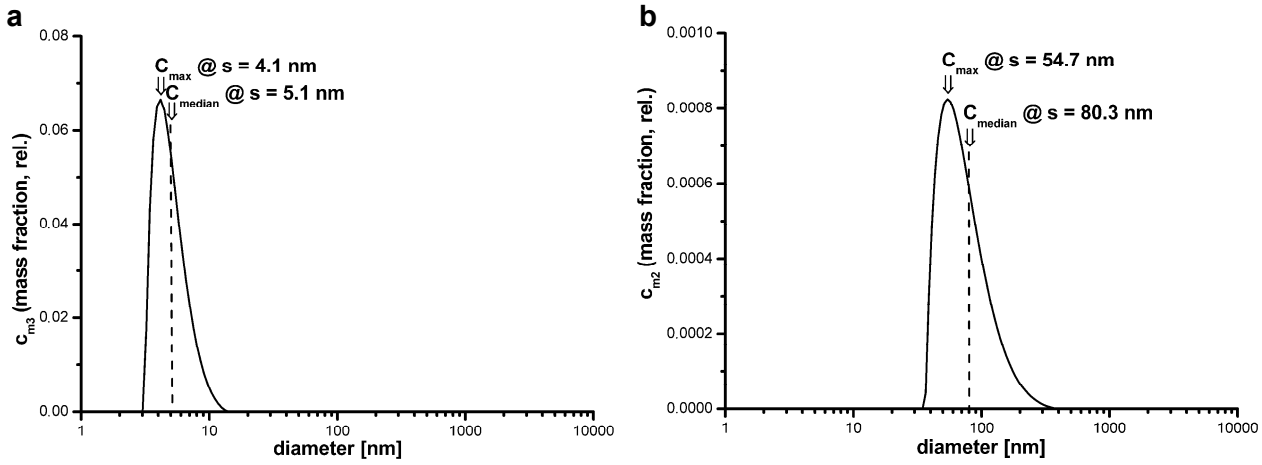

Figure 5.4. Average size estimations by DLS of:
a) bile salt-lipid micelles in the initial solution $FeSSIF_{mod6.5}$
b) liposomes in the bile salt-lipid mixture $FaSSIF_{mod}$ in H_2O 6 d after the dilution of $FeSSIF_{mod6.5}$ (end point).

In a special experiment the liposome formation was prevented by changing the dilution solution for the preparation of $FaSSIF_{mod}$. TM was substituted by a surfactant solution containing a SDS-S2 mixture. Upon dilution the resulting end product (FaSSIF-SDS-S2, $FaSSIF_{SDSS2}$) comprised the same bile salt-lipid compared to $FaSSIF_{mod}$. The static neutron scattering of the samples in 71% D_2O and H_2O after 6 d development is shown in Figure 5.5. The noisy profile (b) of the H_2O sample depicts no additional signal at low q as compared to the contrast enforced D_2O specimen (a). Thus the profile of the sample in 71% D_2O was evaluated.

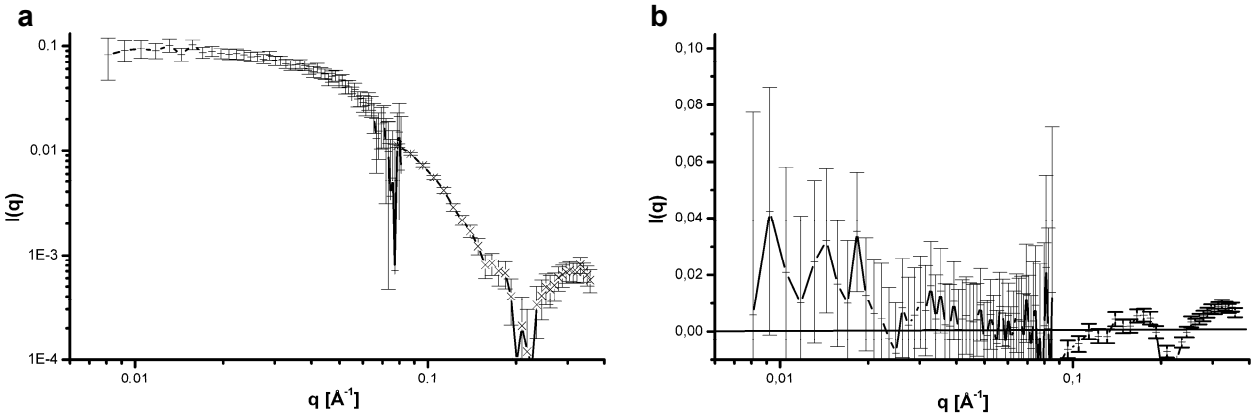

Figure 5.5. Small-angle neutron scattering profiles of the surfactant resolved bile salt-lipid mixture $FaSSIF_{SDSS2}$ in 71% D_2O (a) and H_2O (b) 6 d after the dilution of $FeSSIF_{mod6.5}$ (end point). The profile was estimated at sample-detector distances of 1.2 and 8 m.

The particle size estimation of the surfactant resolved $FaSSIF_{SDSS2}$ particles in 71% D_2O after 6 d development by a Guinier representation of SANS is shown in Figure 5.6. The plot yields a radius of gyration of R_g = 2.96 ± 0.05 nm. The trial of a Kratky-Porod plot yielded no straight line. This indicates the structure of the surfactant resolved $FaSSIF_{SDSS2}$ particles as micelles.

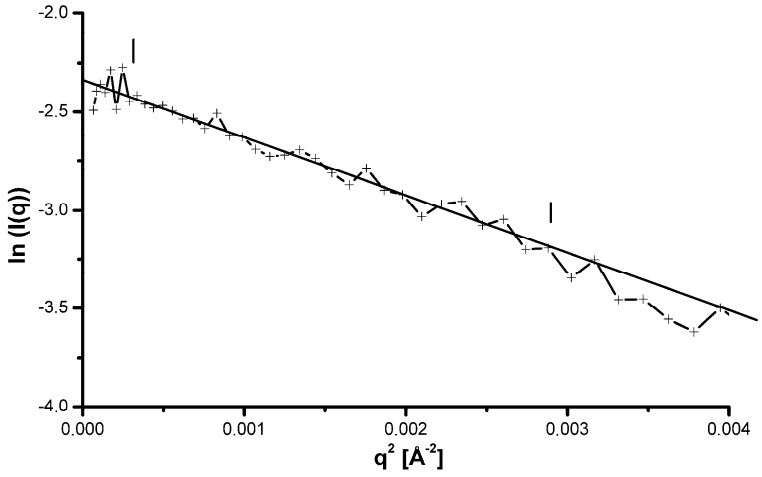

Figure 5.6. SANS evaluation of micelles in the surfactant resolved bile salt-lipid mixture $FaSSIF_{SDSS2}$ in 71% D_2O 6 d after the dilution of $FeSSIF_{mod6.5}$ (end point): the Guinier plot yields a radius of gyration of R_g = 2.96 ± 0.05 nm.

Figure 5.7. depicts the investigation of surfactant resolved $FaSSIF_{SDSS2}$ by DLS. The size distribution was treated as for massive particles according to Equation (5.10). The obtained average particle size was s_{av} = 6.5 nm while the most frequent particle size was s_{max} = 5.3 nm.

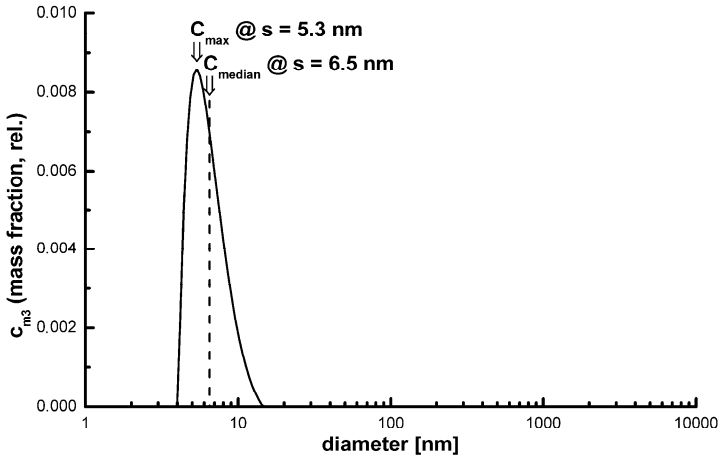

Figure 5.7. Average size estimation of micelles in the surfactant resolved bile salt-lipid mixture $FaSSIF_{SDSS2}$ in 71% D_2O 6 d after the dilution of $FeSSIF_{mod6.5}$ by DLS (300 s).

The structural development of $FeSSIF_{mod6.5}$ to $FaSSIF_{mod}$ in 71% D_2O after dilution by fast mixing was investigated by double beam-time-resolved SANS and DLS. The time-resolved neutron scattering profile is shown in Figure 5.8. as 3D plot with logarithmic time resolution. The data of the early time frames are noisy due to the short span (1 s), while the signal at the shot end (front) is improved by the longer frame width (72.7 s). The duration of the experiment was 1389 s. Figure 5.9. depicts the neutron scattering profile of the last frame. The signal to noise ratio of 500 enabled a further evaluation.

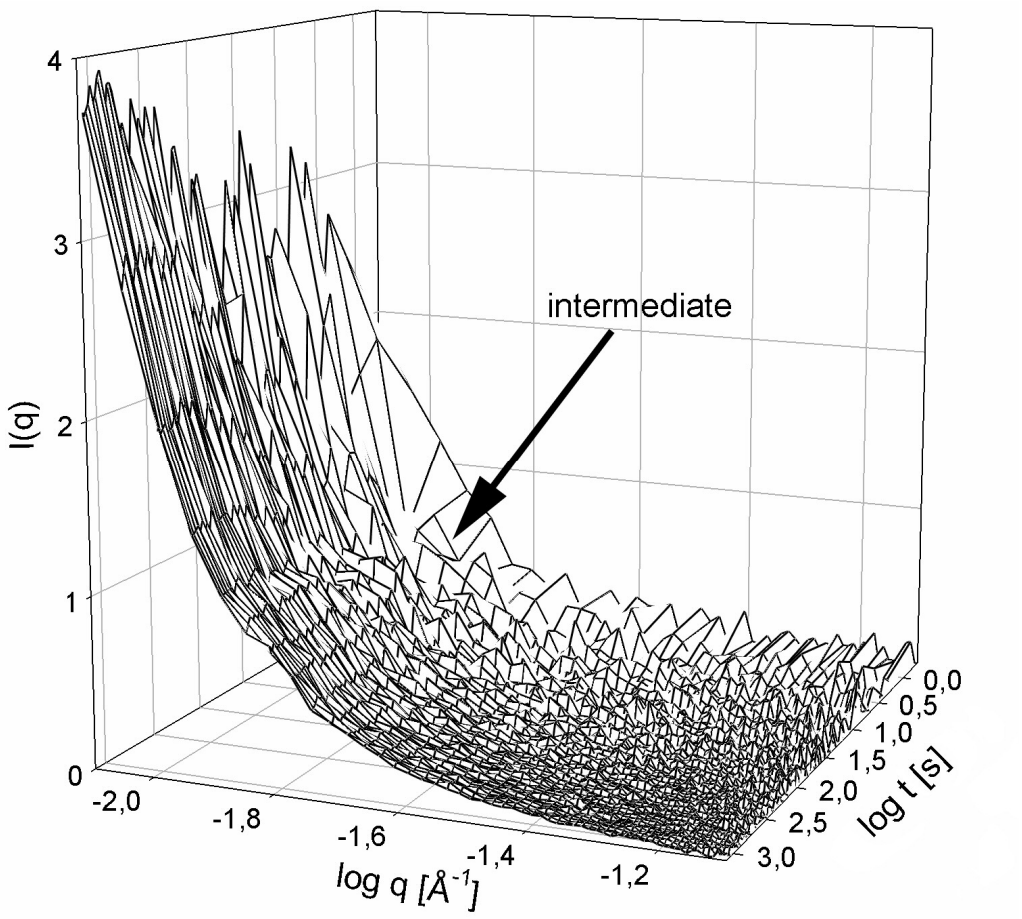

Figure 5.8. Time-resolved neutron scattering profiles of the bile salt-lipid mixture $FaSSIF_{mod}$ in 71% D_2O upon fast dilution of $FeSSIF_{mod6.5}$ with TM with a stopped-flow device: 3D representation (lin-log) of the development in time after dilution.

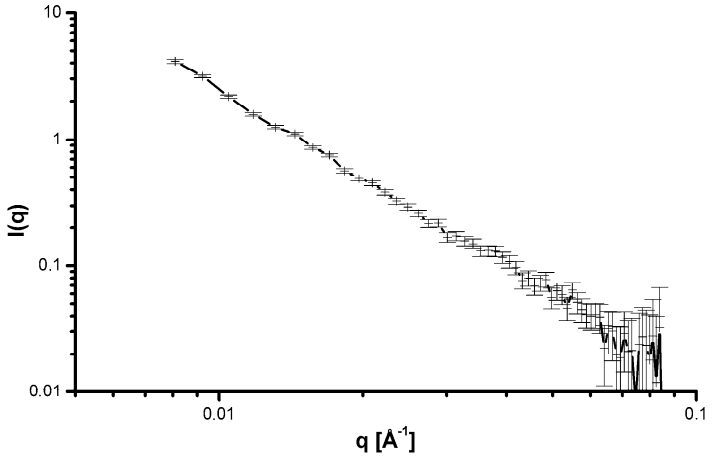

Figure 5.9. SANS of the last time frame of time-resolved neutron scattering at 1389 s.

The evaluation of the neutron scattering profile from the last frame in the time-resolved investigation is shown in Figure 5.10. The Guinier plot (a) yielded a radius of gyration of R_g = 19.91 ± 0.46 nm. The Kratky-Porod plot (b) contained a noisy linear range, which indicates a lipid layer thickness of about d = 4.74 ± 0.63 nm. This indicates liposomes of a size of s = 44.56 ± 1.55 nm.

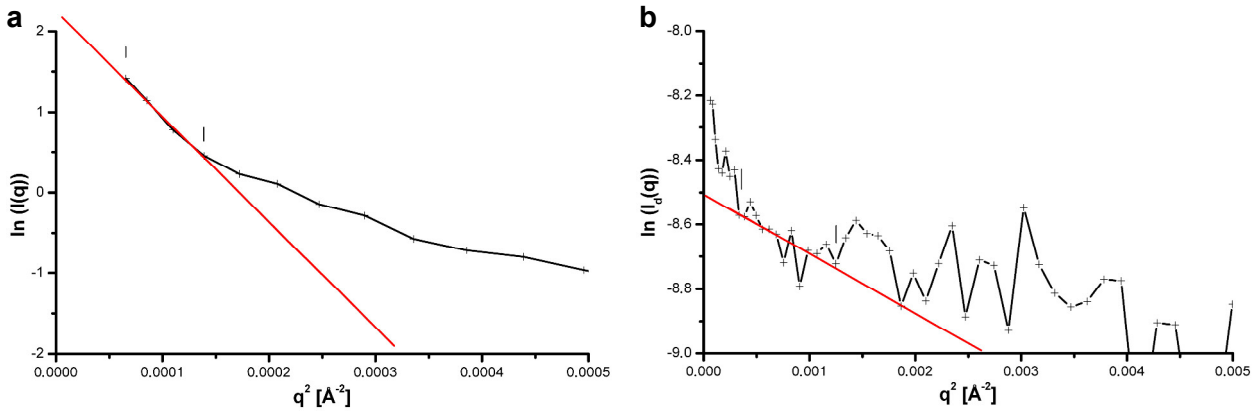

Figure 5.10. SANS evaluation of liposomes in FaSSIF$_{mod}$ (71% D_2O) at 1389 s (last time frame, 72.7 s duration) upon dilution of the bile salt-lipid mixture FeSSIF$_{mod6.5}$:
a) the Guinier plot yields a radius of gyration of R_g = 19.91 ± 0.46 nm
b) the Kratky-Porod representation indicates a lipid layer thickness of about d = 4.74 ± 0.63 nm. The combination yields a liposome size s = 44.56 ± 1.55 nm.

For the kinetic evaluation of the neutron scattering the integral particle scattering after buffer subtraction $I_{int}(t)$ was estimated according to Equation (5.12). Figure 5.11.a depicts the development of the integral particle scattering of the system in 71% D_2O upon time after the concentration jump with logarithmic time scale. The profile consists of three phases: (A) early (t < 3 s), (B) intermediate (3-100 s), and (C) late (> 100 s). The late phase revealed a delayed linear behavior in the semi-logarithmic plot, shown in Figure 5.11.b. The formation of the late product is described by the constant k_3 = 0.00961 ± 0.00125 s^{-1} ($t_{1/2}$ = 72.1 ± 10.8 s). The initial material depicted a relative scattering intensity of I_1= 557 ± 78, the end product a value of I_2 = 917 ± 10. The calculated exponential function is drawn in Figure 5.11.a in green colour, in comparison to a simple linear extrapolation of the late phase (black line). The difference between the experimental data and the late exponential behavior was evaluated further as an evidence of an intermediate.

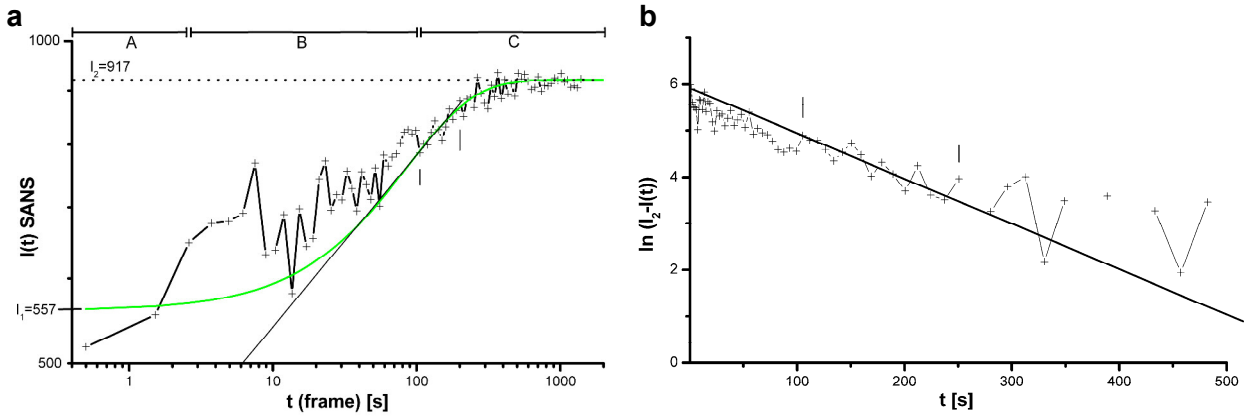

Figure 5.11. a) Biphasic development of integral SANS (buffer subtracted) upon time in FaSSIF$_{mod}$ (71% D_2O) after dilution of the bile salt-lipid mixture FeSSIF$_{mod6.5}$. The late development at long time (range C) is extrapolated by a straight line and exponential function (green);
b) Kinetics of liposome formation upon time after dilution of the bile salt-lipid mixture FeSSIF$_{mod6.5}$ to FaSSIF$_{mod}$ (71% D_2O) estimated by semi-logarithmic plot of SANS data range C.

The difference signal, experiment signal minus late exponential function, is shown in Figure 5.12.a with logarithmic time scale. The profile depicts the peaklike contribution of an intermediate between 3 s and 100 s after the concentration jump. The kinetic evaluation by a semi-logarithmic plot in Figure 5.12.b yielded time constants of k_1 = 0.114 ± 0.025 s^{-1} ($t_{1/2}$ = 6.1 ± 1.7 s) for the formation and k_2 = 0.0178 ± 0.0058 s^{-1} ($t_{1/2}$ = 39.0 ± 18.7 s) for the decay.

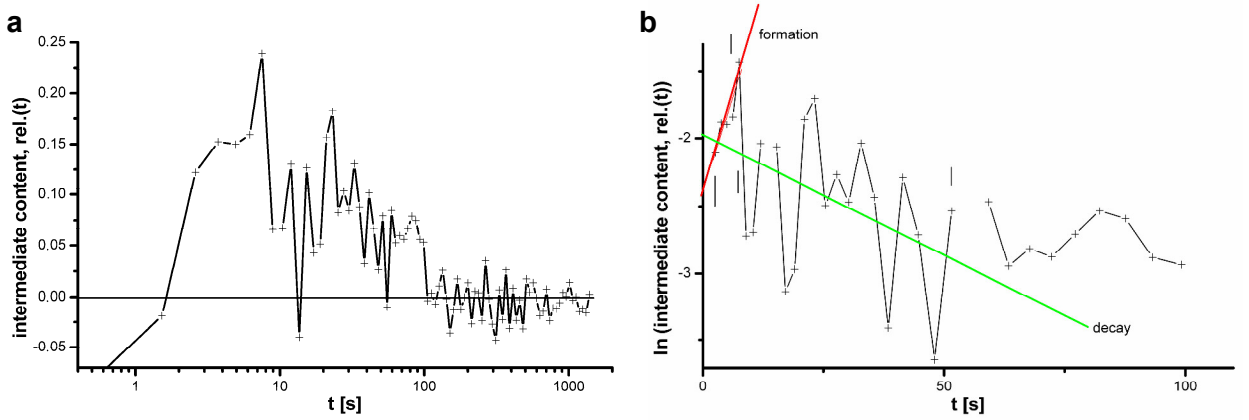

Figure 5.12. a) Development of intermediate signal in integral SANS (buffer subtracted) in FaSSIF$_{mod}$ (71% D_2O) upon time after dilution of the bile salt-lipid mixture FeSSIF$_{mod6.5}$;
b) Formation and decay kinetics of the bile salt-lipid intermediate upon time after dilution of the bile salt-lipid mixture FeSSIF$_{mod6.5}$ to FaSSIF$_{mod}$ (71% D_2O) estimated by semi-logarithmic plot of SANS data range B (Figure 5.11.a).

The structural development after the concentration jump in the same experiment, but analyzed by time-resolved DLS is shown in Figure 5.13.a as 3D representation. The plot depicts the non-weighted distance distributions $S(r)$ after normalization the maximum peak height to unity, which is suitable for comparison of signals from different samples. The development after mixing (back) to equilibrium (front) indicates the transient occurrence of at least three particle populations. The peak shift in the non-weighted time-resolved DLS signal indicates the transformation of particles of 15 nm size to those of 100 nm diameter.

The size distribution at the end of the shot in Figure 5.13.b was weighted to mass contribution of liposomes according to Equation (5.11). The average size was s_{av} = 99.4 nm, the most frequent particles had a diameter of s_{max} = 70.7 nm.

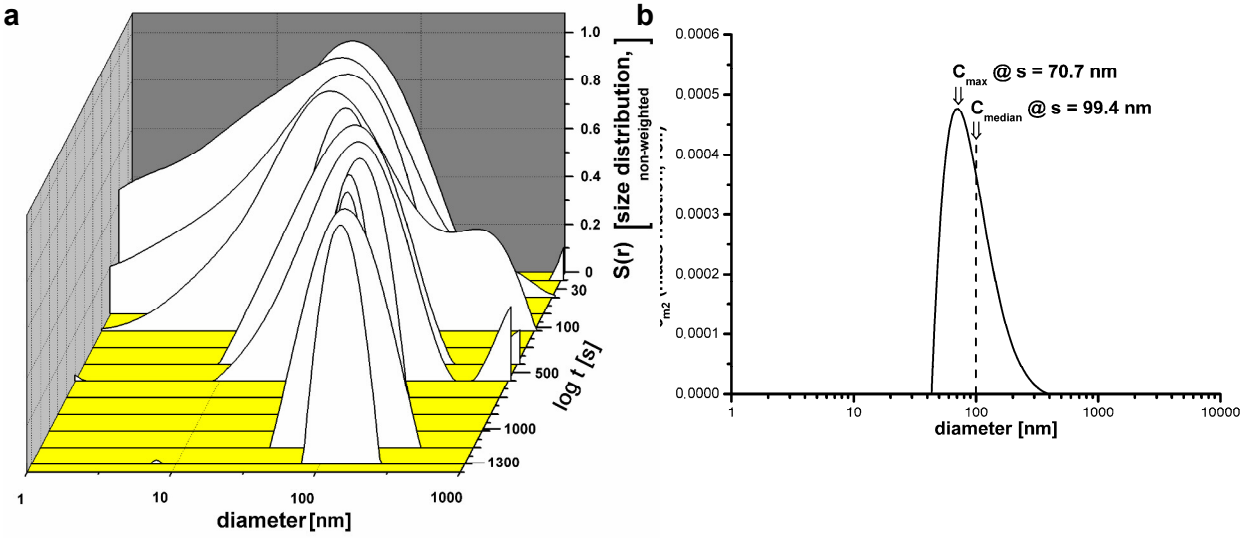

Figure 5.13. a) The particle size distribution (non-weighted, normalized to 1) in TR-DLS upon time after dilution of the bile salt-lipid mixture FeSSIF$_{mod6.5}$ to FaSSIF$_{mod}$ (71% D_2O) shows a peak shift from a broad double peak of small particles to unique large particles. Between 30 and 120 s after the concentration jump an intermediate of 15-110 nm size occurs;
b) Mass-weighted average size distribution $C_{m2}(s)$ of liposomes in the bile salt-lipid mixture FaSSIF$_{mod}$ in 71% D_2O at the end of time development after dilution (front in (a)), obtained with a TR-DLS frame duration of 300 s.

5.5 Discussion

Considering the various routes of administration for new drug entities, the oral route remains the most common. Besides the permeability, the solubility behavior of a drug is a crucial factor of its oral bioavailability. With the increasing number of poorly soluble active substances in the pharmaceutical industry the issue of low bioavailability due to solubility-limited absorption is one of the greatest challenges to formulation scientists. Hydrophobic drugs form intermediate complexes with bile and lipids and their nanostructured assemblies in the gastrointestinal system [156]. This interaction is the key for the development of formulations providing sufficient bioavailability of lipophilic drugs.

A dissolution test capable of evaluating the impact of formulation and manufacturing attributes on drug release from a solid oral drug product under physiological conditions may avoid time- and cost-expensive clinical studies to some extent. To forecast the *in vivo* performance of an active substance after oral administration from *in vitro* data, it is important that the parameters limiting absorption are met in the *in vitro* model. More than ten years ago Galia et al. [26] introduced the biorelevant dissolution media FaSSIF and FeSSIF, representing the pre- and postprandial states in the upper jejunum. Regarding the media composition several important aspects of the luminal fluids were taken into account, namely osmolarity, buffer capacity, pH and especially surface tension. Information about the characteristics of the gastrointestinal fluids, e.g., bile salt and lecithin concentrations in the fasted and fed state, were gathered from the literature [17].

Dissolution data obtained from several poorly soluble but highly permeable compounds were shown to correlate well with observed human pharmacokinetic data gathered under fasted and fed conditions [144]. Regarding this class of compounds the differences in bioavailability in the fasted and the fed state are commonly due to the presence of food which may lead to an increase in solubility and dissolution [157]. Although FaSSIF and FeSSIF are simplified models of the gastrointestinal composition, they have been shown to forecast the effect of food on absorption of poorly soluble drugs and have found application in the pharmaceutical industry to evaluate new drugs and dosage forms. Over the years the biorelevant media have been slightly adjusted to improve the predictions of *in vivo* performance or to render them suitable in permeation studies conducted with cell lines [27]. In a previous study it has been shown that the D/P system combined with the modified biorelevant dissolution media, FaSSIF$_{mod}$ and FeSSIF$_{mod6.5}$, was able to predict the *in vivo* performance in rats of solid oral dosage forms containing the poorly soluble and highly permeable drug fenofibrate [127].

In a further study it was observed that SDS interfered with the vesicular drug solubilizing system of FaSSIF$_{mod}$ and antagonized its solubilization capacity in regards to fenofibrate [145].

This study provides a deeper characterization of the colloidal structures in the bile salt-lipid mixture developed by this interference with SDS via small-angle neutron scattering. Furthermore not only the colloidal structures of FeSSIF$_{mod6.5}$ and FaSSIF$_{mod}$ through static measurements but also the structural development after dilution of FeSSIF$_{mod6.5}$ to FaSSIF$_{mod}$ was investigated. The dilution of FeSSIF$_{mod6.5}$ to FaSSIF$_{mod}$ is both the common preparation method of FaSSIF$_{mod}$ and a simplified simulation of the concentrated bile's fate upon secretion into the small intestine and subsequent transport (Figure 5.14.). The simulation of the fasted state by FaSSIF$_{mod}$ is relevant for the uptake of drugs, which are administered on an empty stomach.

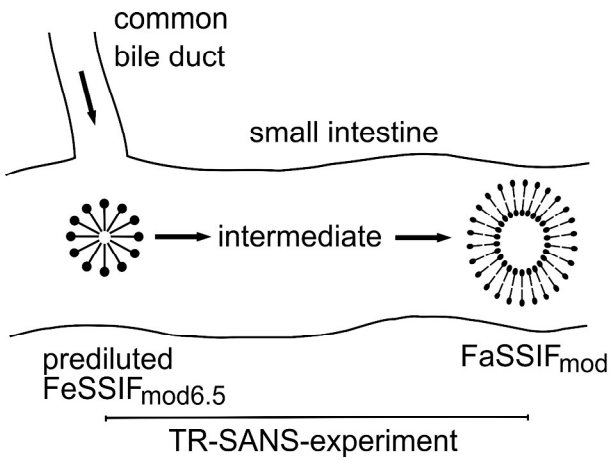

Figure 5.14. Structural dynamics scheme of liposome formation upon dilution of bile salt-lipid mixture FeSSIF$_{mod6.5}$ with subsequent gastrointestinal transport simulating the fasted state.

The structures of micelles, mixed micelles and membrane structures of surfactant-lipid-drug systems may vary between the lower nanometer and the micrometer scale. Those systems may contain different nanoparticles in parallel. A combination of neutron and dynamic light scattering is capable of simultaneous detection of those particles and mixtures. This covers a combined size range of 1 nm to 50 µm with high precision of the SANS range up to 100 nm (at 6 Å wavelength and 8 m distance) and moderate error of 10-20% in the DLS range. Simultaneous SANS-DLS experiments in double beam technique are mandatory, if the lipid- surfactant system undergoes dynamic transitions, or if the sensitive structures are unstable. With the current work we have established a synchronous double beam-time-resolved SANS-DLS technique with sample preparation by fast mixing with a stopped-flow device. The setup with a projecting DLS device according to Figure 5.1. allowed the use of external sample cuvettes in the standard environment of the D11 instrument. The limit in time resolution of 1 s for the SANS investigation and 30 s for the DLS test was given by the technical conditions. Especially the low concentrations of lipid and surfactant were given by the pharmaceutical FaSSIF$_{mod}$/FeSSIF$_{mod6.5}$ system [27], which is much lower as compared to earlier investigations of the physical-chemical

behavior of concentrated bile-lipid systems [34,158]. The SANS signal to noise ratio of the dilute $FaSSIF_{mod}$/$FeSSIF_{mod6.5}$ systems was improved by partial solvent deuteration. The D_2O content was limited to 71% in order to prevent a possible change of sensitive aggregation behavior at high deuteration level [159]. The comparison of the scattering profile of $FaSSIF_{mod}$ with the equivalent solution in H_2O in Figure 5.2. revealed no significant difference, despite the better signal quality of the D_2O sample. It was concluded that the structures in 71% D_2O and H_2O are similar. Thus the time-resolved investigation of the structural dynamics after a concentration jump were done with samples in 71% D_2O buffer.

The end product of the dilution of $FeSSIF_{mod6.5}$ to $FaSSIF_{mod}$ after 6 days development in 71% D_2O was investigated by static SANS and DLS. The neutron scattering revealed a scattering profile typical for unilamellar liposomes (Figure 5.2.a). Narrow side maxima, which would appear in case of multilamellar vesicles were, not detected. The size estimation by Guinier plot with a short linear range (Figure 5.3.a) yielded a radius of gyration of 15 nm. The span of the membrane of d = 4.75 nm was estimated by a Kratky-Porod plot, which depicted a remarkable broad linear range. Thus the particles in $FaSSIF_{mod}$ are large unilamellar liposomes (LUV) of s = 34 nm, similar to those detected in more concentrated systems in the literature [160]. The size distribution of the same system estimated by DLS in Figure 5.4.b revealed a larger average particle diameter of 80 nm. This includes the hydration shell, but possibly a part of the broad size distribution was not seen by the SANS experiment due to the limitation in the q-range. The tenfold expansion of the q-range, possible at the new D11 instrument, was not used as it would have abolished the possibility for time-resolved experiments by intensity reasons.

The investigation of the more concentrated initial solution $FeSSIF_{mod6.5}$ by DLS in Figure 5.4.a indicated small particles of a diameter of 5.1 nm only. As this is too small for the formation of an aqueous lumen these are micelles, as described for similar and more concentrated systems in the literature [146]. The detection of micelles in $FeSSIF_{mod6.5}$ and vesicles in $FaSSIF_{mod}$ is consistent with findings reported in the literature. Despite the huge variety in composition of different biorelevant media the existence of micelles and vesicles can be related to media simulating the fed and the fasted state, respectively [33]. The colloidal structures in different media might solely differ in size and composition, because the particle morphology is affected by the characteristic of the chosen bile salts and phospholipids and the ionic strength of the medium [161].

As a test for the surfactant dependence of the $FeSSIF_{mod6.5}$/$FaSSIF_{mod}$ system the dilution of $FeSSIF_{mod6.5}$ was done with a surfactant mixture of a poloxamer and SDS. The neutron scattering and DLS of this surfactant system, which had the same bile salt-lipid content as $FaSSIF_{mod}$ is shown in Figure 5.5. to Figure 5.7. Both methods indicate small particles. A Kratky-Porod representation of the SANS data (not shown) contained no linear range. Thus no aqueous

lumen was detected. The assumption of spherical particles yields a particle size of $s = R_g \times \sqrt{5}/3$ = 3.8 nm. The value is consistent with the particle size distribution from 3 to 14 nm estimated by DLS (Figure 5.7.) with an average size of s_{av} = 6.5 nm. Thus the surfactant resolved bile salt-lipid particles are micelles.

The time-resolved neutron scattering profiles in Figure 5.8. show the structural development of the freshly prepared $FaSSIF_{mod}$ in the first 23 minutes after dilution from $FeSSIF_{mod6.5}$ by a factor of 3.5. The time resolution (frame width) increased logarithmically by a factor of 1.053 per frame from 1 s to 72.7 s at the end of the shot. Thus the early scattering curves are rather noisy and resemble that of taurocholate micelles from literature [160]. In the subsequent time range of 3 to 100 s (log ~1.5) a temporal peak appeared, which is identified as dynamic intermediate below. At long time (front) the profile developed to a stable signal of large particles.

For a clearer view the last frame of the film is depicted in Figure 5.9. It resembles that of the 6 days old $FaSSIF_{mod}$ shown in Figure 5.2.a. Narrow and intense side maxima, which would appear with multilamellar liposomes were not detected. Also the size estimation of the material in the last film frame in Figure 5.10.a yielded a radius of gyration of R_g = 20 nm, which is a similar value of the 6 days old preparation (15 nm). The estimation of the membrane span by a tentative Kratky-Porod plot in Figure 5.10.b was rather noisy, due to the short exposition time. Nevertheless the obtained coarse value of d = 4.74 ± 0.63 nm is comparable to that of the static sample of d = 4.75. The results indicate that the $FaSSIF_{mod}$ solution contains already 23 min after preparation equivalent particles as after 6 days development, i.e., large unilamellar liposomes LUV.

For the kinetic analysis of the time-resolved neutron scattering the total particle scattering signal after buffer subtraction was integrated. Due to Figure 5.2.a, Figure 5.5.a and Figure 5.8. this integral signal consists in our case by > 95% of the first term of the scattering profiles, which corresponds at constant concentration to the particle size. The time dependent profile of the integral scattering consists of three phases, which are depicted as A, B, C in Figure 5.11.a. In the last period C the final product LUV is formed in an exponential process. The formation kinetics of this is analyzed in Figure 5.11.b by a semi-logarithmic plot. As result a half formation time of 72 s and the initial scattering rate was estimated. The extrapolated exponential formation curve for short time is shown in Figure 5.11.a additionally. In the initial phases A, B up to 100 s after mixing the integral scattering signal showed a significant deviation from the late product contribution. The initial scattering signal up to 2 s corresponds to the scattering of the freshly diluted solution of micelles. In the time regime between 3 and 100 seconds (phase B) an extra signal occurred. This is well seen in the difference signal between experimental curve and the extrapolated late product contribution depicted in Figure 5.12.a. Obviously a metastable intermediate is formed during the first 10 seconds after mixing. It vanishes during the first 2

minutes of the shot. The kinetic analysis of intermediate formation and decay by a semi-logarithmic plot of the difference signal is depicted in Figure 5.12.b. With the limited resolution of the experiment the formation of the intermediate occurs with a half formation time of 6 s. The half life time for the decay was 39 s.

The synchronous time-resolved DLS investigation of the same sample had a constant time resolution of 30 s. The formation of the late product LUV is clearly detected by the peak shift of the unweighted size distribution in Figure 5.13.a in the time regime > 100 s. The investigation of the final product during 300 s shown in Figure 5.13.b as the mass weighted size distribution yielded an average particle size of 99 nm and a most frequent size of 71 nm. These values are comparable to the estimation by SANS, if one takes into account, that the DLS size analysis includes the hydration shell, and the limitation of the SANS profile at low scattering vector *q*, which is equivalent to a large particle cut off. The occurrence of the intermediate is in the DLS profile visible in the short time range, i.e., in the first four frames up to 120 s. The broad shoulder in the second frame after mixing may correspond to an intermediate mixture.

The presented method of combined structural investigation by time-resolved neutron small-angle and dynamic light scattering in double beam experiments allows the estimation of the structural development in a broad size range from 1 nm to 50 µm. The limited precision of the DLS size estimations in the large particle regime (> 200 nm) of 20 % is acceptable as the structure of smaller particles is obtained more precisely by the neutron scattering. The resolution of the structural dynamics and development is 1-5 s with single shot experiments, as in the presented investigation, and 0.1-1 s in multiple repetition experiments.

The metastable intermediate detected in the current investigation obviously consists of bile salt-lipid aggregates, probably mixed micelles. For mixed micelles in the chemical and temporal equilibrium the structures were investigated extensively in the literature [146,162]. The structure of the metastable dynamical micelles detected here has to be resolved by later investigations. The intermediate micelles may play a role for drug uptake by solubilizing hydrophobic drugs leading to an enforced uptake.

5.6 Acknowledgments

We thank for support by the Bundesministerium für Forschung und Technologie (BMBF, grant no. 05KS7UMA) and the Institute Laue Langevin, Grenoble, France.

Discussion

The current work unveils the importance of determining the effects of the dosage form excipients on solubility and permeability of a drug, enabling the prediction of its *in vivo* performance. In chapter 2 it was shown that the D/P system is able to predict the *in vivo* performance of different fenofibrate IR formulations in rats and to simulate the effect of food on the absorption of fenofibrate. A self-developed lipid microparticle formulation was among the fenofibrate formulations investigated. Previously performed *in vitro* measurements (e.g., *in vitro* dissolution) revealed that this formulation failed to significantly diminish the food effect of fenofibrate due to several reasons which are beyond the scope of this thesis. Therefore, this formulation was additionally applied in these studies to encompass a broad spectrum of IR fenofibrate formulations, from very poor to excellent. For the development of an IVIVC several formulations displaying different performances *in vivo* which can be reflected *in vitro* are necessary.

The establishment of an IVIVC is more cumbersome when the pharmacokinetic parameters of different formulations vary only slightly because the finding of a differentiating *in vitro* method may be difficult. This was the case for the six fenofibrate IR tablet formulations which were tested in two *in vivo* human studies (see chapters 3 and 4). Since all tablets were subjected to a bioequivalence study they exhibited only slight differences in their *in vivo* performance. No significant difference was detected regarding the $AUC_{0\text{-}inf}$ values, whereas an obvious variation in C_{max} was detected.

Reviewing the literature it might be suggested that the *in vivo* performance of these fenofibrate tablets could be simulated through their dissolution properties because dissolution is commonly the absorption rate limiting parameter for a BCS class II drug (see section 1.2.3). The application of several *in vitro* methods led to the conclusion that a combination of *in vitro* solubility and permeation measurements was able to differentiate between the formulations of five tablets manufactured by the same technique. This *in vitro* data could be successfully correlated with the C_{max} values obtained in humans (see section 4.4). However, no differentiation was seen based solely on the *in vitro* dissolution properties.

It has been stated in section 1.2.3 that *in vitro* dissolution and permeation studies should be conducted under physiologically relevant conditions (e.g., dissolution volume, permeation area). This would preferentially include simultaneous determination of dissolution and permeation, since both processes are related *in vivo*. The promising D/P system could not be used due to an adaption of the *in vitro* dose/dissolution volume ratio to more realistic *in vivo* conditions (see section 1.1.2.3). Increasing the concentrations of formulation excipients (e.g., SDS) would have destroyed the Caco-2 monolayer used in the D/P system.

An equilibrium dialysis device comprising cellulose membranes was the method selected to examine the permeation of fenofibrate (see chapter 3). Assuming a dissolution volume of 50 ml *in vivo*, a complete dosage form could not be applied to the apical side of the permeation unit as only a maximum volume of 4 ml was accepted. The application of an appropriate fraction of each tablet to the apical chamber would have resulted in undetectable low fenofibrate concentrations permeated into the receiver chamber. This was confirmed by dissolution studies conducted with complete dosage forms in 50 ml $FaSSIF_{mod}$ which resulted in less than 0.5% of the fenofibrate dose in solution (see section 3.5).

Therefore, dissolution and permeation assays were conducted separately with a subsequent combination of both data sets (see chapters 3 and 4). Dissolution assays were substituted by solubility measurements, since dissolution studies showed no potential to differentiate between the tablets matching their *in vivo* performance (see sections 3.4 and 3.5). It was attempted to simulate the *in vivo* conditions as closely as possible by utilizing the surfactant compositions of the fenofibrate formulations in biorelevant medium to both assays. Different surfactant concentrations were tested to get a deeper scientific insight into the contributions of different surfactant compositions to oral absorption and the mechanisms of altering dissolution and/or permeation.

It might be argued that a dialysis membrane is not representative of physiological conditions. Certainly, transport through a porous membrane is not able to substitute the multivariate processes involved in drug permeation. But the permeation experiments with dialysis membranes were able to unveil the incorporation of dissolved fenofibrate into micelles as potential explanation of the *in vivo* performance of the six IR tablets (see chapter 3). As a change in the dose/dissolution volume ratio increased the excipient concentrations in the medium, Caco-2 monolayers could not be used. Although Caco-2 assays might be considered as standard for permeation studies, they nevertheless do not contain all characteristics of the intestinal epithelium, as has been outlined in section 1.1.1. This might be the reason why admittedly various compounds of all BCS classes have been tested in the aforementioned dissolution/Caco-2 systems but studies with compounds significantly taken up by transporters are missing.

Moreover, large interlaboratory variability has been reported for Caco-2 permeability studies since this heterogeneous cell population is exposed to different selection pressures in different laboratories [6]. On the contrary, the use of an artificial membrane provides more reproducible data. Further advantages of an artificial membrane to a Caco-2 cell monolayer are the better resistance to various pH values, sheer force, different osmolarities and toxic excipients to mention the most important. The application of an artificial membrane instead of a cell monolayer in a dissolution/permeation device would allow an expansion of the permeation

area/dissolution volume ratio, since artificial membranes are available in any shape and size. The permeation area provided by the Caco-2 cell monolayer is narrowed by the specified dimensions of the Transwell® device. An enlarged permeation area in a dissolution/permeation device would resemble more closely the intestinal epithelium, since the foldings, villi and microvilli provide a vast permeation area *in vivo*.

Due to the small area of the Caco-2 monolayer, the dissolved drug accumulates at the donor site of the monolayer, explaining the common failure of transporter mediated uptake studies in dissolution/permeation devices. In addition, since transporters are expressed to a lesser extent than *in vivo* they might be saturated or overrun by the dissolved compound throughout the assay. *In vivo*, this phenomenon is observed only at peak concentrations, whereas transporter affinity is relevant at lower drug concentrations. Therefore, transporter studies using Caco-2 cells might be conducted as separate assays for mechanistic analyses. These would reveal whether a compound is passively or actively transported through the intestinal epithelium and, in case of an active transport, the related transporter. Furthermore, relevant excipient effects on drug permeation could be investigated (see section 1.2.3).

Concerning the simulation of *in vivo* dissolution it seems that the paradigm of displaying sink conditions *in vitro* does not resemble the actual situation in the intestine. Adjustment of the *in vitro* dissolution volume to the actual fluid volumes in the GI tract (see section 1.1.2.3) disclosed that non-sink conditions will at least partly prevail throughout the *in vivo* dissolution of poorly water-soluble drugs. However, *in vitro* dissolution studies performed with the fenofibrate IR tablets in 50 ml biorelevant media resulted in less than 0.5% fenofibrate in solution. Thus, no differentiation between the formulations was possible. It is assumed that the sink conditions have to be simulated in a manner, comparable to the *in vivo* situation. The sink of dissolved drug *in vivo* is provided by permeation across the membrane into the central circulation. Therefore, this should be mimicked in a dissolution/permeation device by offering a vast permeation area and sink conditions comparable to *in vivo* conditions. When the appropriate dose to dissolution volume is taken into account the actual intestinal drug and excipient concentrations would prevail. This might expose the different formulation effects on dissolution as it has been suggested by Langguth et al. [95]. In the solubility studies the contribution of the excipients to the solubility of fenofibrate emerged by applying this aforementioned condition (see chapter 4).

Furthermore, the influence of formulation excipients on drug permeation could be monitored simultaneously as it has been investigated in a separate permeation study (see chapter 3). The major issue of such a dissolution/permeation device is the choice of an appropriate permeation unit, as has been discussed throughout this thesis. An interesting approach has been reported by Kale et al. (see section 1.3.4.2) in which chicken intestine was utilized as permeation unit. The application of an animal intestine instead of an artificial membrane implies as major

drawback the animal intrinsic interindividual variability. Apart from this, animal intestine segments seem not to be viable *in vitro* in the presence of biorelevant media, as has been shown by Patel et al. [47]. This excludes animal intestine as potential *in vitro* surrogate for human intestinal epithelium and additionally promotes the application of a resistant artificial membrane in a dissolution/permeation device.

A promising approach in terms of simulating *in vivo* drug permeation with an artificial membrane has been introduced by Corti et al. (see section 1.1.1). The artificial membrane permeability of 21 at least partially passive transported drugs was successfully correlated to their fraction absorbed in humans. The examined compounds encompassed the whole range of permeation characteristics, varying from poorly to highly permeable. 13 of the substances chosen are recommended by the FDA for validation of *in vitro* permeation methods, including hydrophilic ones, such as atenolol, aciclovir and metformin. The potential of this artificial membrane system to predict human fraction absorbed was greater than that obtained for the same set of drugs with the commonly used Caco-2 permeation method. Corti et al. used a flat artificial membrane with a diameter of only 47 mm which were mounted in a diffusion cell for their permeation studies. A considerably larger permeation unit had to be provided in a dissolution/permeation device to approach the actual dissolution volume/permeation area ratio *in vivo* (see section 1.1).

The same train of thought was followed in the area of dialysis therapy. Here, the dialysis performance was improved by changing the dialysis format from a flat sheet to the hollow fiber geometry [163]. Transferred to a modified dissolution/permeation device the small flat Caco-2 monolayer could be substituted by an artificial membrane (Corti et al.) shaped as a tube. Based on the results of this thesis further modifications of the dissolution/permeation approach should be realized. Dissolution should take place in approximately 50 ml dissolution volume. This fluid could circulate through a flow through dissolution cell under closed system conditions. Almost the entire tubing system should be composed of the artificial membrane. The tubing system could be immersed in a beaker comprising the receiver medium. As realized in the D/P system, the acceptor medium should contain BSA to maintain sink conditions for drug permeation throughout the experiment. This might better simulate *in vivo* permeation as well as dissolution because non-sink conditions may at least partly prevail during the dissolution of poorly water-soluble drugs. Therefore, the different formulation effects (e.g., different excipients or excipient concentrations) might have a more appropriate impact on the *in vitro* drug dissolution, reflecting their contribution to the *in vivo* performance. For example, the obtained solubility and permeation data from the five RD tablets (see section 4.4) should be reflected in the dissolution and permeation profiles gathered from this modified dissolution/permeation device.

The concept of combining a small dissolution volume with a vast permeation area *in vitro* to simulate *in vivo* oral drug absorption has been already stated and partly realized by Dibbern et

al. (see section 1.3.1). In their resorption model Resomat, a small dissolution volume of 50-100 ml simulates the fluid volume in the GI tract. The authors discussed in a publication [54] that the *in vivo* permeation barrier should be represented by a membrane being as large as possible. However, the Resomat is equipped with a membrane of only 10 cm^2 permeation area, thus displaying a small permeation area/dissolution volume ratio.

This ratio would significantly increase by using the described tubing system. Such a dissolution/permeation approach might be applicable as a low cost, high-throughput screening system for drugs and drugs formulated as solid oral dosage forms in the early development phase. The dynamic conditions in this system would reduce the thickness of the unstirred water layer adhering to the membrane surface which has been shown to disturb permeation studies of highly permeable compounds under static conditions [38]. Any biorelevant media regardless of their pH could be applied if an artificial membrane were in use. To simulate more closely the *in vivo* situation the permeation membrane could be impregnated with a mixture of polyglycolysed glycerides. Moreover, the application of an artificial membrane should result in high repeatability for a series of formulations in contrast to animal and human studies. *In vivo* studies exhibit commonly large biological variations and therefore require large groups of individuals to be able to discriminate between different formulations. Furthermore, the pharmacokinetic data include all factors of absorption providing little information for further improvement of the drug formulation, especially at an early stage.

The described dissolution/permeation system might elucidate the contributions of formulation characteristics to dissolution and permeation of orally administered drug products. This approach would be based on the promising solubility and permeation methods introduced in this thesis. Additionally, crucial information about compounds belonging to BCS classes III and IV in terms of a potential IVIVC could be provided by investigating both important determinants of oral absorption, dissolution and permeation. Additionally, the investigation of compounds which seem to be unproblematic concerning permeation could unveil influences of the formulation properties on the permeation step. This has been displayed in *in vitro* permeation studies for the formulated BCS class II drug, fenofibrate (see chapter 3). In these studies two potential processes of fenofibrate uptake which might be influenced by the IR tablet properties could not be investigated. This will be shortly discussed.

Formulation B was disregarded when the IVIVC for the fenofibrate IR tablets was established (see section 4.4). Its good *in vivo* performance might be attributed to the small particle size of fenofibrate (< 200 nm) in this formulation, leading either to an increased dissolution rate [91] and/or to an increased adhesiveness of the particles to the epithelium [95,164]. Both these potential cases were not investigated since the assays were conducted with micronized fenofibrate. To examine the latter only a cell layer could have exhibited the microvilli necessary

to simulate the potential larger contact area between drug and intestinal barrier (see section 1.1.1).

The second potential process of fenofibrate permeation which might be influenced by the IR formulation characteristics was facilitated by uptake via liposomes containing bile salts. Chen et al. [165] reported an increased oral bioavailability of fenofibrate by using liposomes containing a bile salt compared to micronized fenofibrate capsules, although their *in vitro* release argued the opposite. The authors suggested an alternative absorption mechanism for liposomes as explanation for the better *in vivo* performance. This would imply that the vesicular system of $FaSSIF_{mod}$ might promote the absorption of fenofibrate via two modes, namely through the solubilization and facilitated permeation of fenofibrate. An appropriate cell layer would be required for an examination of the second potential process of fenofibrate uptake. Due to the toxicity of the formulation excipients, the use of cell lines had to be excluded in both described cases.

The combination of *in vitro* dissolution and permeation studies under physiologically relevant conditions might substitute *in vitro* dissolution measurements as the absolute standard for the development of an IVIVC. It has been stated repeatedly that *in vitro* dissolution studies should be optimized for each drug and dosage form to establish an IVIVC [17,166,167]. This confirms the inability of the current *in vitro* dissolution methods to simulate *in vivo* conditions as no standard method is suitable for all kinds of drug formulations.

An *in vitro* dissolution/permeation approach could be further elaborated by addition of a stomach simulating unit, use of enzymes, simulation of the peristaltic movements, introduction of a meal or simulation of the dilution of bile as it has been conducted in the TR-SANS study (see chapter 5), to mention a few. These properties have been partly implemented in the dissolution/hollow fiber system by Blanquet et al. (see section 1.3.4.1) which is widely used in nutrition studies. However, only few oral dosage forms have been studied with this system which may be ascribed to the costly and complex realization of a study. This leads to the conclusion that an ideal dissolution/permeation device should be easy to handle and simulate the multivariate processes involved in drug absorption, in a reasonable way, for a successful application as high-throughput screening system for drugs and drug formulations. With a permeation system analyzing active and passive transport processes the scope of compounds could be expanded to all BCS classes.

Summary

This current work focused on the simulation of *in vivo* dissolution and permeation in order to be able to predict the *in vivo* performance of orally administered fenofibrate immediate release formulations. Therefore, the effects of the formulation surfactants on *in vivo* solubility and permeation of fenofibrate, under physiologically relevant excipient concentrations were emphasized.

It was shown that the surfactant sodium dodecyl sulfate may decrease rather than increase the solubility of fenofibrate *in vivo*, although it is commonly used and assumed to raise the solubility of hydrophobic drugs. This was related to the interference of sodium dodecyl sulfate with the vesicular system of the biorelevant medium, $FaSSIF_{mod}$, and therefore its solubilization capacity. The impact of sodium dodecyl sulfate on the vesicular drug solubilizing system was investigated by several *in vitro* experiments, such as dynamic light scattering, cryogenic transmission electron microscopy and small-angle neutron scattering. These techniques detected the disappearance of the vesicle system under physiologically relevant sodium dodecyl sulfate concentrations. Additionally, the secretion of bile into the intestine was simulated by dilution of the fed state biorelevant medium $FeSSIF_{mod6.5}$, to result in the fasted state model $FaSSIF_{mod}$. The structural development was investigated with simultaneous time-resolved neutron and dynamic light scattering in a novel double beam technique.

Moreover, *in vitro* permeation studies revealed that sodium dodecyl sulfate concentrations inversely correlated with fenofibrate permeability. This effect was attributed to micellar entrapment of fenofibrate, preventing its permeation across the dialysis membrane. Through combination of the observed permeation and solubility data a good *in vitro/in vivo* correlation regarding C_{max} values in humans could be established for five fenofibrate formulations which were based on the same manufacturing technique.

Due to toxicity concerns associated with sodium dodecyl sulfate, the use of the dissolution/permeation system could not be employed in the development of the *in vitro/in vivo* correlation. In the first part of the thesis (chapter 2) the simultaneous evaluation of dissolution and permeation using the dissolution/permeation system has shown its ability to predict the *in vivo* performance in rats of different fenofibrate formulations and to simulate the food effect on the absorption of fenofibrate. In the second part of the thesis (chapters 3 and 4) the dose/dissolution volume ratio was adjusted to recently reported *in vivo* findings, resulting in increased excipient concentrations *in vitro*. Therefore, the dissolution/permeation system which contained the susceptible Caco-2 monolayer had to be substituted by the separate determinations of the solubility and permeation data.

To date, no single *in vitro* method is able to simulate one-to-one the multivariate processes involved in *in vivo* oral drug absorption. However, this thesis has shown that through the application and/or interplay of several *in vitro* methods, the prediction of the *in vivo* performance of fenofibrate immediate release tablets were possible under adjusted *in vitro* dissolution volume conditions. Furthermore, the influences of formulation excipients on drug absorption were detected questioning the indiscriminate application of sodium dodecyl sulfate in drug products.

Besides the experimental part, the major characteristics and their potential implementation in a dissolution/permeation device were discussed based on the promising realization of the *in vitro* solubility and permeation methods. The results presented in the current work will hopefully encourage a reassessment of the current methods to simulate *in vivo* dissolution and permeation in order to expand the applications of *in vitro/in vivo* correlation and further minimize the number of animal studies.

References

1. Amidon GL, Lennernäs H, Shah VP, Crison JR: A theoretical basis for a biopharmaceutic drug classification: the correlation of in vitro drug product dissolution and in vivo bioavailability. Pharm Res 1995;12:413-420.
2. DeSesso JM, Jacobson CF: Anatomical and physiological parameters affecting gastrointestinal absorption in humans and rats. Food Chem Toxicol 2001;39:209-228.
3. Weaver LT, Austin S, Cole TJ: Small intestinal length: a factor essential for gut adaptation. Gut 1991;32:1321-1323.
4. Croyle MC, Walter E, Janich S, Roessler BJ, Amidon GL: Role of Integrin Expression in Adenovirus-Mediated Gene Delivery to the Intestinal Epithelium. Hum Gene Ther 1998;9:561-573.
5. Hodin RA, Matthews JB: Small intestine. In Norton JA, Bollinger RR, Chang AE, Lowery SF, Mulvihill SJ, Pass HI, Thompson RW (eds.). Surgery: basic science and clinical evidence. New York, Springer 2008:963-990.
6. Artursson P, Palm K, Luthman K: Caco-2 monolayers in experimental and theoretical predictions of drug transport. Adv Drug Deliv Rev 1996;22:67-84.
7. Loftsson T, Konradsdottir F, Másson M: Influence of aqueous diffusion layer on passive drug diffusion from aqueous cyclodextrin solutions through biological membranes. Pharmazie 2006;61:83-89.
8. Humberstone AJ, Charman WN: Lipid-based vehicles for the oral delivery of poorly water soluble drugs. Adv Drug Deliv Rev 1997;25:103-128.
9. Bohets H, Annaert P, Mannens G, Anciaux K, Verboven P, Meuldermans W, Lavrijsen K: Strategies for absorption screening in drug discovery and development. Curr Top Med Chem 2001;1:367-383.
10. Langguth P, Lee KM, Spahn-Langguth H, Amidon GL: Variable gastric emptying and discontinuities in drug absorption profiles: Dependence of rates and extent of cimetidine absorption on motility phase and pH. Biopharm Drug Dispos 1994;15:719-746.
11. Levine RR: Factors affecting gastrointestinal absorption of drugs. Amer J Digest Dis 1970;15:171-188.
12. Oomen AG, Hack A, Minekus M, Zeijdner E, Cornelis C, Schoeters G, Verstraete W, Van de Wiele T, Wragg J, Rompelberg CJM: Comparison of five in vitro digestion models to study the bioaccessibility of soil contaminants. Environ. Sci. Technol 2002;36:3326-3334.
13. Davis SS, Hardy JG, Fara JW: Transit of pharmaceutical dosage forms through the small intestine. Gut 1986;27:886-892.
14. Sunesen VH, Vedelsdal R, Kristensen HG, Christrup L, Müllertz A: Effect of liquid volume and food intake on the absolute bioavailability of danazol, a poorly soluble drug. Eur J Pharm Sci 2005;24:297-303.
15. Evans DF, Pye G, Bramley R, Clark AG, Dyson TJ, Hardcastle JD: Measurement of gastrointestinal pH profiles in normal ambulant human subjects. Gut 1988;29:1035-1041.
16. Sugano K, Okazaki A, Sugimoto S, Tavornvipas S, Omura A, Mano T: Solubility and dissolution profile assessment in drug discovery. Drug Metab Pharmacokinet 2007;22:225-254.
17. Dressman JB, Amidon GL, Reppas C, Shah VP: Dissolution testing as a prognostic tool for oral drug absorption: immediate release dosage forms. Pharm Res 1998;15:11-22.
18. Jantratid E, Janssen N, Reppas C, Dressman JB: Dissolution Media Simulating Conditions in the Proximal Human Gastrointestinal Tract: An Update. Pharm Res 2008;25:1663-1676.
19. Custodio JM, Wu CY, Benet LZ: Predicting drug disposition, absorption/elimination/transporter interplay and the role of food on drug absorption. Adv Drug Deliv Rev 2008;60:717-733.
20. Schiller C, Froehlich CP, Giessmann T, Siegmund W, Monnikes H, Hosten N, Weitschies W: Intestinal fluid volumes and transit of dosage forms as assessed by magnetic resonance imaging. Aliment Pharmacol Ther 2005;22:971-979.

21. Hanson R, Gray V: Handbook of Dissolution Testing 3rd ed.; Dissolution Technologies. DE, Inc.: Hockessin 2004.
22. Haubrich WS, Schaffner F, Berk JE: Bockus gastroenterology, 5th ed. Philadelphia. WB Saunders, 1995.
23. Singh BN: Effects of food on clinical pharmacokinetics. Clin Pharmacokinet 1999;37:213-255.
24. Charman WN, Rogge MC, Boddy AW, Berger BM: Effect of food and a monoglyceride emulsion formulation on danazol bioavailability. J Clin Pharmacol 1993;33:381-386.
25. FDA: Guidance for Industry: Food-Effect Bioavailability and Fed Bioequivalence Studies. 2002.
26. Galia E, Nicolaides E, Horter D, Lobenberg R, Reppas C, Dressman JB: Evaluation of various dissolution media for predicting in vivo performance of class I and II drugs. Pharm Res 1998;15:698-705.
27. Kataoka M, Masaoka Y, Sakuma S, Yamashita S: Effect of food intake on the oral absorption of poorly water-soluble drugs: in vitro assessment of drug dissolution and permeation assay system. J Pharm Sci 2006;95:2051-2061.
28. Lind ML, Jacobsen J, Holm R, Mullertz A: Development of simulated intestinal fluids containing nutrients as transport media in the Caco-2 cell culture model: Assessment of cell viability, monolayer integrity and transport of a poorly aqueous soluble drug and a substrate of efflux mechanisms. Eur J Pharm Sci 2007;32:261-270.
29. Hernell O, Staggers JE, Carey MC: Physical-chemical behavior of dietary and biliary lipids during intestinal digestion and absorption. 2. Phase analysis and aggregation states of luminal lipids during duodenal fat digestion in healthy adult human beings. Biochemistry 1990;29:2041-2056.
30. Borgström B: Partition of lipids between emulsified oil and micellar phases of glyceride-bile salt dispersions. J Lipid Res 1967;8:598-608.
31. Nielsen FS, Gibault E, Ljusberg-Wahren H, Arleth L, Pedersen JS, Mullertz A: Characterization of prototype self-nanoemulsifying formulations of lipophilic compounds. J Pharm Sci 2007;96:876-892.
32. Fatouros DG, Walrand I, Bergenstahl B, Müllertz A: Colloidal Structures in Media Simulating Intestinal Fed State Conditions with and Without Lipolysis Products. Pharm Res 2008;26:361–374.
33. Sunesen VH, Pedersen BL, Kristensen HG, Müllertz A: In vivo in vitro correlations for a poorly soluble drug, danazol, using the flow-through dissolution method with biorelevant dissolution media. Eur J Pharm Sci 2005;24:305-313.
34. Mazer NA, Benedek GB, Carey MC: Quasielastic light-scattering studies of aqueous biliary lipid systems. Mixed micelle formation in bile salt-lecithin solutions. Biochemistry 1980;19:601-615.
35. Hjelm RP, Thiyagarajan P, Alkan H: A small-angle neutron scattering study of the effects of dilution on particle morphology in mixtures of glycocholate and lecithin. J Appl Crystallogr 1988;21:858-863.
36. Wei H, Löbenberg R: Biorelevant dissolution media as a predictive tool for glyburide a class II drug. Eur J Pharm Sci 2006;29:45-52.
37. Deferme S, Annaert P, Augustijns P: In Vitro Screening Models to Assess Intestinal Drug Absorption and Metabolism. In Ehrhardt C, Kim KJ (eds.). Drug Absorption Studies. US, Springer 2008:182-215.
38. Corti G, Maestrelli F, Cirri M, Zerrouk N, Mura P: Development and evaluation of an in vitro method for prediction of human drug absorption II. Demonstration of the method suitability. Eur J Pharm Sci 2006;27:354-362.
39. Artursson P, Karlsson J: Correlation between oral drug absorption in humans and apparent drug permeability coefficients in human intestinal epithelial (Caco-2) cells. Biochem Biophys Res Comm 1991;175:880-885.
40. Pinto M, Robine-Leon S, Appay MD, Kedinger M, Triadou N, Dussaulx E, Lacroix B, Simon-Assmann P, Haffen K, Fogh J: Enterocyte-like differentiation and polarization of the human colon carcinoma cell line Caco-2 in culture. Biol. Cell 1983;47:323-330.

41. Karlsson J, Kuo SM, Ziemniak J, Artursson P: Transport of celiprolol across human intestinal epithelial (Caco-2) cells: mediation of secretion by multiple transporters including P-glycoprotein. Br J Pharmacol 1993;110:1009-1016.
42. Lennernäs H, Palm K, Fagerholm U, Artursson P: Comparison between active and passive drug transport in human intestinal epithelial (Caco-2) cells in vitro and human jejunum in vivo. Int J Pharm 1996;127:103-107.
43. Friedman DI, Amidon GL: Passive and carrier-mediated intestinal absorption components of two angiotensin converting enzyme (ACE) inhibitor prodrugs in rats: enalapril and fosinopril. Pharm Res 1989;6:1043-1047.
44. Cavet ME, West M, Simmons NL: Transport and epithelial secretion of the cardiac glycoside, digoxin, by human intestinal epithelial (Caco-2) cells. Br J Pharmacol 1996;118:1389-1396.
45. Wetterich U, Spahn-Langguth H, Mutschler E, Terhaag B, Rösch W, Langguth P: Evidence for intestinal secretion as an additional clearance pathway of talinolol enantiomers: concentration-and dose-dependent absorption in vitro and in vivo. Pharm Res 1996;13:514-522.
46. Artursson P, Ungell AL, Löfroth JE: Selective paracellular permeability in two models of intestinal absorption: cultured monolayers of human intestinal epithelial cells and rat intestinal segments. Pharm Res 1993;10:1123-1129.
47. Patel N, Forbes B, Eskola S, Murray J: Use of Simulated Intestinal Fluids with Caco-2 Cells and Rat Ileum. Drug Dev Ind Pharm 2006;32:151-161.
48. Fleisher D, Li C, Zhou Y, Pao LH, Karim A: Drug, meal and formulation interactions influencing drug absorption after oral administration. Clinical implications. Clin Pharmacokinet 1999;36:233-254.
49. Wagner D, Spahn-Langguth H, Hanafy A, Koggel A, Langguth P: Intestinal drug efflux: formulation and food effects. Adv Drug Deliv Rev 2001;50:13-31.
50. Brouwers J, Tack J, Lammert F, Augustijns P: Intraluminal drug and formulation behavior and integration in in vitro permeability estimation: A case study with amprenavir. J Pharm Sci 2006;95:372-383.
51. Aungst BJ: Intestinal permeation enhancers. J Pharm Sci 2000;89:429-442.
52. Rosano HL, Schulman JH, Weisbuch JB: Mechanism of the selective flux of salts and ions through nonaqueous liquid membranes. Ann N Y Acad Sci 1961;92:457-496.
53. Koch H: Ein einfaches Gerät zur Simulierung der Resorption von Arzneistoffen und Metaboliten in vitro. Dtsch Apoth Ztg 1977;117:1239-1243.
54. Dibbern HW, Scholz GH: Resorptions-Modellversuche mit künstlichen Lipoidmembranen. Arzneimittelforschung 1969;19:1140-1145.
55. Ginski MJ, Taneja R, Polli JE: Prediction of dissolution-absorption relationships from a continuous dissolution/Caco-2 system. AAPS PharmSci 1999;1:27-38.
56. Kataoka M, Masaoka Y, Yamazaki Y, Sakane T, Sezaki H, Yamashita S: In vitro system to evaluate oral absorption of poorly water-soluble drugs: simultaneous analysis on dissolution and permeation of drugs. Pharm Res 2003;20:1674-1680.
57. Kobayashi M, Sada N, Sugawara M, Iseki K, Miyazaki K: Development of a new system for prediction of drug absorption that takes into account drug dissolution and pH change in the gastro-intestinal tract. Int J Pharm 2001;221:87-94.
58. Sugawara M, Kadomura S, He X, Takekuma Y, Kohri N, Miyazaki K: The use of an in vitro dissolution and absorption system to evaluate oral absorption of two weak bases in pH-independent controlled-release formulations. Eur J Pharm Sci 2005;26:1-8.
59. He X, Kadomura S, Takekuma Y, Sugawara M, Miyazaki K: A new system for the prediction of drug absorption using a pH-controlled Caco-2 model: Evaluation of pH-dependent soluble drug absorption and pH-related changes in absorption. J Pharm Sci 2004;93:71-77.
60. He X, Sugawara M, Kobayashi M, Takekuma Y, Miyazaki K: An in vitro system for prediction of oral absorption of relatively water-soluble drugs and ester prodrugs. Int J Pharm 2003;263:35-44.

61. Motz SA, Klimundová J, Schaefer UF, Balbach S, Eichinger T, Solich P, Lehr CM: Automated measurement of permeation and dissolution of propranolol HCl tablets using sequential injection analysis. Anal Chim Acta 2007;581:174-180.
62. Minekus M, Marteau P, Havenaar R, Huis in'T Veld JHJ: A multicompartmental dynamic computer-controlled model simulating the stomach and small intestine. ATLA 1995;23:197-209.
63. Larsson M, Minekus M, Havenaar R: Estimation of the bioavailability of iron and phosphorus in cereals using a dynamic in vitro gastrointestinal model. J Sci Food Agric 1997;74:99-106.
64. Verwei M, Arkbage K, Havenaar R, van den Berg H, Witthoft C, Schaafsma G: Folic acid and 5-methyltetrahydrofolate in fortified milk are bioaccessible as determined in a dynamic in vitro gastrointestinal model. J Nutr 2003;133:2377-2383.
65. Krul C, Luiten-Schuite A, Baan R, Verhagen H, Mohn G, Feron V, Havenaar R: Application of a dynamic in vitro gastrointestinal tract model to study the availability of food mutagens, using heterocyclic aromatic amines as model compounds. Food Chem Toxicol 2000;38:783-792.
66. Souliman S, Blanquet S, Beyssac E, Cardot JM: A level A in vitro/in vivo correlation in fasted and fed states using different methods: applied to solid immediate release oral dosage form. Eur J Pharm Sci 2006;27:72-79.
67. Kale VV, Kasliwal RH, Avari JG: Attempt to Design Continuous Dissolution–Absorption System Using Everted Intestine Segment for In Vitro Absorption Studies of Slow Drug Release Formulations. Diss Tech May 2007:31-36.
68. Timmins P, Dennis AB, Vyas KA: Biphasic controlled release delivery system for high solubility pharmaceuticals and method. US Patent 6,475,521 2002.
69. Nelson E: Solution rate of theophylline salts and effects from oral administration. J Am Pharm Assoc 1957;46:607-614.
70. Levy G, Leonards JR, Procknal JA: Development of in vitro dissolution tests which correlate quantitatively with dissolution rate-limited drug absorption in man. J Pharm Sci 1965;54:1719-1722.
71. FDA: Guidance for Industry: Extended Release Oral Dosage Forms: Development, Evaluation, and Application of In Vitro/In Vivo Correlations. 1997.
72. Agency EM: Guideline on the investigation of bioequivalence. CPMP/EWP/QWP/1401/98 2008.
73. Eddington ND, Marroum P, Uppoor R, Hussain A, Augsburger L: Development and internal validation of an in vitro-in vivo correlation for a hydrophilic metoprolol tartrate extended release tablet formulation. Pharm Res 1998;15:466-473.
74. Mojaverian P, Rosen J, Vadino WA, Liebowitz S, Radwanski E: In-vivo/in-vitro correlation of four extended release formulations of pseudoephedrine sulfate. J Pharm Biomed Anal 1997;15:439-445.
75. Takka S, Sakr A, Goldberg A: Development and validation of an in vitro–in vivo correlation for buspirone hydrochloride extended release tablets. J Control Release 2003;88:147-157.
76. Chapman MJ: Pharmacology of fenofibrate. Am J Med 1987;83:21-25.
77. Faergeman O: Hypertriglyceridemia and the fibrate trials. Curr Opin Lipidol 2000;11:609-614.
78. Farnier M, Picard S: Diabetes: Statins, fibrates, or both? Curr Atheroscler Rep 2001;3:19-28.
79. Illingworth DR: Management of hyperlipidemia: goals for the prevention of atherosclerosis. Clin Invest Med 1990;13:211-218.
80. Steinhilber D, Schubert-Zsilavecz M: Molekularpharmakologie und medizinische Chemie der Fibrate. Pharm. Unserer Zeit 2007;36:108-112.
81. Dollery C: Therapeutic Drugs, vol. 1. Edinburgh, Churchill Livingstone 1991.
82. Chiou WL, Barve A: Linear correlation of the fraction of oral dose absorbed of 64 drugs between humans and rats. Pharm Res 1998;15:1792-1795.

83. Weil A, Caldwell J, Strolin-Benedetti M: The metabolism and disposition of fenofibrate in rat, guinea pig, and dog. Drug Metab Dispos 1988;16:302-309.
84. Hanafy A, Spahn-Langguth H, Vergnault G, Grenier P, Tubic Grozdanis M, Lenhardt T, Langguth P: Pharmacokinetic evaluation of oral fenofibrate nanosuspensions and SLN in comparison to conventional suspensions of micronized drug. Adv Drug Deliv Rev 2007;59:419-426.
85. Granero GE, Ramachandran C, Amidon GL: Dissolution and solubility behavior of fenofibrate in sodium lauryl sulfate solutions. Drug Dev Ind Pharm 2005;31:917-922.
86. Balfour JA, McTavish D, Heel RC: Fenofibrate. A review of its pharmacodynamic and pharmacokinetic properties and therapeutic use in dyslipidaemia. Drugs 1990;40:260-290.
87. Filippatos T, Milionis HJ: Treatment of hyperlipidaemia with fenofibrate and related fibrates. Expert Opin Investig Drugs 2008;17:1599-1614.
88. Guay DRP: Update on fenofibrate. Cardiovasc Drug Rev 2002;20:281-302.
89. Shepherd J: The fibrates in clinical practice: focus on micronised fenofibrate. Atherosclerosis 1994;110:55-63.
90. Mishra AK, Vachon MG, Guivarc'h PH, Snow RA, Pace GW: IDD technology: oral delivery of water-insoluble drugs using phospholipid-stabilized microparticulate IDD formulations. In Rathbone MJ, Hadgraft J, Roberts MS (eds.). Modified-release drug delivery technology. New York, Marcel Dekker 2003:151-157.
91. Jinno J, Kamada N, Miyake M, Yamada K, Mukai T, Odomi M, Toguchi H, Liversidge GG, Higaki K, Kimura T: Effect of particle size reduction on dissolution and oral absorption of a poorly water-soluble drug, cilostazol, in beagle dogs. J Control Release 2006;111:56-64.
92. Merisko-Liversidge E, Liversidge GG, Cooper ER: Nanosizing: a formulation approach for poorly-water-soluble compounds. Eur J Pharm Sci 2003;18:113-120.
93. Perrut M, Jung J, Leboeuf F: Enhancement of dissolution rate of poorly-soluble active ingredients by supercritical fluid processes Part I: Micronization of neat particles. Int J Pharm 2005;288:3-10.
94. Heng D, Ogawa K, Cutler DJ, Chan HK, Raper JA, Ye L, Yun J: Pure drug nanoparticles in tablets: what are the dissolution limitations? J Nanopart Res 2009;DOI 10.1007/s11051-009-9759-y.
95. Langguth P, Hanafy A, Frenzel D, Grenier P, Nhamias A, Ohlig T, Vergnault G, Spahn-Langguth H: Nanosuspension formulations for low-soluble drugs: pharmacokinetic evaluation using spironolactone as model compound. Drug Dev Ind Pharm 2005;31:319-329.
96. Abdalla A, Klein S, Mader K: A new self-emulsifying drug delivery system (SEDDS) for poorly soluble drugs: characterization, dissolution, in vitro digestion and incorporation into solid pellets. Eur J Pharm Sci 2008;35:457-464.
97. Porter CJ, Trevaskis NL, Charman WN: Lipids and lipid-based formulations: optimizing the oral delivery of lipophilic drugs. Nat Rev Drug Discov 2007;6:231-248.
98. Motz SA, Schaefer UF, Balbach S, Eichinger T, Lehr CM: Permeability assessment for solid oral drug formulations based on Caco-2 monolayer in combination with a flow through dissolution cell. Eur J Pharm Biopharm 2007;66:286-295.
99. Charman WN, Porter CJH, Mithani S, Dressman JB: Physicochemical and physiological mechanisms for the effects of food on drug absorption: The role of lipids and pH. J Pharm Sci 1997;86:269-282.
100. Persson EM, Gustafsson AS, Carlsson AS, Nilsson RG, Knutson L, Forsell P, Hanisch G, Lennernäs H, Abrahamsson B: The effects of food on the dissolution of poorly soluble drugs in human and in model small intestinal fluids. Pharm Res 2005;22:2141-2151.
101. Holm P, Norling T: A tablet comprising a fibrate. WO 2006084475 2006.
102. Cavallari C, Rodriguez L, Albertini B, Passerini N, Rosetti F, Fini A: Thermal and fractal analysis of diclofenac/Gelucire 50/13 microparticles obtained by ultrasound-assisted atomization. J Pharm Sci 2005;94:1124-1134.

103. Passerini N, Perissutti B, Moneghini M, Voinovich D, Albertini B, Cavallari C, Rodriguez L: Characterization of carbamazepine-Gelucire 50/13 microparticles prepared by a spray-congealing process using ultrasounds. J Pharm Sci 2002;91:699-707.
104. Rodriguez L, Passerini N, Cavallari C, Cini M, Sancin P, Fini A: Description and preliminary evaluation of a new ultrasonic atomizer for spray-congealing processes. Int J Pharm 1999;183:133-143.
105. Hauss DJ: Oral lipid-based formulations. Adv Drug Deliv Rev 2007;59:667-676.
106. Jannin V, Musakhanian J, Marchaud D: Approaches for the development of solid and semi-solid lipid-based formulations. Adv Drug Deliv Rev 2008;60:734-746.
107. Jaspart S, Piel G, Delattre L, Evrard B: Solid lipid microparticles: formulation, preparation, characterisation, drug release and applications. Expert Opin. Drug Deliv 2005;2:75-87.
108. O'Driscoll CM, Griffin BT: Biopharmaceutical challenges associated with drugs with low aqueous solubility-The potential impact of lipid-based formulations. Adv Drug Deliv Rev 2008;60:617-624.
109. Porter CJ, Pouton CW, Cuine JF, Charman WN: Enhancing intestinal drug solubilisation using lipid-based delivery systems. Adv Drug Deliv Rev 2008;60:673-691.
110. Pouton CW: Formulation of poorly water-soluble drugs for oral administration: Physicochemical and physiological issues and the lipid formulation classification system. Eur J Pharm Sci 2006;29:278-287.
111. Yamashita S, Furubayashi T, Kataoka M, Sakane T, Sezaki H, Tokuda H: Optimized conditions for prediction of intestinal drug permeability using Caco-2 cells. Eur J Pharm Sci 2000;10:195-204.
112. Yamaoka K, Tanigawara Y, Nakagawa T, Uno T: A pharmacokinetic analysis program (multi) for microcomputer. J Pharmacobiodyn 1981;4:879-885.
113. Heinzel G, Woloszczak R, Thomann P: TopFit. Version 2.0. Pharmacokinetic and Pharmacodynamic Data Analysis System for the PC. Stuttgart, G. Fischer, 1993.
114. Peterson ML, Hickey MB, Zaworotko MJ, Almarsson Ö: Expanding the Scope of Crystal Form Evaluation in Pharmaceutical Science. J Pharm Sci 2006;9:317-326.
115. Dai WG, Pollock-Dove C, Dong LC, Li S: Advanced screening assays to rapidly identify solubility-enhancing formulations: High-throughput, miniaturization and automation. Adv Drug Deliv Rev 2008;60:657-672.
116. Corsini A, Bellosta S, Davidson MH: Pharmacokinetic Interactions Between Statins and Fibrates. Am J Cardiol 2005;96:44-49.
117. Adam A, Schrimpl L, Schmidt PC: Some Physicochemical Properties of Mefenamic Acid. Drug Dev Ind Pharm 2000;26:477-487.
118. Rasenack N, Müller BW: Dissolution Rate Enhancement by in Situ Micronization of Poorly Water-Soluble Drugs. Pharm Res 2002;19:1894-1900.
119. Swanepoel E, Liebenberg W, de Villiers MM, Dekker TG: Dissolution Properties of Piroxicam Powders and Capsules as a Function of Particle Size and the Agglomeration of Powders. Drug Dev Ind Pharm 2000;26:1067-1076.
120. Cao X, Gibbs ST, Fang L, Miller HA, Landowski CP, Shin HC, Lennernäs H, Zhong Y, Amidon GL, Yu LX: Why is it Challenging to Predict Intestinal Drug Absorption and Oral Bioavailability in Human Using Rat Model. Pharm Res 2006;23:1675-1686.
121. Fagerholm U: Prediction of human pharmacokinetics-gastrointestinal absorption. J Pharm Pharmacol 2007;59:905-916.
122. Merle L, Dangoumau J, Balabaud C: Effect of food and light schedule on bile flow in the rat. Cell Mol Life Sci 1978;34:764-765.
123. Zhao YH, Abraham MH, Le J, Hersey A, Luscombe CN, Beck G, Sherborne B, Cooper I: Evaluation of rat intestinal absorption data and correlation with human intestinal absorption. Eur J Med Chem 2003;38:233-243.
124. Zwart LL, Rompelberg CJM, Sips A, Welink J, Engelen JGM: Anatomical and physiological differences between various species used in studies on the pharmacokinetics and toxicology of xenobiotics. A review of literature. RIVM report 623860010, National Institute of Public Health and the Environment 1999.

125. Lobenberg R, Kramer J, Shah VP, Amidon GL, Dressman JB: Dissolution testing as a prognostic tool for oral drug absorption: dissolution behavior of glibenclamide. Pharm Res 2000;17:439-444.
126. Irvine JD, Takahashi L, Lockhart K, Cheong J, Tolan JW, Selick HE, Grove JR: MDCK (Madin-Darby canine kidney) cells: A tool for membrane permeability screening. J Pharm Sci 1999;88:28-33.
127. Buch P, Langguth P, Kataoka M, Yamashita S: IVIVC in oral absorption for fenofibrate immediate release tablets using a dissolution/permeation system. J Pharm Sci 2009;98:2001-2009.
128. Kesisoglou F, Panmai S, Wu Y: Nanosizing-Oral formulation development and biopharmaceutical evaluation. Adv Drug Deliv Rev 2007;59:631-644.
129. Ryde T, Gustow EE, Ruddy SB, Jain R, Patel R, Wilkins MJ: Nanoparticulate fibrate formulations. US Patent 7,276,249 2007.
130. Serbest G, Horwitz J, Barbee K: The effect of poloxamer-188 on neuronal cell recovery from mechanical injury. J Neurotrauma 2005;22:119-132.
131. Bennion BC, Tong LKJ, Holmes LP, Eyring EM: Kinetics of sodium lauryl sulfate micelle dissociation by a light-scattering temperature-jump technique. J Phys Chem 1969;73:3288-3289.
132. Busoi C, Rotaru M, Oghina B, Surmeian M, It P: Method of Purifying a Surfactant by Ultrafiltration. WO/2006/084902 2006.
133. Wanka G, Hoffmann H, Ulbricht W: Phase diagrams and aggregation behavior of poly(oxyethylene)-poly(oxypropylene)-poly(oxyethylene) triblock copolymers in aqueous solutions. Macromolecules 1994;27:4145-4159.
134. Shah VP, Hunt JP, Fairweather WR, Prasad VK, Knapp G: Influence of dioctyl sodium sulfosuccinate on the absorption of tetracycline. Biopharm Drug Dispos 1986;7:27-33.
135. Luner PE, Vander Kamp D: Wetting behavior of bile salt-lipid dispersions and dissolution media patterned after intestinal fluids. J Pharm Sci 2001;90:348-359.
136. Anderberg EK, Artursson P: Epithelial transport of drugs in cell culture. VIII: Effects of sodium dodecyl sulfate on cell membrane and tight junction permeability in human intestinal epithelial (Caco-2) cells. J Pharm Sci 1993;82:392-398.
137. Anderberg EK, Nyström C, Artursson P: Epithelial transport of drugs in cell culture. VII: Effects of pharmaceutical surfactant excipients and bile acids on transepithelial permeability in monolayers of human intestinal epithelial(Caco-2) cells. J Pharm Sci 1992;81:879-887.
138. Ingels F, Deferme S, Destexhe E, Oth M, Van den Mooter G, Augustijns P: Simulated intestinal fluid as transport medium in the Caco-2 cell culture model. Int J Pharm 2002;232:183-192.
139. Nagarajan R, Wang CC: Solution Behavior of surfactants in ethylene glycol: Probing the existence of a CMC and of micellar aggregates. J Colloid Interface Sci 1996;178:471-482.
140. Coello A, Meijide F, Nunez ER, Tato JV: Aggregation behavior of bile salts in aqueous solution. J Pharm Sci 1996;85:9-15.
141. Kossena GA, Boyd BJ, Porter CJ, Charman WN: Separation and characterization of the colloidal phases produced on digestion of common formulation lipids and assessment of their impact on the apparent solubility of selected poorly water-soluble drugs. J Pharm Sci 2003;92:634-648.
142. Hjelm Jr RP, Thiyagarajan P, Alkan-Onyuksel H: Organization of phosphatidylcholine and bile salt in rodlike mixed micelles. J Phys Chem 1992;96:8653-8661.
143. Leng J, Egelhaaf SU, Cates ME: Kinetics of the Micelle-to-Vesicle Transition: Aqueous Lecithin-Bile Salt Mixtures. Biophys J 2003;85:1624-1646.
144. Dressman JB, Reppas C: In vitro-in vivo correlations for lipophilic, poorly water-soluble drugs. Eur J Pharm Sci 2000;11 Suppl 2:S73-80.
145. Buch P, Holm P, Thomassen JQ, Scherer D, Branscheid R, Kolb U, Langguth P: IVIVC for Fenofibrate Immediate Release Tablets Using Solubility and Permeability as In Vitro Predictors for Pharmacokinetics. J Pharm Sci 2010.

146. Okazaki A, Mano T, Sugano K: Theoretical dissolution model of poly-disperse drug particles in biorelevant media. J Pharm Sci 2008;97:1843-1852.
147. Lieutenant K, Lindner P, Gahler R: A new design for the standard pinhole small-angle neutron scattering instrument D11. J Appl Crystallogr 2007;40:1056-1063.
148. Guinier A: La diffraction des rayons X aux tres petits angles; application a l'etude de phenomenes ultramicroscopiques. Ann. Phys.(Paris) 1939;12:161-237.
149. Porod G: Die Abhängigkeit der Röntgen-Kleinwinkelstreuung von Form und Grösse der kolloiden Teilchen in verdünnten Systemen. IV. Acta Phys. Austriaca 1948;2:255–292.
150. Kratky O: X-ray small angle scattering with substances of biological interest in diluted solutions. Prog Biophys 1963;13:105-173.
151. Nawroth T, Conrad H, Dose K: Neutron small angle scattering of liposomes in the presence of detergents. Physica B 1989;156:477-480.
152. Carrozzino JM, Fuguet E, Helburn R, Khaledi MG: Characterization of small unilamellar vesicles using solvatochromic [pi]* indicators and particle sizing. J Biochem Biophys Methods 2004;60:97-115.
153. Peters R, Georgalis Y, Saenger W: Accessing lysozyme nucleation with a novel dynamic light scattering detector. Acta Cryst 1998;54:873-877.
154. Hofmann AM, Wurm F, Huehn E, Nawroth T, Langguth P, Frey H: Hyperbranched polyglycerol-based lipids via oxyanionic polymerization: toward multifunctional stealth liposomes. Biomacromolecules 2010;11:568-574.
155. Zackrisson M, Stradner A, Schurtenberger P, Bergenholtz J: Small-angle neutron scattering on a core-shell colloidal system: a contrast-variation study. Langmuir 2005;21:10835-10845.
156. MacGregor KJ, Embleton JK, Lacy JE, Perry EA, Solomon LJ, Seager H, Pouton CW: Influence of lipolysis on drug absorption from the gastro-intestinal tract. Adv Drug Deliv Rev 1997;25:33-46.
157. Welling PG: Effects of food on drug absorption. Annu Rev Nutr 1996;16:383-415.
158. Walter A, Vinson PK, Kaplun A, Talmon Y: Intermediate structures in the cholate-phosphatidylcholine vesicle-micelle transition. Biophys J 1991;60:1315-1325.
159. Lo Nostro P, Stubicar N, Chen SH: Isotopic effect in phase separation of dioctanoylphosphatidylcholine/water micellar solutions. Langmuir 1994;10:1040-1043.
160. Long MA, Kaler EW, Lee SP: Structural characterization of the micelle-vesicle transition in lecithin-bile salt solutions. Biophys J 1994;67:1733-1742.
161. Meyuhas D, Bor A, Pinchuk I, Kaplun A, Talmon Y, Kozlov MM, Lichtenberg D: Effect of Ionic Strength on the Self-Assembly in Mixtures of Phosphatidylcholine and Sodium Cholate* 1. J Colloid Interface Sci 1997;188:351-362.
162. Small DM, Penkett SA, Chapman D: Studies on simple and mixed bile salt micelles by nuclear magnetic resonance spectroscopy. Biochim Biophys Acta 1969;176:178-189.
163. Vienken J, Bowry S: Quo vadis dialysis membrane? Artif Organs 2002;26:152-159.
164. Lenhardt T, Vergnault G, Grenier P, Scherer D, Langguth P: Evaluation of Nanosuspensions for Absorption Enhancement of Poorly Soluble Drugs: In Vitro Transport Studies Across Intestinal Epithelial Monolayers. AAPS J 2008;10:435-438.
165. Chen Y, Lu Y, Chen J, Lai J, Sun J, Hu F, Wu W: Enhanced bioavailability of the poorly water-soluble drug fenofibrate by using liposomes containing a bile salt. Int J Pharm 2009;376:53-60.
166. Uppoor VR: Regulatory perspectives on in vitro (dissolution)/in vivo (bioavailability) correlations. J Control Release 2001;72:127-132.
167. Yihong QIU, Lirong LIU, Gz ZG, Yisheng C, William P: Developing solid oral dosage forms: pharmaceutical theory & practice. Oxford, Elsevier Ltd 2008.

A. Appendix

A.1 Illustration of the observed surfactant-FaSSIF$_{mod}$ interactions

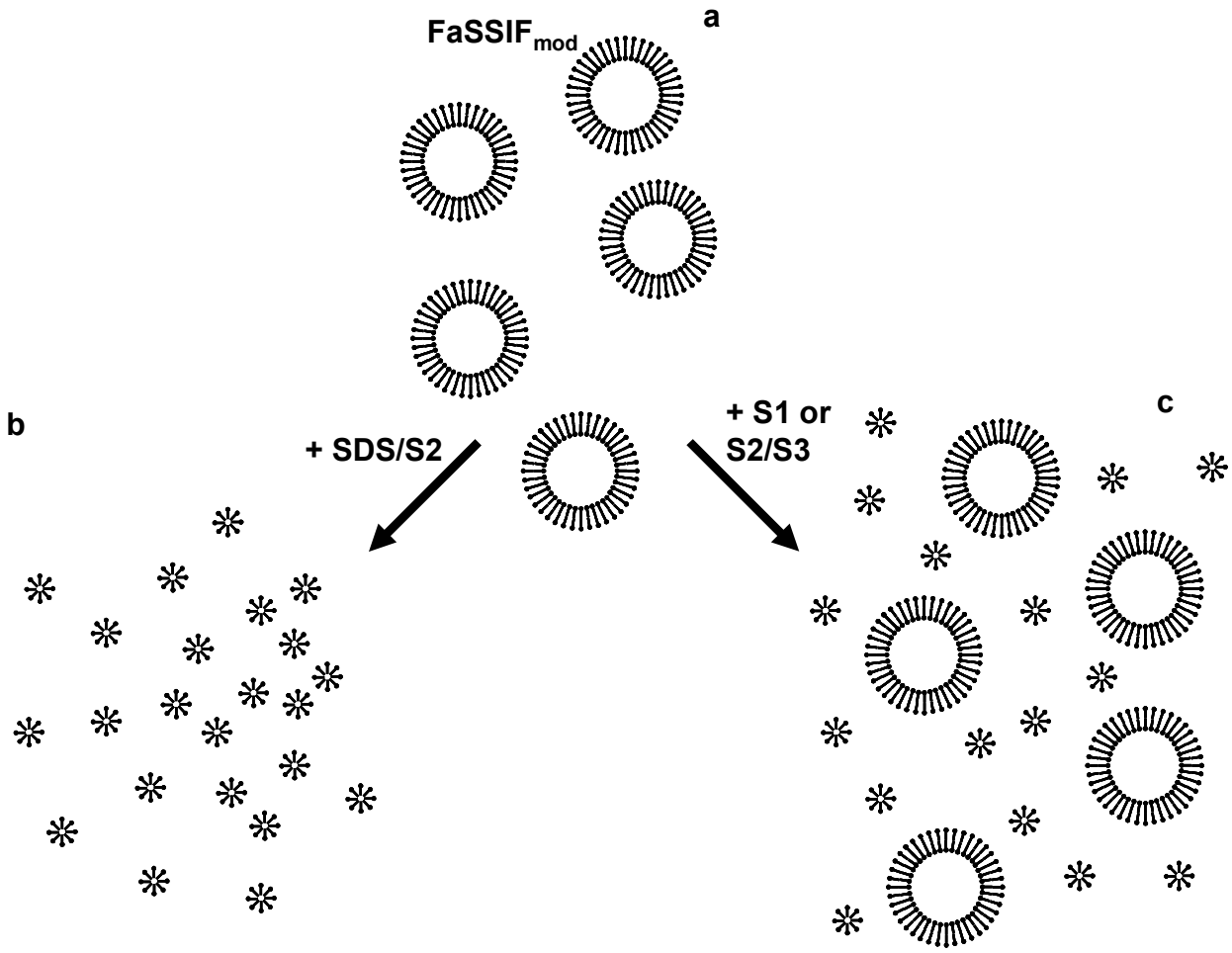

Figure A.1. Illustration of the structural changes when the surfactant compositions of formulations H-J (SDS/S2) (b) and the surfactant compositions of formulations A or G (S1 and S2/3 are commercial surfactants) (c) are dissolved in FaSSIF$_{mod}$ (a) to a final concentration of 0.1% (see section 4.4). In the first case the surfactants interfere with the vesicular system of FaSSIF$_{mod}$ (a) and finally micelles are formed (b). In the second case vesicles and micelles coexist (c). The given percentage reference the main surfactant in the formulation.

A.2 Two human *in vivo* studies with fenofibrate IR tablet formulations

Clinical study 1

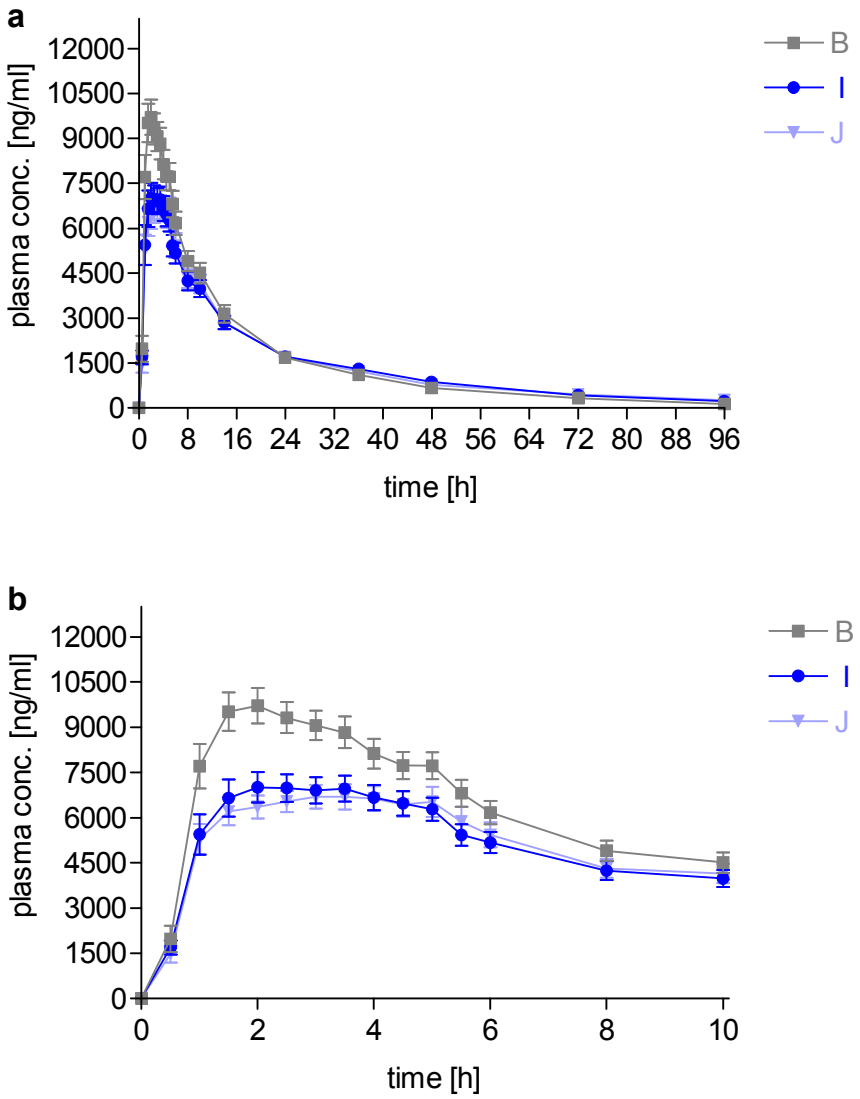

Figure A.2. Average (± SD) fenofibric acid plasma concentrations in humans (n ≥ 12) after oral administration of different fenofibrate formulations (clinical study 1, see section 3.3). The complete plasma profiles (a) and for a better differentiation between the formulations the first 10 hours of the plasma profiles are shown (b).

Clinical study 2

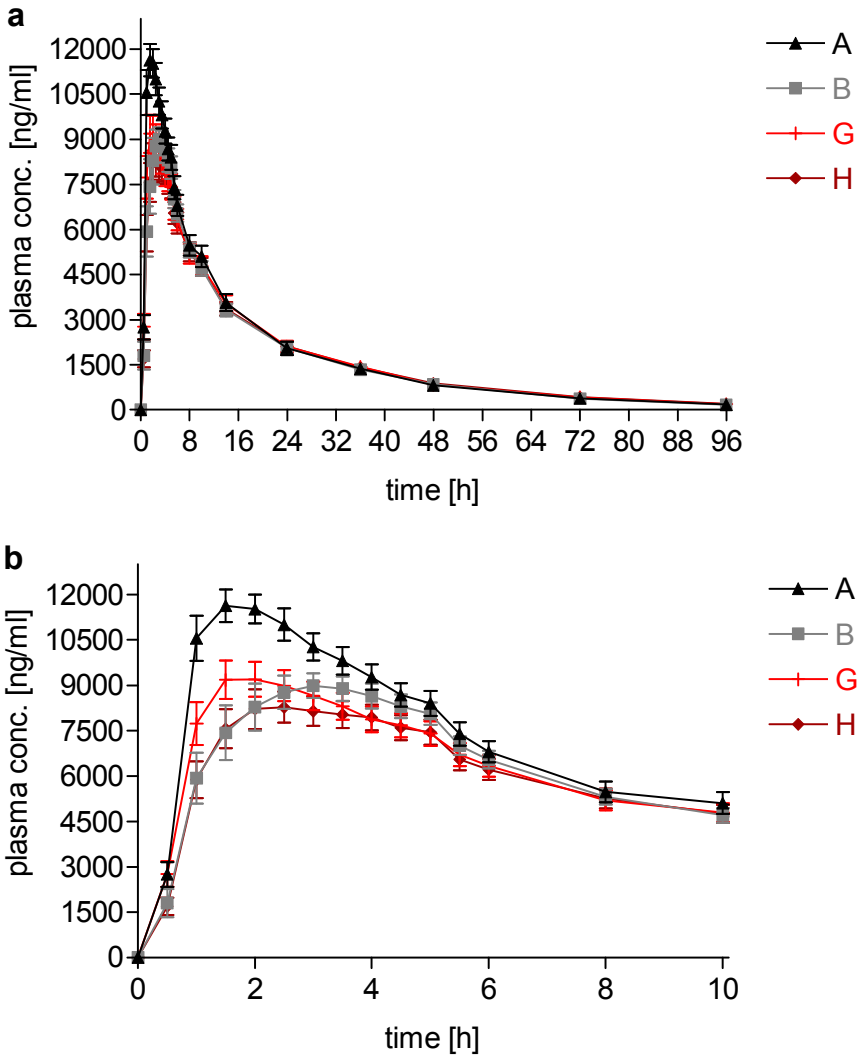

Figure A.3. Average (± SD) fenofibric acid plasma concentrations in humans (n ≥ 12) after oral administration of different fenofibrate formulations (clinical study 2, see section 3.3). The complete plasma profiles (a) and for a better differentiation between the formulations the first 10 hours of the plasma profiles are shown (b).

A.3 Surface tension measurements

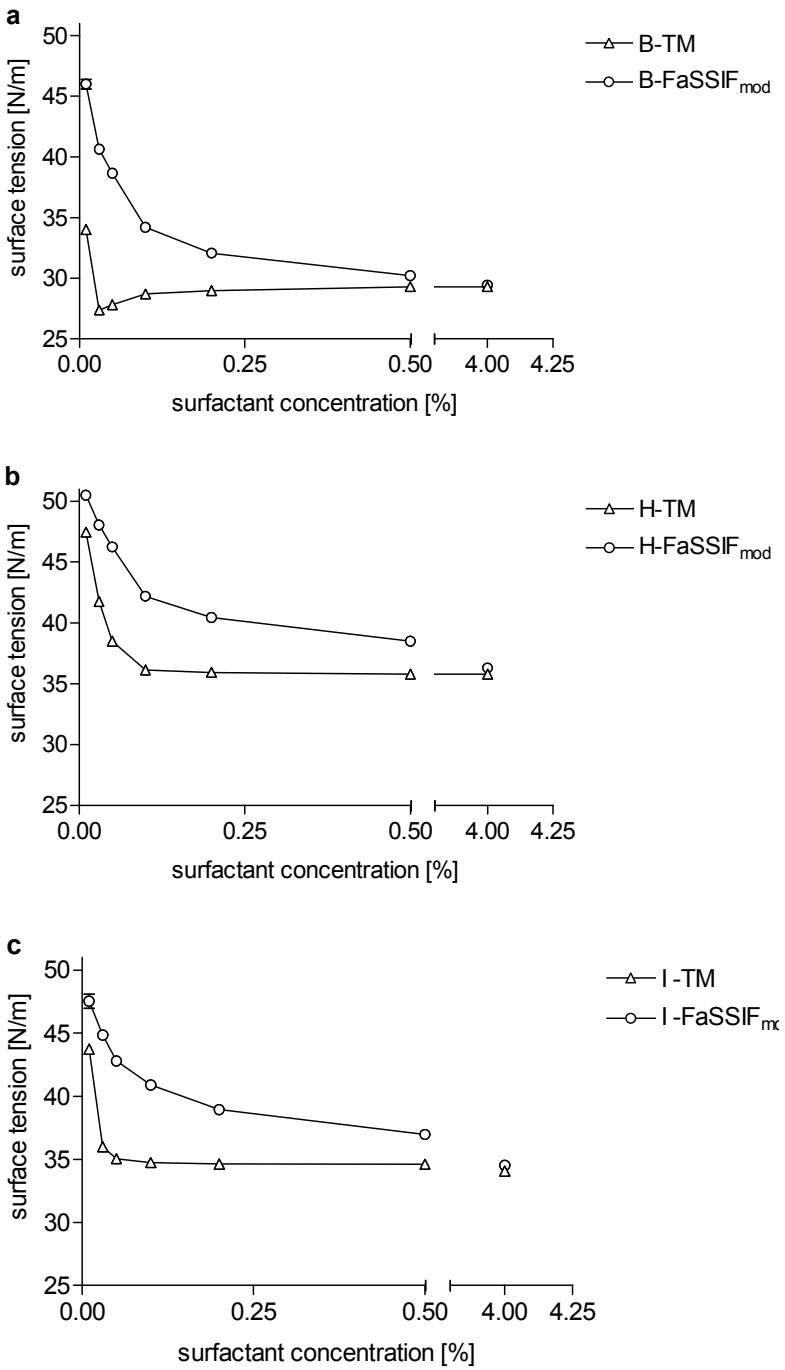

Figure A.4. Surface tension as a function of surfactant composition for formulations B (a), H (b) and I (c) in transport medium and FaSSIF$_{mod}$. The given percentages reference the main surfactant in the formulation. Each data point is the mean ± SD of three independent experiments.

A.4 Time-resolved small-angle neutron scattering measurements

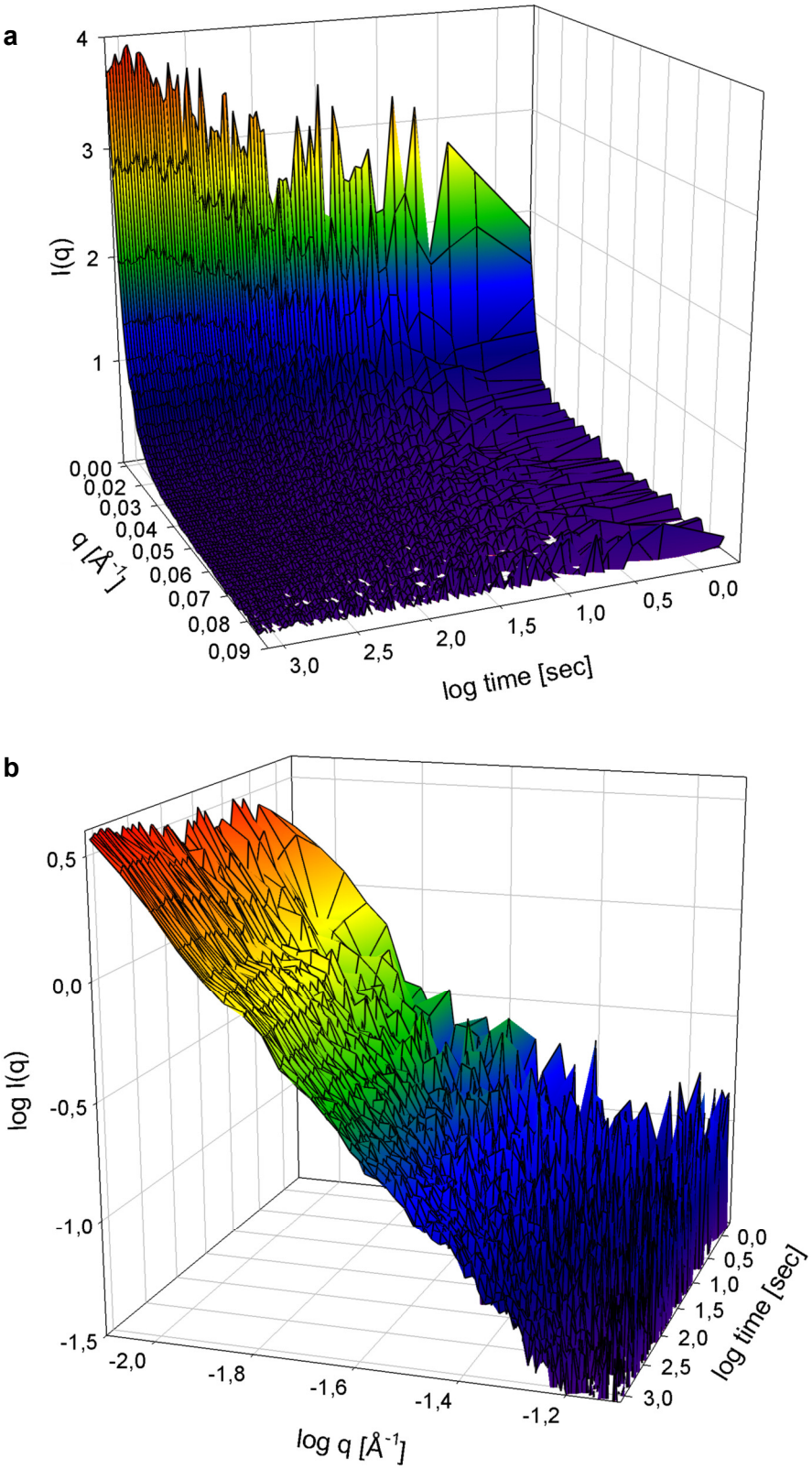

Figure A.5. Time-resolved neutron scattering profiles of the bile salt-lipid mixture FaSSIF$_{mod}$ in 71% D_2O upon fast dilution of FeSSIF$_{mod6.5}$ with transport medium with a stopped-flow device: 3D representations (lin-lin (a) and log-log (b)) of the development after dilution.

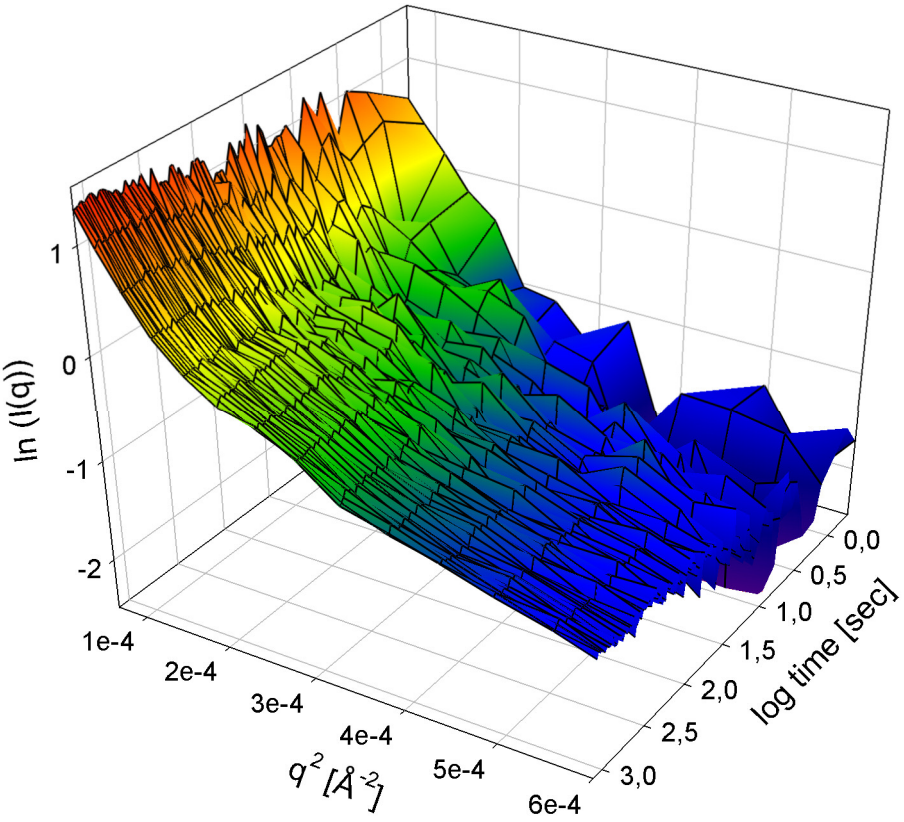

Figure A.6. 3D representation of the particle size development by Guinier plots of neutron scattering after dilution of $FeSSIF_{mod6.5}$ with transport medium with a stopped-flow device to $FaSSIF_{mod}$ (71% D_2O).

Publications and poster presentations

Buch P, Langguth P, Kataoka M, Yamashita S: IVIVC in oral absorption for fenofibrate immediate release tablets using a dissolution/permeation system. J Pharm Sci 2009;98:2001-2009

Buch P, Holm P, Thomassen JQ, Scherer D, Kataoka M, Yamashita S, Langguth P: IVIVR in oral absorption for fenofibrate immediate release tablets using dissolution and dissolution permeation methods. Pharmazie (in press)

Buch P, Holm P, Thomassen JQ, Scherer D, Branscheid R, Kolb U, Langguth P: IVIVC for fenofibrate immediate release tablets using solubility and permeability as *in vitro* predictors for pharmacokinetics. J Pharm Sci (in press)

Nawroth T, Buch P, Buch K, Langguth P, Schweins R: Liposome formation from bile salt-lipid micelles in the digestion and drug delivery model $FaSSIF_{mod}$ estimated by combined time-resolved neutron and dynamic light scattering. (in preparation)

Buch P, Holm P, Thomassen JQ, Scherer D, Kataoka M, Yamashita S, Langguth P: *In vitro*/*in vivo* relationship for fenofibrate IR tablets using dissolution and dissolution permeation methods Poster at the 36th Annual Meeting & Exposition of the Controlled Release Society, 18th-22nd Jul 2009, Copenhagen, Denmark